COMPARISON BETWEEN TURKISH AND JORDAN STANDARDS FROM GEOTECHNICAL EARTHQUAKE ENGINEERING ASPECTS

SHAFEEQ MOHAMMAD HAWA

IŞIK UNIVERSITY
JANUARY, 2024

COMPARISON BETWEEN TURKISH AND JORDAN STANDARDS FROM GEOTECHNICAL EARTHQUAKE ENGINEERING ASPECTS

SHAFEEQ MOHAMMAD HAWA

Işık University, School of Graduate Studies, Civil Engineering Master Program, 2024

This thesis has been submitted to Işık University School of Graduate Studies for a Master's Degree. (MA).

IŞIK UNIVERSITY

JANUARY, 2024

IŞIK UNIVERSITY

GRADUATE SCHOOL OF SCIENCE AND ENGINEERING

COMPARISON BETWEEN TURKISH AND JORDAN STANDARDS FROM
GEOTECHNICAL EARTHQUAKE ENGINEERING ASPECTS

SHAFEEQ MOHAMMAD HAWA

APPROVED BY:

Assist. Prof. Ehsan ETMİNAN (Thesis Advisor)	Işık University
Assist. Prof. Önder UMUT	Işık University
Assist. Prof. Kaveh DEHGHANIAN	Istanbul Aydın University

APPROVAL DATE: 22/01/2024

COMPARISON BETWEEN TURKISH AND JORDAN STANDARDS FROM GEOTECHNICAL EARTHQUAKE ENGINEERING ASPECTS

ABSTRACT

This thesis focuses on a comparative analysis of geotechnical earthquake engineering standards in Turkey and Jordan. The importance lies in ensuring that these standards are safe and economically viable, meeting each country's specific geotechnical and ground motion requirements. The study comprehensively examines both nations' earthquake and ground motion characteristics, reviewing relevant papers. The research is organized into six chapters, including recommendations. The thesis delves into the evolution of standards in both countries, considering feedback from researchers and the impact of past earthquakes on human life and infrastructure. It also explores the geotechnical earthquake phenomena resulting from earthquakes, such as landslides and liquefaction. The study reveals differences in codes due to variations in geological conditions, soil properties, and seismic locations. However, it also identifies noteworthy similarities. Additionally, the research analyzes the impact of earthquakes on soil by simulating two seismic events: the Düzce earthquake in Turkey and the Dead Sea earthquake in Jordan. PLAXIS 3D software, as a finite element method, is employed to observe deformations in the mesh, foundation, and piles, providing insights into the effects of seismic activity on these structural elements. The study emphasizes that Turkey encounters more frequent ground motion events than Jordan, and earthquakes in Turkey demonstrate a higher peak ground acceleration. Furthermore, even though Jordan experiences fewer earthquakes, the potential impact could be severe in the event of their occurrence. The similarities in earthquake effects identified through PLAXIS analysis indicate the presence of high peak ground acceleration, posing a significant risk in Turkey. This risk extends to Jordan, particularly during moderate earthquakes. This observation sheds light on why Jordan may have implemented stringent requirements in its building codes, aligning with the standards set by Turkey in some sections.

GEOTEKNİK DEPREM MÜHENDİSLİĞİ YÖNÜNDEN TÜRK VE ÜRDÜN STANDARTLARININ KARŞILAŞTIRILMASI

ÖZET

Bu tez, Türkiye ve Ürdün'deki geoteknik deprem mühendisliği standartlarının karşılaştırmalı analizine odaklanmaktadır. Önemli olan, bu standartların güvenli ve ekonomik açıdan uygulanabilir olmasını, her ülkenin kendine özgü geoteknik ve yer hareketi gereksinimlerini karşılamasını sağlamaktır. Bu çalışma, ilgili belgeleri gözden geçirerek her iki ülkenin deprem ve yer hareketi özelliklerini kapsamlı bir şekilde inceliyor. Bu araştırma öneriler de dahil olmak üzere altı bölüm halinde düzenlenmiştir. Tez, araştırmacılardan gelen geri bildirimleri ve geçmiş depremlerin insan yaşamı ve altyapı üzerindeki etkisini dikkate alarak her iki ülkedeki standartların gelişimini incelemektedir. Ayrıca heyelan ve zemin sıvılaşma gibi depremlerden kaynaklanan jeoteknik deprem olaylarını da araştırmaktadır. Bu çalışma, jeolojik koşullar, toprak özellikleri ve sismik konumlardaki değişiklikler nedeniyle kodlardaki farklılıkları ortaya koymaktadır. Ancak aynı zamanda dikkate değer benzerlikleri de tanımlar. Araştırma ayrıca iki sismik olayı simüle ederek depremlerin toprak üzerindeki etkisini analiz ediyor: Türkiye'deki Düzce depremi ve Ürdün'deki Ölü Deniz depremi. PLAXIS 3D yazılımı, sonlu elemanlar yöntemi olarak kafes, temel ve kazıklardaki deformasyonları gözlemlemek için kullanılır ve sismik aktivitenin bu yapısal elemanlar üzerindeki etkilerine dair içgörü sağlar. Çalışma, Türkiye'nin Ürdün'e göre daha sık yer hareketi olaylarıyla karşılaştığını ve Türkiye'deki depremlerin daha yüksek pik yer ivmesi gösterdiğini vurguluyor. Ayrıca, Ürdün'de daha az deprem yaşansa da, depremlerin meydana gelmesi halinde potansiyel etki daha şiddetli olabilir. PLAXIS analiziyle tespit edilen deprem etkilerindeki benzerlikler, Türkiye'de önemli bir risk oluşturan yüksek pik yer ivmesinin varlığına işaret etmektedir. Bu risk, özellikle orta dereceli depremler sırasında Ürdün'e kadar uzanmaktadır. Bu gözlem, Ürdün'ün inşaat mevzuatında neden bazı bölümlerde Türkiye'nin belirlediği standartlara uygun olarak katı gereklilikler uygulamış olabileceğine ışık tutuyor.

Anahtar Kelimeler: Türkiye Bina Deprem Yönetmeliği 2018, Ürdün Bina Deprem Yönetmeliği 2022, PLAXIS 3D Analizi, Kazık Temeli, Geoteknik Deprem Analizi

ACKNOWLEDGEMENTS

TABLE OF CONTENTS

LIST OF TABLES

LIST OF FIGURES

LIST OF ABBREVIATIONS

AFAD :   Disaster and Emergency Management Authority of Turkey

BKS   :   Building usage class (TBEC-2018)

CPT   :   Cone penetration test

DD-1 :   Maximum expected earthquake ground motion

DD-2 :   Standard design earthquake ground motion

DD-3 :   Frequently expected earthquake ground motion

DD-4 :   Service level earthquake ground motion

DSFS :   Dead Sea fault system

DSTF :   Dead Sea transform fault

E   :   Energy released of earthquake (ergs)

E50   :   Modulus of elasticity (kN/m²)

F_a, F_S :   Local ground effect coefficients for short period region (JBEC-2022 and TBEC-2018)

F_L :   Liquefaction resistance (JBEC-2022)

JSO   :   Jordan Seismological Observatory

NAFS :   North Anatolian fault system

PEER :   Pacific Earthquake Engineering Research Center

Ra   :   Load reduction factor (JBEC-2022)

rd   :   Stress reduction coefficient

R_F :   Stress of earthquake that causes liquefaction (kPa) (JBEC-2022)

R_i :   Equivalent average shear stress (JBEC-2022)

RSN :   Record Sequence Numbers

SD_1 :   Design spectral acceleration coefficient for 1.0 second period (TBEC-2018)

SD_S :   Short-period design spectral acceleration coefficient (dimensionless) (TBEC-2018

SM$_1$: Design spectral acceleration coefficient for 1.0 second period (dimensionless) (JBEC-2022)

SM$_S$: Short-period design spectral acceleration coefficient (dimensionless) (JBEC-2022)

SPT : Standard penetration test

S$_S$: Short period map spectral acceleration coefficient (dimensionless)

S$_T$: The spectral response acceleration factor

T$_a$: Dominant natural vibrational period calculated empirically (sec) (JBEC-2022)

TBEC-2018: Turkish Building Earthquake Code-2018

TEC : Turkish Earthquake Code

TpA : Dominant natural vibrational period calculated empirically (sec) (TBEC-2018)

u$_q$: Minimum uniaxial compressive strength

V : Base shear force (kN)

W : Total weight of the building (kN)

LIST OF SYMBOLS

$(N_{60})_{30}$:   Average number of standard penetrations blows in the upper 30 meters

ΔP_{su} :   Dynamic water pressure (kN/m^2)

Δt :   Time difference (sec)

μ :   Poisson's ratio

A_0 :   The effective ground acceleration coefficient

a_{max} :   Peak horizontal acceleration at the ground surface (m/s^2)

A_t :   Equivalent area used in the empirical natural vibration period account (m^2)

A_T :   Spectral acceleration coefficient

b_c, b_q, b_γ: Foundation base slope coefficients

C :   Cohesion strength of the soil (kPa)

CB :   Signifies the drilling drill diameter correction coefficient

CE :   Denotes the energy ratio correction coefficient

C_M :   Design earthquake moment magnitude correction coefficient

CR :   Rod length correction coefficient

$CRR_{M7.5}$:   Moment size 7.5 earthquake rate

CS :   Stands for the sampler type correction coefficient

C_t :   The coefficient used in the empirical natural vibration period calculation

C_u :   Undrained shear strength (kPa)

d_c, d_q, d_γ: The foundation depth coefficients (dimensionless)

d_{su} :   Height of the wall below the water level (TBEC-2018)

F :   Force

$F_{\gamma d}, F_{qd}, F_{cd}$:   Factors that depend on foundation depth and determined according to table available on the code depending on the width and length of the foundation

$F_{\gamma i}, F_{qi}, F_{ci}$:   Loading curvature coefficients

$F_{\gamma s}$, F_{qs}, F_{cs}: Factors that depend on shape of the foundation and determined according to table available on the code depending on the width and length of the foundation

g   :   Gravitational acceleration (m/s^2)

G   :   Wind load (kN)

g_c, g_q, g_γ: Foundation soil slope coefficients

G_{max} :   Maximum shear modulus

H   :   Lateral seismic load (kN)

H_N :   Total height of the upper part of the building above the basements (m)

I   :   The importance factor of the building

i_c, i_q, i_γ :   Loading curvature coefficients

K_a :   Coefficient of active earth pressure

k_h :   Horizontal static-equivalent earthquake coefficient

K_p :   Coefficient of passive earth pressure

M   :   Magnitude of earthquake

M_0 :   Seismic moment

M_{11} :   The moment resulting from bending around the horizontal axis (kN.m/m)

M_2 :   The bending moment around the second axis (bending moment around the x-axis)

M_{22} :   The bending moment resulting from bending around the vertical axis (kN.m/m)

M_3 :   The bending moment around the third axis (bending around the z-axis)

N_γ, N_q, N_c: Factors of bearing capacity of soil, and determining from tables available in the code depending on angle of soil shear resistance

P   :   live load (kN)

qk   :   Maximum foundation bearing capacity (kN/m^2) (TBEC-2018)

q_u :   Maximum foundation bearing capacity (kN/m^2) (JBEC-2018)

r   :   Coefficients of retaining structures

R   :   load reduction factor (TBEC-2018)

R_a :   Load reduction factor (JBEC-2022)

rd   :   Stress reduction coefficient

R_F :   Stress of earthquake that causes the liquefaction (kPa) (JBEC-2022)

R_i :   Equivalent average shear stress (JBEC-2022)

S_1 : Map spectral acceleration coefficient for 1.0 seconds period [dimensionless]

s_c, s_q, s_γ: The foundation shape coefficients (dimensionless)

t : Time (sec)

u_q : Minimum uniaxial compressive strength

V_s : Shear wave velocity (m/s)

W : Total weight of the building (kN)

z : Height of the wall below the water level (JBEC-2022)

β : The inclination angle of the ground surface behind the wall relative to the horizontal (degrees)

γ_b : The buoyant unit weight of soil (kN/m^3)

δ_d : The friction angle between ground and wall (degrees)

θ : The angle from the face of wall to the vertical, depending on the static-equivalent earthquake coefficient (rad).

ρ : Density of the soil

σ'_v : The effective stress at specific point of soil (kN/m^2)

σ'_{vo} : Effective vertical stress

σ_v : The total stress at specific point of soil (kN/m2)

σ_{vo} : Total vertical stress

$\tau_{earthquake}$: Stress of earthquake that causes the liquefaction (kPa)

τ_R : liquefaction resistance (TBEC-2018)

φ : Angle of internal friction of soil (Degree)

Φ'_d : The angle of shearing resistance of the soil (rad)

ψ : The angle of the wall measured relative to the horizontal (from the horizontal in front of the wall to the back of the wall) (rad)

$C\dot{u}$: The damping matrix with velocity

F_1 : Local ground effect coefficient for a period of 1.0 seconds (TBEC-2018)

F_v : Local ground effect coefficient for a period of 1.0 seconds (JBEC-2022)

Ku : The stiffness matrix with displacement

T_B : Horizontal elastic design acceleration spectrum corner period (sec)

T_A : Horizontal elastic design acceleration spectrum corner period (sec)

$m\ddot{u}$: The mass matrix with acceleration

CHAPTER 1

1. INTRODUCTION

Comprehending the Earth's motion and distinguishing the soil strata and their constituents and attributes are fundamental and significant sciences in engineering. They serve as the basic building blocks for constructing engineering structures. Geotechnical earthquake engineering is relatively new compared to many other branches of civil engineering. The field of geotechnical earthquake engineering experienced significant growth following seismic events in various locations around the globe, such as Alaska and Niigata, Japan, in 1964. This study is of great significance due to the importance of the subject matter it explores, which is geotechnical earthquake engineering. This field focuses on understanding the seismic hazards associated with earthquakes and finding ways to mitigate them. It sheds light on the complex dynamics of the earth's plates and the characteristics of seismic waves. It provides insight into calculating ground motion parameters and accurately determining dynamic soil properties. The negative consequences of not adhering to the appropriate rules and regulations in geotechnical engineering are apparent in the significant damages that can occur, not only in physical infrastructure but also in economic, social, and political aspects. Hence, it is crucial to ensure that the correct rules and laws are consistently applied in geotechnical engineering to minimize the impact of seismic hazards and mitigate the associated risks (Kramer, 1996).

Given the critical importance of this subject, the investigation into the geotechnical earthquake engineering standards employed in Turkey and Jordan is undertaken. The objective is to unveil distinctions between the two sets of criteria and ascertain any weaknesses or deficiencies therein. The intention is to harness the strengths inherent

in each standard and address gaps, enhancing engineering solutions' efficacy. This endeavor aspires to positively influence economic, social, and political facets, ultimately mitigating the harmful effects of earthquakes.

Comparing the geotechnical earthquake standards of Turkey and Jordan has become even more crucial following the devastating earthquake that struck Turkey and Syria on February 6th, 2023. This earthquake resulted in significant human and material losses, with over 50000 fatalities and thousands of people injured. Since earthquakes of this magnitude are not new, it is essential to rely on standards to minimize the damage caused, starting with the geotechnical aspects (Naddaf, 2023).

1.1 Research Problem and Research Question

The research problem revolves around the geotechnical earthquake engineering standards applied in Turkey and Jordan. The primary focus is to examine the similarities and differences between these standards. Key research questions that arise include:

- What similarities and differences exist in Turkey and Jordan's geotechnical earthquake engineering standards, and what accounts for these variations?
- How effective are these standards in ensuring seismic safety?
- How can seismic activity affect soil and foundations based on recorded earthquakes in Turkey and Jordan?

Furthermore, the investigation aims to identify the challenges encountered in implementing these standards in both countries. By addressing these research questions, a comprehensive understanding of the standards' effectiveness and areas for improvement can be gained, contributing to enhancing seismic safety measures in Turkey and Jordan. Both Turkey and Jordan are situated in seismically active regions. While Jordan is generally considered less prone to earthquakes than Turkey, it still contains some functional areas and may experience frequent seismic activity.

Understanding and comparing these countries' geotechnical earthquake engineering standards can provide insights into their preparedness and resilience in mitigating seismic risks, which allows for assessing the effectiveness of existing standards and identifies areas for improvement. In addition, Turkey and Jordan have experienced devastating earthquakes in the past, resulting in significant loss of life and damage to infrastructure. By comparing their geotechnical earthquake engineering

standards, lessons can be learned from past experiences, successes, and failures. This knowledge can guide future improvements in standards to enhance seismic safety. Also, the geotechnical conditions, geological formations, and building practices can vary between countries and regions. So, this study comparing the standards in Turkey and Jordan offers an opportunity to explore how these factors influence the design and implementation of geotechnical earthquake engineering measures. Comparing standards between different countries, such as Turkey and Jordan, promotes international collaboration and knowledge exchange. It fosters a deeper understanding of diverse approaches, best practices, and innovations in geotechnical earthquake engineering, benefiting the two countries and the broader global community.

1.2 Objectives and Contributions of the Study

The objectives of the study can be clarified in the following points:

1. To compare and analyze the geotechnical earthquake engineering standards in Turkey and Jordan, examining their similarities and differences. This will involve thoroughly examining each standard's design criteria, requirements, and methodologies.

2. To evaluate the effectiveness of the geotechnical earthquake engineering standards in ensuring seismic safety. This assessment will examine the historical performance of structures designed based on these standards and consider any significant differences in the observed performance between the two countries.

3. To propose recommendations for improvement and highlight best practices from both standards. By identifying strengths and weaknesses in each standard, the study aims to provide valuable insights into potential areas of improvement and suggest measures to enhance seismic safety.

4. Analyze the dynamic behavior of the foundation and soil using PLAXIS software.

Hence, the study is expected to comprehensively comprehend Turkey's and Jordan's geotechnical earthquake engineering standards. This will provide valuable insights into the specific provisions, design approaches, and requirements unique to each country. Furthermore, the study will offer a broader perspective on seismic design practices and strategies through a comparative analysis, highlighting the similarities and differences between the standards. Additionally, by evaluating the effectiveness

of these standards in ensuring seismic safety, the study will assess their performance and identify potential areas that can be refined or improved.

1.3 Methodology

Study the standards of Turkey's and Jordan's geotechnical earthquakes and find the differences.

The methodology employed in this study begins by providing a concise background on the importance of geotechnical earthquake engineering and highlighting the significance of comparing the standards in Turkey and Jordan. This comparison aims to identify any weaknesses or gaps in the existing standards and propose more effective measures for seismic safety. This discussion will be covered in the first chapter, along with an exploration of the research problem, research questions, objectives, and expected contributions of the study. Moving on to the second chapter, a comprehensive literature review will be presented, covering the fundamental principles of geotechnical earthquake engineering. This chapter will also delve into an overview of seismic hazards, soil dynamics, and previous geotechnical earthquake engineering research in Jordan and Turkey. The third chapter will analyze Jordan and Turkey's most significant seismic activities. A comparative examination of these earthquakes and their impact on both countries will be conducted, with a specific focus on the role and effects of soil. The fourth chapter will extensively review the geotechnical engineering standards in Jordan and Turkey. This chapter will include a comparative analysis of these standards, highlighting their similarities and differences to evaluate their effectiveness in ensuring seismic safety. The penultimate chapter presents case studies involving designing and analyzing a circular raft pile foundation using PLAXIS software. The analysis will encompass ground motion data from earthquakes in Turkey and Jordan, selected based on the seismic events in each region. This analysis will adhere to the earthquake standards of Turkey and Jordan, providing insights into the effects of seismic activity on the soil and foundation.

This chapter will culminate the research, presenting the key outcomes and insights obtained throughout the study.

CHAPTER 2

2. LITERATURE REVIEW

This chapter presents a comprehensive literature review on the fundamentals of earthquake engineering, aiming to facilitate an understanding of geotechnical engineering and the standards employed in different countries. The discussion covers the causes of earthquakes, plate boundaries, faults, and seismic waves. Additionally, an overview is provided on seismic hazards and soil dynamics, underscoring the significance of the study. Furthermore, the chapter includes a review of previous research conducted in the field of geotechnical earthquake engineering in both Turkey and Jordan.

2.1 Geotechnical Earthquake Engineering Fundamentals

Since earthquakes cannot be prevented, engineers face the challenge of selecting the most effective approach to minimize their impact. This places a significant responsibility on engineers to implement construction projects by standards that account for seismic risks.

Implementing geotechnical earthquake engineering standards necessitates a comprehensive approach encompassing all aspects of the operation. Therefore, when studying this field, it is imperative to understand various factors, starting with ground motion and the propagation of waves and their effects on the soil. Additionally, the resistance of foundations to seismic shaking should be carefully considered. Furthermore, it is crucial to comprehend the hazards associated with seismic activity, particularly their impact on soil behavior. Attention must also be given to the quality of construction materials, avoiding the use of subpar material

and preventing the overloading of structural elements beyond their capacity or unexpected circumstances. It is essential to arrange structural elements based on their weight, with heavier elements placed beneath lighter ones, while also considering the nature of materials used in these elements, be it steel or reinforced concrete (Elnashai, Sarno and Kwon, 2015).

2.1.1 Causes of Earthquake

In seismology, it is widely recognized that earthquakes are primarily caused by abrupt displacement along tectonic faults, resulting in a substantial release of accumulated stress and the subsequent release of seismic energy. This phenomenon, commonly called "quick slip," is characterized by rapid fault slippage and consequential seismic activity. However, it is essential to acknowledge that earthquakes can be induced by other factors besides the fast sliding along tectonic faults. Instances such as atomic explosions and large-scale landslides, involving the sudden movement of considerable volumes of rock, soil, or debris down slopes or hillsides, can also contribute to seismic events. Furthermore, the behavior of tectonic faults can be influenced by volcanic activity through various mechanisms. For instance, the movement of magma underneath a volcano can induce deformation and alter stress conditions in the surrounding crust, potentially impacting nearby faults. Volcanic processes, including magma intrusion, volcanic eruptions, and associated ground deformation, can potentially initiate or trigger seismic activity, including rapid slip events along faults (Srbulov, 2011).

The figure illustrates the fault geometry before and after displacement, which produces the earthquake.
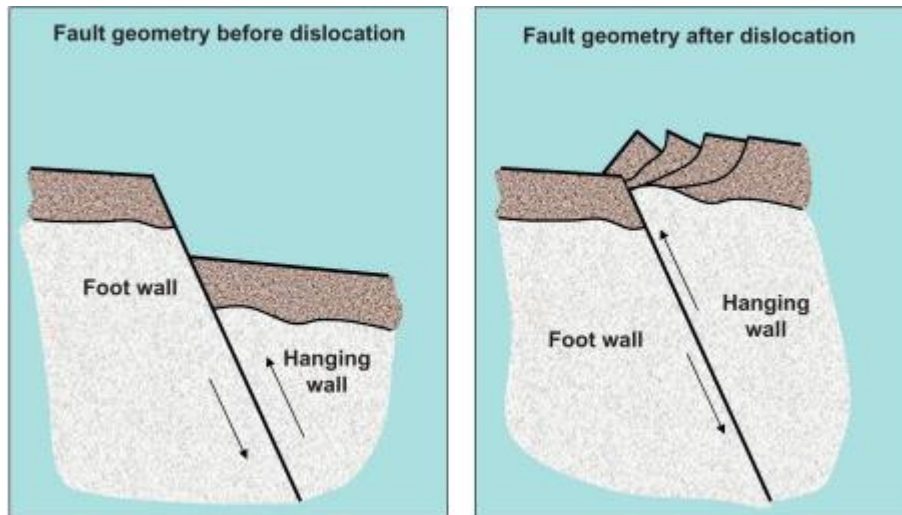
Figure 2.1. Fault displacement (reverse fault displacements) (Glass, 2013)

This figure illustrates the displacement of the fault, which may result in the burial of a layer under one layer while remaining close to the other layer.
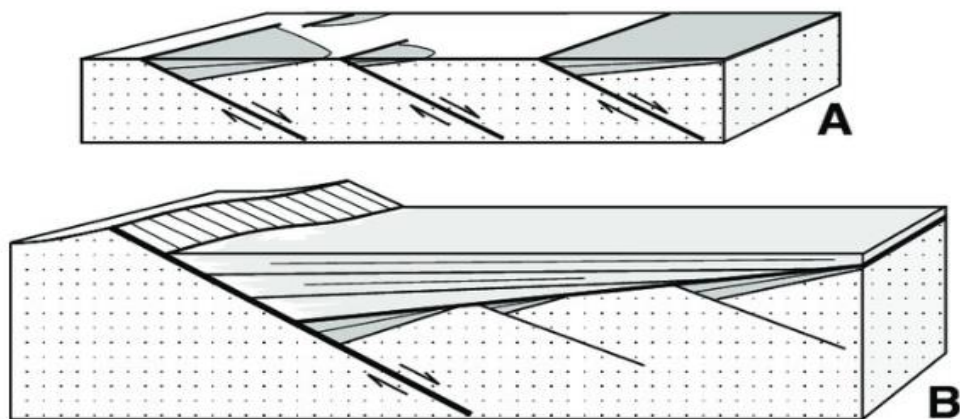
Figure 2.2. Fault displacement (Glass, 2013)

Tectonic plates encompass oceanic and continental crust and the uppermost segment of the mantle. These plates constitute the lithosphere, defined as rigid rock slabs with an average thickness of 100 kilometers. The thickness of the crust varies irregularly, ranging from 25 to 60 kilometers beneath continents, while in oceanic regions, it measures approximately 4 to 6 kilometers. However, young mountain ranges can exhibit crustal thicknesses of up to 60 to 70 kilometers. The internal composition of tectonic plates is known to be intricate, displaying a diverse geological makeup. Furthermore, the plates include the mantle, extending to depths between 30

7

and 2,900 kilometers. Positioned beneath the crust, the mantle constitutes an integral part of Earth's interior, primarily composed of dense silicate rocks (Elnashai, Sarno and Kwon, 2015). The figure illustrates the internal structure of the earth.
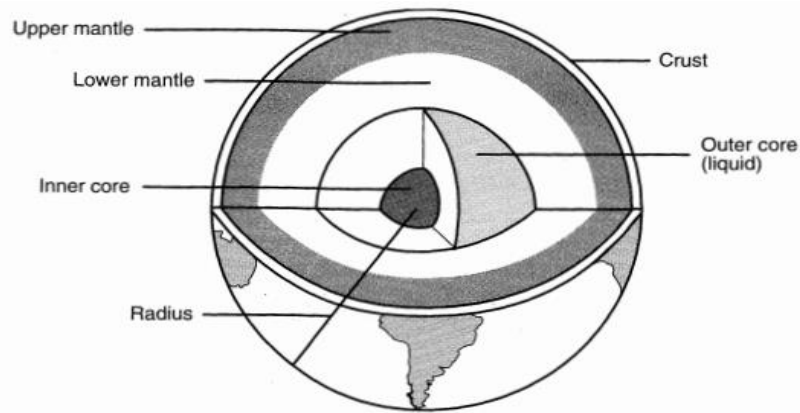
Figure 2.3. Internal structure of the earth (Kramer, 1996).

2.1.2 Plate Boundaries

Plate boundaries represent dynamic zones where significant geological activity occurs. These boundaries are crucial in earthquakes, marking the regions where tectonic plates interact. There are three primary types of plate boundaries:

Divergent Boundaries: Divergent boundaries occur when tectonic plates move apart. This movement leads to the upward migration of magma from the asthenosphere, creating a new crust. This process, known as seafloor spreading, is commonly observed along mid-ocean ridges, where fresh oceanic crust is formed.

Convergent Boundaries: Convergent boundaries form when tectonic plates collide or move towards each other. The type of convergence depends on the nature of the plates involved. In cases where an oceanic plate collides with a continental plate, the denser marine plate typically subducts beneath the continental plate, giving rise to a subduction zone. This subduction process often leads to forming volcanic arcs and mountain ranges. When two continental plates collide, rocks' immense pressure and folding can develop extensive mountain systems.

Transform Boundaries: Transform boundaries occur when tectonic plates slide past each other horizontally. Fault lines, such as the famous San Andreas Fault in California characterize these boundaries. Transform boundaries facilitate the lateral movement between plates, causing earthquakes as the plates slip past each other (Kramer, 1996). The figure illustrates the types of plate boundaries.

8
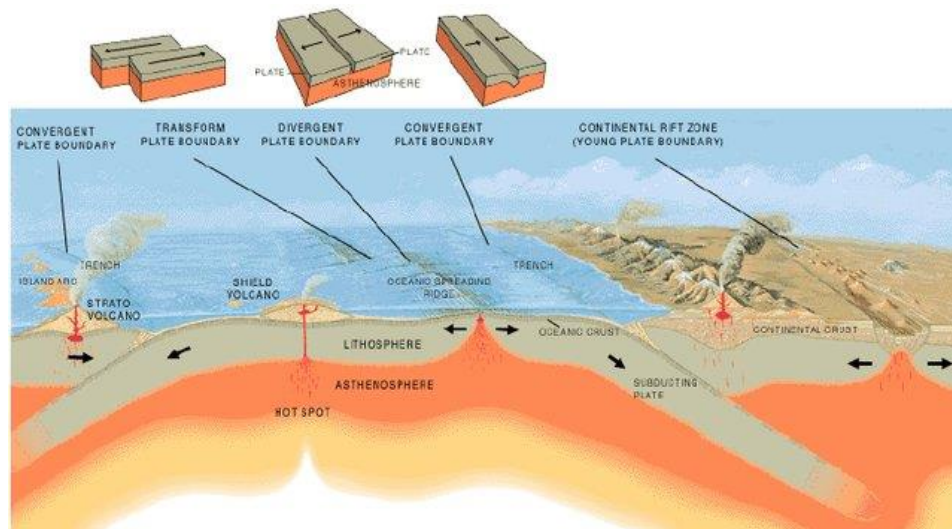
Figure 2.4. The main types of plate boundaries (Sandwell, 2001)

2.1.3   Faults

Faults and plate tectonics are closely related and interconnected. Comprehending plate tectonics entails explaining the motion of substantial, rigid plates that constitute the Earth's lithosphere, encompassing the crust and upper mantle. This description also accounts for the interaction between these plates. These plates are constantly moving and interact along their boundaries, primarily defined by faults. Faults are the surface expressions of the interactions between tectonic plates. They are the zones where the rocks on either side of the fault have moved relative to each other. Faults form due to the stresses and forces exerted on the Earth's crust caused by the movement of tectonic plates. These faults can stretch across significant distances, sometimes covering tens of kilometers, even though their existence may not be readily apparent in surface topography. It is important to note that a fault does not necessarily indicate an imminent earthquake, as many faults can be inactive or have limited seismic activity. In most earthquakes, fault rupture may not reach the earth's surface, meaning the fault occurs at depths below the observable surface.

This highlights the complexity of earthquake occurrence and the challenges associated with predicting seismic events solely based on visible fault lines (Kramer, 1996).

The occurrence of earthquakes is attributed to the weakness of faults and their movement. Rock friction plays a significant role along the edges of faults, generating seismic waves that propagate along the fault. During earthquakes, there are changes in

9

shear stress, strength anisotropy, and regular and environmental stress near the fault. As energy is released from the fault, it increases the pressure of the surrounding area, triggering seismic events such as earthquakes (Dong and Luo, 2022).

- Fault types

Faults are classified based on the type of movement, which can be horizontal, vertical, or inclined. The upper block of rock above the fault surface is called the hanging wall, while the lower block below the fault surface is called the footwall. Compression causes the Earth's crust to lengthen vertically, resulting in a normal dip-slip fault, where the hanging wall slides down relative to the footwall.

Normal faults are primarily associated with tensional forces and commonly occur in regions undergoing extension. In some instances, blocks of rock between two normal faults may drop downward, forming a trough-like structure called a graben. Conversely, blocks of rock uplifted between two normal faults are referred to as horsts (Rafferty, 2011).

Furthermore, faults can also exhibit inclined movement, where blocks of rock are dropped along an inclined fault surface. These faults are known as tilted fault blocks. Reverse dip-slip faults are formed due to compressional forces acting horizontally. In these faults, the hanging wall moves upward relative to the footwall. The figure illustrates the normal, reverse dip-slip faults.
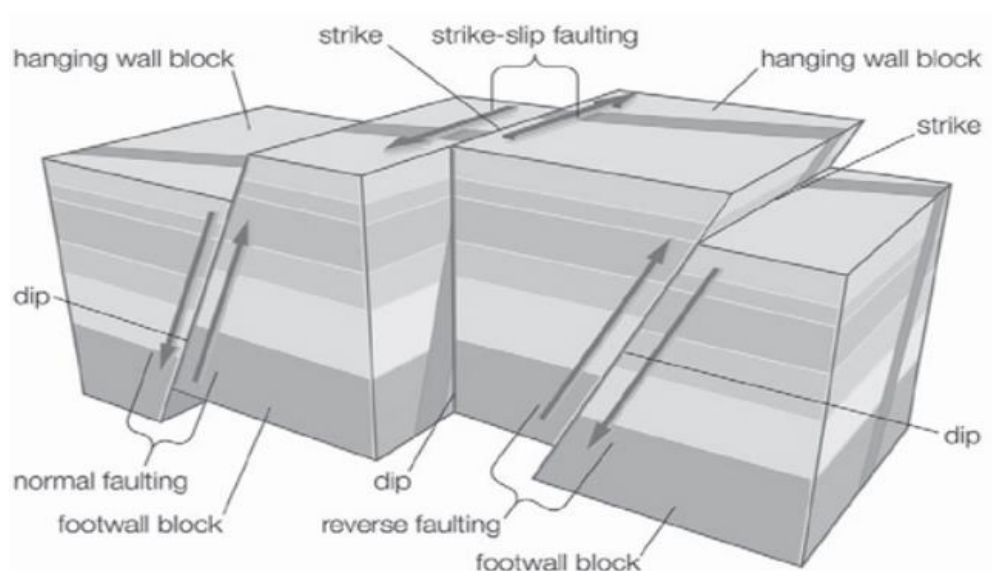
Figure 2.5. The normal, reverse dip-slip faults (Rafferty, 2011).

Strike-slip faults, or transcurrent, wrench, or lateral faults, are formed due to horizontal compression. The release of energy in these faults involves the horizontal displacement of rocks, occurring parallel to the compressional force. The fault plane associated with strike-slip faults is almost vertical, and the relative movement between the blocks laterally along the fault plane. These faults are widely observed and commonly found at the boundaries where oceanic and continental tectonic plates converge at oblique angles.

Oblique fault movement combines vertical and horizontal displacements along a fault plane. Unlike pure vertical (dip-slip) or horizontal (strike-slip) faults, oblique faults exhibit a diagonal or inclined motion. The movement can involve both vertical displacement (upward or downward) and horizontal displacement (left or right) simultaneously or in varying proportions. Oblique faults are commonly associated with complex tectonic settings where multiple forces act on the Earth's crust, resulting in a combination of vertical and horizontal stress components. This type of fault movement is often observed in regions with a significant element in both compression and shear forces acting on the rocks (Rafferty, 2011).

2.1.4   Seismic Waves

The construction design should consider site effects, which pertain to the characteristics of the local site conditions. These include the mechanical properties of near-surface geological formations, ground surface, and subsurface geometry. Side effects can lead to the deformation of seismic waves, such as their amplification, significant spatial variability in seismic ground motion, and shifts in frequency content. Considering these factors when designing constructions is crucial to ensure their resilience to seismic events. The propagation of seismic waves is influenced by topography, including canyons, slopes, and hills. These topographic effects can impact the waves' duration, intensity, and frequency content. Such terrain features can cause variations in wave behavior, changing how the waves propagate and interact with the surrounding environment (Asimaki and Mohammadi, 2018).

Different types of seismic waves are generated during an earthquake, including body and surface waves. Body waves consist of P-waves and S-waves. P-waves, also known as primary waves, are longitudinal waves that compress and rarefy materials as they propagate through them, similar to sound waves. They travel parallel to the

direction of wave propagation and can travel through various mediums, such as solids and fluids. On the other hand, S-waves, or secondary waves, are transverse waves that induce shear deformation as they travel through materials. S-waves propagate perpendicular to the direction of wave travel and can have both vertical and horizontal movements.

P-waves and S-waves propagate through the Earth's interior, contributing to seismic energy release during an earthquake (Sheare, 2001).

The figure illustrates the deformations produced by P and S waves.
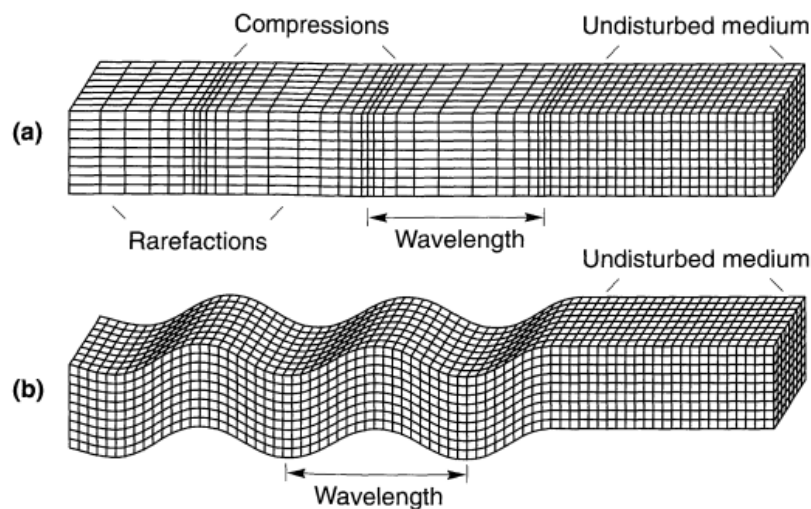
Figure 2.6. Body waves (Kramer, 1996)

As these waves interact with the Earth's surface layers, they give rise to surface waves. Surface waves include Rayleigh waves and Love waves. Rayleigh waves result from the interaction between P-waves and vertical shear waves at the Earth's surface. They cause particles to move in elliptical paths, with decreasing amplitudes at greater depths. Rayleigh waves are more prominent at longer distances from the earthquake source.

On the other hand, love waves are generated through the interaction of horizontal shear (SH) waves with a soft surface layer lacking vertical particle motion. Love waves propagate along the Earth's surface, causing horizontal ground motion in a side-to-side movement.

Surface waves, comprising Rayleigh waves and Love waves, significantly impact ground motion, particularly at greater distances from the earthquake source. Their amplitudes are generally higher than body waves, resulting in more intense

shaking. Consequently, beyond a certain distance, surface waves become the primary contributors to peak ground motions (Shearer, 2001). The figure illustrates the deformations produced by surface waves.
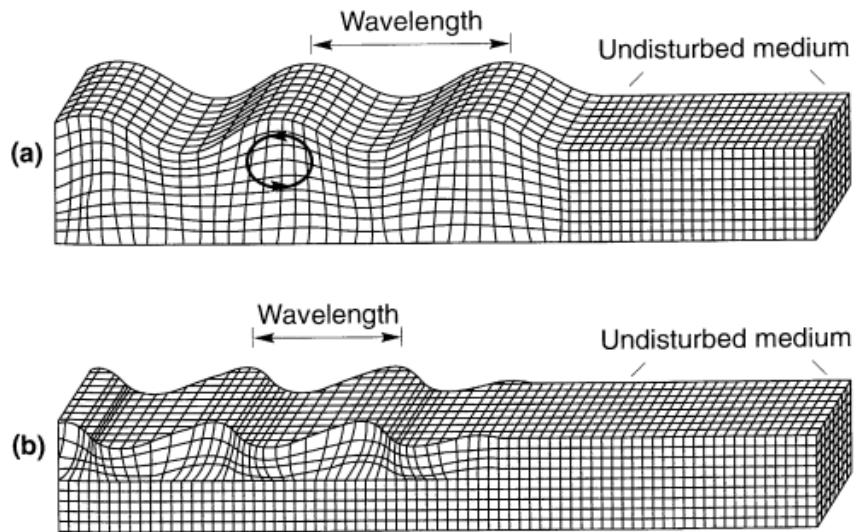
Figure 2.7. Surface waves (Kramer, 1996)

The table compares the different types of seismic waves based on their nature, particle motion, speed, amplitude, and frequency. The speed is indicated relative to each other, with P-waves being the fastest and Love waves being the slowest. The amplitude and frequency are given in a general sense, with higher or lower values compared to other waves.

Table 2.1 A comparison of the types of seismic waves (Shearer, 2001)

Seismic Wave	Nature	Particle Motion	Speed	Amplitude	Frequency
P-waves	Longitudinal	Compressional	Fastest	Lower to moderate	Broad frequency range
S-waves	Transverse	Shear	Slower than P-waves	Lower to moderate	Broad frequency range
Rayleigh waves	Rolling motion	Elliptical	Slower than S-waves	Higher than body waves	Lower frequency range
Love waves	Side-to-side	Horizontal	Slower than S-waves	Higher than body waves	Higher frequency range

2.1.5 Size of Earthquake

The size of an earthquake is a critical factor in comprehending its influence on the Earth's surface and human communities. It involves the assessment of multiple seismic parameters, such as magnitude, intensity, and extent, which offer valuable insights into the characteristics and consequences of the earthquake. By measuring and quantifying an earthquake's size, scientists can categorize and compare seismic events, assess their potential hazards, and devise strategies to minimize their detrimental impacts. Various scales and measurements are employed to describe the size of an earthquake, each capturing different aspects of the seismic activity, including its magnitude and intensity.

Earthquake magnitude quantifies the total energy released during an earthquake. Magnitude scales, such as the Richter or moment magnitude scale (Mw), provide a numerical value reflecting the earthquake's relative strength. A higher magnitude indicates a more powerful quake and implies a more significant release of energy.

$$\log_{10} E = 11.4 + 1.5M \tag{2.1}$$

It's important to note that the Richter scale is logarithmic, meaning that each whole number increase on the scale represents a tenfold increase in the amplitude of the seismic waves and approximately 31.6 times more energy released.

Surface waves are utilized in determining the moment magnitude scale, which can be expressed through the following equation:

$$MW = \frac{\log_{10} M\circ}{1.5 - 10.73} \tag{2.2}$$

The seismic moment measures the total energy released by an earthquake. It represents the product of the average displacement of rocks along a fault, the area of the fault surface that slips, and the rigidity of the rocks involved. It provides a quantitative measure of the strength or magnitude of an earthquake.

Earthquake Intensity:

Earthquake intensity refers to the subjective evaluation of an earthquake's effects and strength at a specific location. It provides information about the degree of ground shaking and the observed impact on structures, the natural environment, and human activities. Unlike earthquake magnitude, which quantifies the energy released by an earthquake, intensity focuses on the actual consequences and how people perceive the shaking. Intensity assessments rely on various intensity scales, with the Modified Mercalli Intensity (MMI) scale being the most widely recognized. The MMI scale classifies earthquake effects into different intensity levels, ranging from I (not felt) to XII (destruction). These levels are determined based on observed damage, personal experiences, and factors such as the distance from the earthquake's source. For example, individuals may describe an earthquake as weak if they do not feel it, while others might characterize it as violent due to building collapses and loss of life. It's important to note that intensity values can vary significantly between locations, even for earthquakes of the same magnitude, due to differences in local geological conditions, building structures, and other factors. Assessing earthquake intensity provides valuable information for understanding the localized impact of an earthquake, evaluating potential damage, and informing emergency response efforts. It is an ancient measure of earthquake magnitude that considers the observed consequences and human perception of the shaking. By collecting intensity data from various locations, scientists can map the spatial distribution of shaking and improve our understanding of earthquake characteristics and behavior (Shearer, 2001).

The following table illustrates the Modified Mercalli Intensity (MMI) Scale of 1931, which employs Roman numerals ranging from (I) to (XII). The scale provides a classification of earthquake intensity, with (I) representing the mildest and (XII) indicating the most extreme and destructive impacts.

Table 2.2 Modified Mercalli Intensity (MMI) Scale of 1931 (Kramer, 1996)

Intensity Level	Description
I	Not felt.
II	Weak - Felt only by a few individuals under favorable conditions.
III	Weak - It felt noticeable indoors, especially on the upper floors.
IV	Light - Felt indoors by many, outdoors by few.
V	Moderate - Felt by nearly everyone, objects may be shaken.
VI	Strong - Felt by all, many people were alarmed, and some heavy furniture moved.
VII	Very strong - Difficult to stand, noticed by drivers.
VIII	Severe - Buildings are damaged, and chimneys may fall.
IX	Violent - General panic, buildings severely damaged or collapse.
X	Extreme - Many buildings are destroyed; bridges may collapse.
XI	Extreme - Few structures are left standing, with ground cracks and landslides.
XII	Extreme - Destruction, waves seen on the ground surface.

2.2 Overview of Seismic Hazards and Soil Dynamics

Seismic hazards refer to the potential risks and dangers associated with earthquakes. They encompass various phenomena and effects that can occur during and after an earthquake, posing threats to human life, infrastructure, and the environment. Understanding seismic hazards is crucial for assessing an area's vulnerability, implementing appropriate safety measures, and developing effective emergency response plans. Critical seismic hazards include ground shaking, structural hazards, surface rupture, ground displacement, liquefaction, landslides, tsunamis, and aftershocks.

2.2.1   Ground Shaking

Seismic waves travel rapidly from the epicenter and propagate through the Earth's crust. These waves can cause prolonged shaking that may persist for minutes. The impact of the shaking can be catastrophic for structures and individuals near the epicenter, depending on factors such as the earthquake's magnitude and the characteristics of the local terrain. Ground shaking is widely recognized as the primary seismic hazard as it is the root cause of all other earthquake-related risks. Consequently, regions with lower ground shaking generally experience fewer or negligible secondary hazards. However, during episodes of intense ground shaking, a broad range of seismic hazards can arise, resulting in extensive damage and significant risks to infrastructure and human safety. Ground shaking levels can vary within a small area due to variations in soil characteristics. As seismic waves travel through the Earth's layers, they eventually reach the soil, which can significantly influence the amplitude and intensity of the shaking. Certain types of soil can amplify the seismic waves, leading to more vital ground shaking, while other types of soil can dampen or attenuate the waves, resulting in reduced shaking. Therefore, the composition and properties of the earth play a crucial role in determining the ground-shaking levels experienced in a particular location (Kramer, 1996).

To analyze probabilistic seismic hazards using Probabilistic Seismic Hazard Analysis (PSHA), the focus should no longer be on searching for the worst-case ground motion intensity. Instead, it is crucial to consider all potential ground motions that could occur. To attain this objective, it is essential to consider several key points:

1. Identification of earthquake sources capable of producing destructive ground motions.
2. Assessment of the possible magnitudes of earthquakes that could occur.
3. Evaluation of the distances between potentially affected sites and the earthquake sources.
4. Prediction of the resulting distribution of ground motion intensity based on factors such as earthquake magnitude, distance, and other relevant parameters.
5. Integration of uncertainties regarding earthquake size, location, and ground motion intensity using the total probability theorem (Baker, 2013).

2.2.2 Liquefaction

Understanding liquefaction and its potential effects is crucial for engineers, urban planners, and policymakers in earthquake-prone regions. By considering the risk of liquefaction in the design and construction of infrastructure, appropriate measures can be taken to enhance the resilience and safety of communities in the face of seismic events. Liquefaction is a phenomenon that occurs in loosely saturated soil, such as sand, when the soil transitions from a solid state to a liquid state due to the increase in pore water pressure caused by ground shaking. This phenomenon results in a loss of soil strength and stability, significantly damaging structures and infrastructure.

Liquefaction can occur near bodies of water such as rivers. This is because the presence of water can significantly influence soil liquefaction potential. The soil may have a higher water content or be more saturated in areas close to rivers or other water bodies, increasing its liquefaction susceptibility. The water-filled pores in the soil act as lubricants, reducing the effective stress and making the soil more prone to losing its strength and behaving like a liquid during seismic shaking (Idriss and Boulanger, 2008). The phenomenon of liquefaction can be categorized into two groups: cyclic mobility and flow liquefaction.

Flow liquefaction is a type of liquefaction phenomenon that can have profound and impactful consequences. It is characterized by flow failures, which are extreme instabilities in the soil. Flow liquefaction occurs when the shear stress required to maintain the static equilibrium of a soil mass, known as static shear stress, surpasses the shear strength of the soil in its liquefied state. When flow liquefaction is triggered, it induces significant deformations driven by the static shear stresses acting on the soil.

The cyclic stresses experienced by the soil can push it into an unstable state where its strength decreases sufficiently to allow the static stresses to initiate flow failures. Flow liquefaction failures are recognized for their sudden initiation, rapid progression, and the considerable distances over which the liquefied materials can travel. In essence, flow liquefaction involves the loss of soil strength in its liquefied state, resulting in the rapid flow and displacement of soil materials. This phenomenon can have severe implications for structures and infrastructure in the affected area.

Cyclic mobility is a significant phenomenon that can result in substantial deformations. It occurs when the shear resistance of the liquefied soil is more significant than its static shear strength. These deformations predominantly occur during earthquakes and are commonly referred to as lateral spreading. Lateral spreading can manifest on gently sloping terrain or flat ground near bodies of water. The following table compares flow liquefaction and cyclic mobility.

Table 2.3 Comparison between flow liquefaction and cyclic mobility (Idriss and Boulanger, 2008)

	Flow Liquefaction	Cyclic Mobility
Definition	Tremendous instabilities, known as flow failures, result in large deformations driven by static shear stresses.	Significant deformations occurring during earthquakes are referred to as lateral spreading.
Shear Stress vs. Shear Strength	The shear stress required for static equilibrium exceeds the shear strength of the liquefied soil.	The shear resistance of the liquefied soil is more significant than its static shear strength.
Triggering Factors	Static shear stress surpasses shear strength in a liquefied state.	The shear resistance of the soil is lower than its static shear strength.
Deformation Type	Rapid flow and displacement of soil materials.	Lateral spreading of soil due to seismic activity.
Occurrence	This is commonly observed in areas with flowable soils.	It can manifest on gently sloping or flat ground near bodies of water.
Initiation Speed	Sudden initiation and rapid development.	Develops during earthquakes.
Displacement Distance	Materials can move over significant distances.	Lateral spreading occurs in the vicinity of the affected area.

Flow failure is one of the most severe consequences of liquefaction. It is a catastrophic ground failure phenomenon that involves the lateral displacement of large masses of soil over significant distances, often tens of meters. This displacement occurs due to the loss of bearing strength in liquefied soil. Another phenomenon associated with liquefaction is the formation of sand boils. During liquefaction, groundwater is subjected to high pressure, causing it to rush to the surface. This upward flow of groundwater results in sand or sediment-filled water jets, known as

sand boils. These sand boils serve as an indicator of the elevated groundwater pressures induced by liquefaction. Both flow failure and sand boils are significant indicators of the damaging effects of liquefaction. They can lead to extensive damage to structures, infrastructure, and the natural environment. Understanding these phenomena is crucial for assessing the risks associated with liquefaction and implementing appropriate mitigation measures. It is important to note that mitigating the hazards of flow failure and sand boils requires proper engineering and geotechnical approaches. Efforts such as ground improvement techniques, suitable foundation design, and adequate drainage systems can help reduce the susceptibility to liquefaction and minimize the associated risks (Kramer, 1996).

The figure illustrates sand boils in the Loma Prieta.

Figure 2.8. Sand boil in Loma Prieta, California, earthquake of October 17, 1989 (Kramer, 1996).

2.2.3 Landslides

Seismic motion can trigger violent landslides, destroying buildings, bridges, and infrastructure. Entire villages and towns can be wiped out or buried beneath the surface. This can be observed in the accompanying figure. Landslides do not only occur because of liquefaction. Still, they can also be caused by slope failures previously considered stable but could not withstand the ground shaking. These slope

failures can lead to significant damage and pose risks to human life and property. It is essential to recognize that landslides induced by seismic activity can have severe consequences. They highlight the need to consider slope stability and implement appropriate engineering measures and land-use planning practices that follow the standards to mitigate the risks associated with ground shaking and potential landslides. By understanding the factors contributing to slope failures and implementing effective strategies, we can work towards minimizing the impacts of landslides triggered by seismic events.

Figure 2.9. Before the landslide for Peruvian earthquake 1970 (Kramer, 1996).

Figure 2.10. After the landslide for Peruvian earthquake 1970 (Kramer, 1996).

Kleefer divided the landslide characteristics into three groups: disrupted and falls, coherent slides, and lateral spreads and flow.

Table 2.4 Landslides type (Rodriguez, Bommer and Chandler, 1999)

Landslides Type	Name
Disrupted Slides and Falls	Rock falls
	Rock slides
	Rock avalanches
	Soil fall
	Disrupted soi
	Soil avalanche
Coherent Slides	Rock slump
	Rock block slides
	Soil slumps
	Soil block slides
	Slow earth flows
Lateral Spreads and Flows	Soil lateral spreads
	Rapid soil flows
	Subaqueous landslides

2.3 Previous Research on Geotechnical Earthquake Engineering in Turkey and Jordan

2.3.1 Previous Research on Geotechnical Earthquake Engineering in Turkey

2.3.1.1 Landslides in Northwestern Anatolia

According to studies conducted between 1959 and 1994, it has been found that Turkey is prone to earthquake-related damage, with landslides accounting for approximately 27% of all natural hazards. To further understand the distribution of landslides in Turkey, a comprehensive study was conducted in 1997. The investigation mapped landslides throughout the country using a topographic base map scale of 1:25,000. As in the table, the landslides were also classified based on their relative depths.

Table 2.5 Landslides classification according to depths (Duman, Çan, Emre, Keçer, Doğan, Ateş and Durmaz, 2005)

Depth	Classification
Less Than 5m	Shallow
larger Than 5m	Deep-Seated

A study conducted in northwestern Anatolia, Turkey, focused on detecting landslides in the region. The findings revealed that various landslides affected approximately 7.1% of the area. The study covered a total area of 93,081 km^2. Additionally, it was observed that a significant proportion of the landslides in the region were deep-seated, with a ratio of 8020 out of 10,007. These results provide valuable insights into the occurrence and characteristics of landslides in this area of Turkey (Duman, Çan, Emre, Keçer, Doğan, Ateş and Durmaz, 2005).

2.3.1.2 Amplification and Liquefaction

A site survey used shallow seismic methods to characterize geotechnical earthquake parameters and investigate phenomena such as soil amplification and liquefaction. The study focused on 161 strong-motion stations located in Turkey. Boreholes were drilled at each station, reaching a depth of 30 meters, to gather data on the soil profiles. An integrated data acquisition system was employed to capture shallow seismic data. This system involved generating controlled impacts, recording ground motion using geophones, and storing the recorded signals with high fidelity using Geode recording units. To estimate the P-wave velocity near the surface, nonlinear travel time tomography and arrival times were extracted from the shot records. The S-wave velocity was determined through Rayleigh-wave inversion. Soil profiles at the stations were determined using standard penetration tests conducted at a depth of 1.5 meters. The figure illustrates the 161 Turkish national grid distribution for strong-motion seismograph stations.
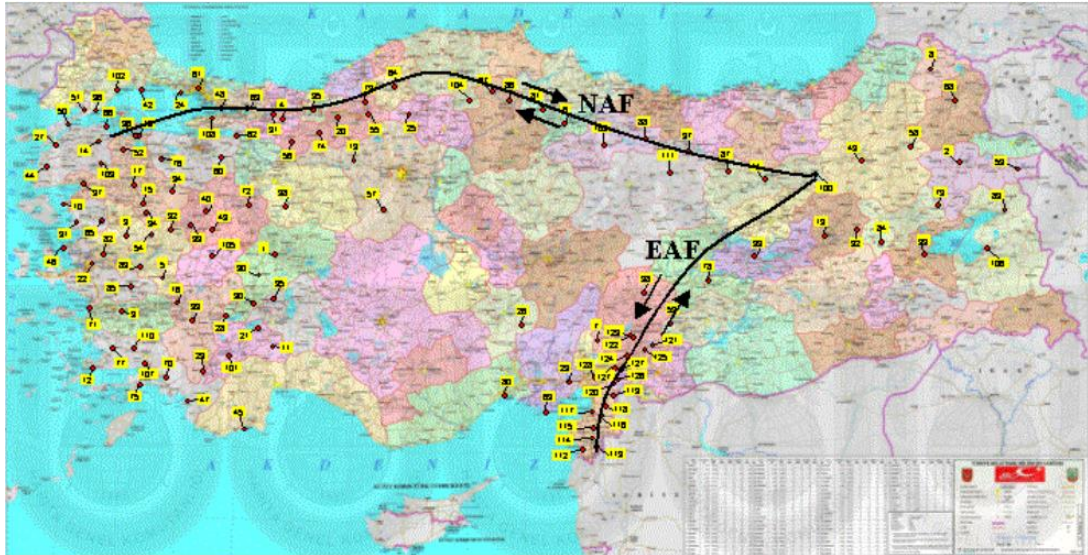
Figure 2.11. Turkish national grid for strong-motion seismograph stations (Bakir, Eser, Akkar and Iravul, 2011).

The figure demonstrates the correlation between seismic velocities and borehole data for a particular station. Notably, the S-wave velocities and SPT N values exhibited remarkable consistency in most stations located in alluvial soils. However, there may be discrepancies between the S-wave velocity and SPT N values due to variations at specific borehole locations. The findings of this study will contribute to future soil investigations, enabling the determination of soil liquefaction potential, amplification characteristics, geotechnical earthquake parameters, and variations in ground motion acceleration. The results will be available through a centralized internet-based database, facilitating access and utilization of the obtained information (Bakir, Eser, Akkar and Iravul, 2011).
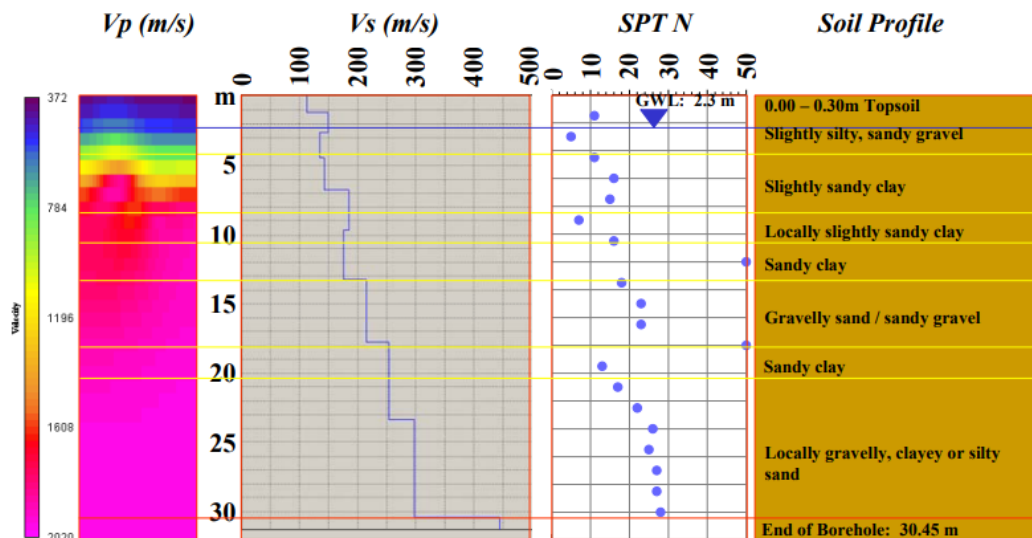
Figure 2.12. Example for the results of seismic and geotechnical investigations at the site of station (Bakir, Eser, Akkar and Iravul, 2011).

2.3.1.3 Rize Landslides

Every year, Rize in northern Turkey experiences landslides because of heavy rainfall. Understanding the soil characteristics in this area is crucial for minimizing human and material losses. Such a study helps comprehend soil stabilization performance, map landslides triggered by rainfall, and determine rainfall intensity and duration thresholds. The main objective of this study was to analyze the properties of residual soils formed from the decomposition of volcanic rocks. This soil is known to contribute significantly to shallow landslides triggered by rainfall. Specifically, the focus was on landslides with a shallow depth of less than 5 meters, which exhibit a rapid flow-type behavior. A total of 12 disturbed and undisturbed soil samples were collected from the landslide-prone area for analysis. The hand vane test determined In-situ undrained shear strength, indicating similar soil characteristics around and inside the landslide mass. The soil was identified as fine-grained, with a liquid limit reaching up to 87% and a relatively low pH of 5.3. Regarding mechanical properties, the soil samples were subjected to regular stress loads of up to 65 kPa. Seventy-two direct shear tests were conducted on undisturbed soil samples under two conditions: saturated, with an average internal friction angle of 36.3°, and unsaturated. Unconfined compression tests were performed with stress levels reaching 52 kPa, while the hand vane tests recorded up to 103 kPa pressures. This study provides valuable insights into their behavior by investigating the characteristics of these residual soils. It helps

establish a basis for soil stabilization measures and developing landslide hazard maps. The findings contribute to understanding the strength and stability of the soils under different stress conditions, thereby aiding in assessing and managing landslide risks in the area. The heavy rainfall in Gündoğdu town occurred in August 2010. The first day recorded rainfall of 166.6 mm, while the second day recorded rainfall of 52.5 mm, which means that in two days, the average rainfall for August was surpassed. The table presents the resulting losses from this rainfall event.

Table 2.6 Gündoğdu town losses due to rainfall (Uyeturk, Huraj, Bayraktarogly and Huseyinpasaogly, 2022)

Parameter	Value
Casualties	13
Destroyed Houses	174
Houses Requiring Restoration	96
Government Expenditure	$6.5 million
Infrastructure Repair Costs	Water pipelines, sewage systems, roads, etc.
Affected Farmers	1276
Affected Farmland Area	30 million m^2
Mainly Affected Crop	Tea plantations

The residual soils found in Rize are formed through the weathering process of alkaline volcanic rocks, pyroclastic rocks, and rhyolitic tuffs with basaltic-andesitic properties. The region's humidity contributes to significant chemical weathering of the exposed volcanic units and shallow subsurface layers. The average specific gravity of 27 samples was 2.59, following the ASTM D854 standard. Grain size distribution analysis was conducted on 31 samples, with 25 classified as fine-grained soils. The clay-size fractions were found to be as high as 39%. The grain size distribution is presented in the figure.
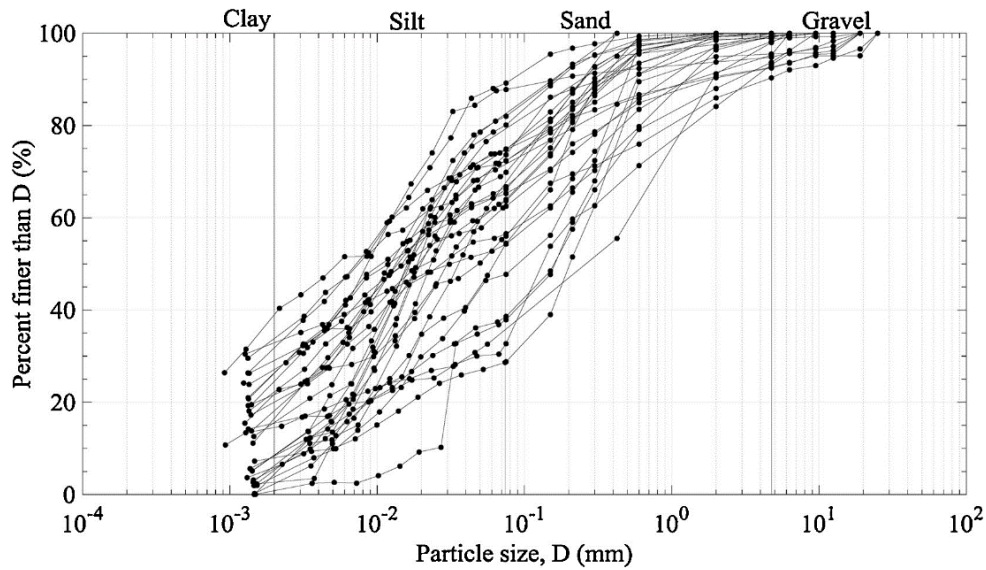
Figure 2.13. Grain size distribution for 31 samples (Uyeturk, Huraj, Bayraktarogly and Huseyinpasaogly, 2022).

The study on residual soils derived from volcanic rocks in Rize revealed several findings related to the landslides in the area. It was observed that the preparation of the samples, explicitly drying, impacted the liquid limit, reducing it by up to 30%. This factor should be considered when determining the Atterberg limits. Halloysite minerals were also detected in the soil samples, constituting approximately 27% of the composition. This classification places the soil in the medium to extra-sensitive category. Furthermore, the soil exhibited low dry unit weight, high porosity, and a high void ratio (Uyeturk, Huraj, Bayraktarogly and Huseyinpasaogly, 2022).

2.3.1.4 Çanakkale Earthquakes

Çanakkale, also known as Dardanelles, is a region spanning Asia and Europe. It is characterized as an active tectonic area and experienced an earthquake magnitude of 6.8 in 2014. The earthquake primarily occurred in thick alluvial deposits. This study aimed to identify areas within Çanakkale susceptible to earthquake hazards based on site conditions. 110 boreholes were drilled at geophysical measurement stations to cover the study area. The study employed multi-channel analysis of surface waves (MASW) and microtremor (MT) measurements. Shear velocity at a depth of 30 meters was also examined, and a map of vibration periods was generated by analyzing the MT time series. The city of Çanakkale is home to over 150,000 residents and is situated on

alluvial ground influenced by tectonic faults. The figure provided illustrates the extent of the study area.
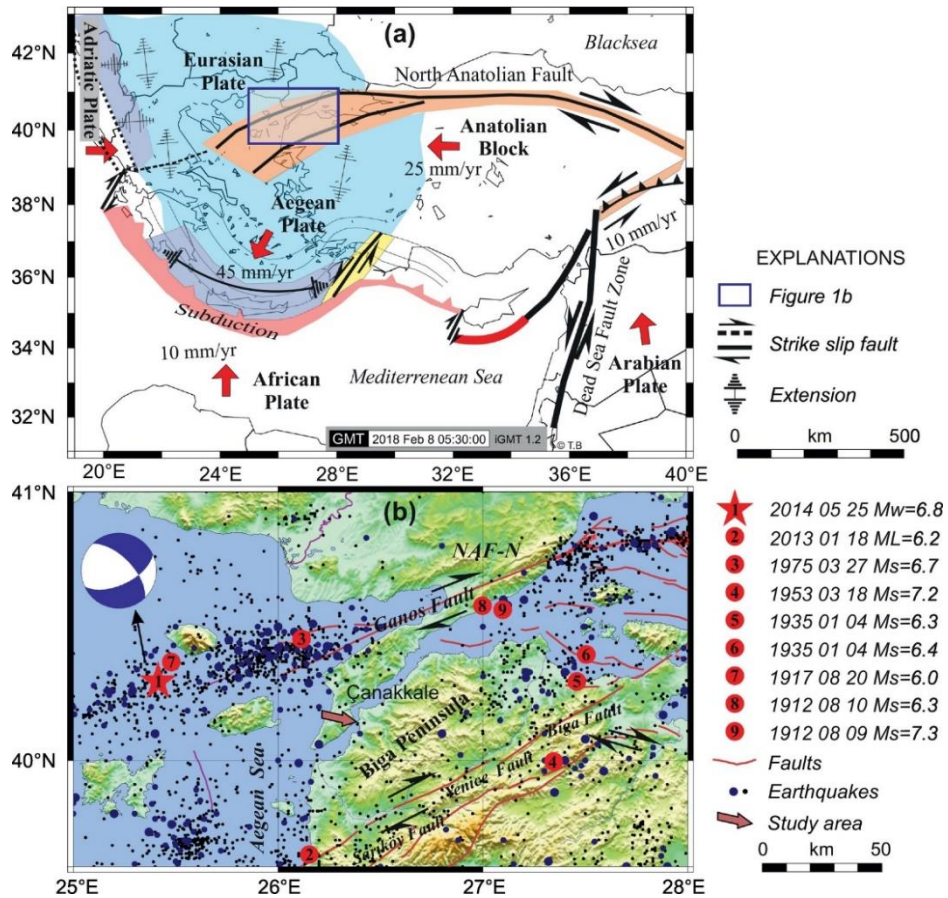
Figure 2.14. Area of study (Çanakkale) (Beklar, Demirci, Ekinci and Buyuksarac, 2019)

The geological context of Çanakkale is characterized by marine sediments dating back to the middle Miocene-Pliocene period. These sediments are classified into two main groups: Gazhanedere and Alçıtepe. The Gazhanedere group comprises Upper Miocene-aged sandstone, conglomerate units, and mudstone. On the other hand, the Alçıtepe group is composed of bioclastic limestones. The sediments on the northern and southern sides of Çanakkale are considered less consolidated. The provided figure illustrates the geological framework of Çanakkale (Beklar, Demirci, Ekinci and Buyuksarac, 2019).
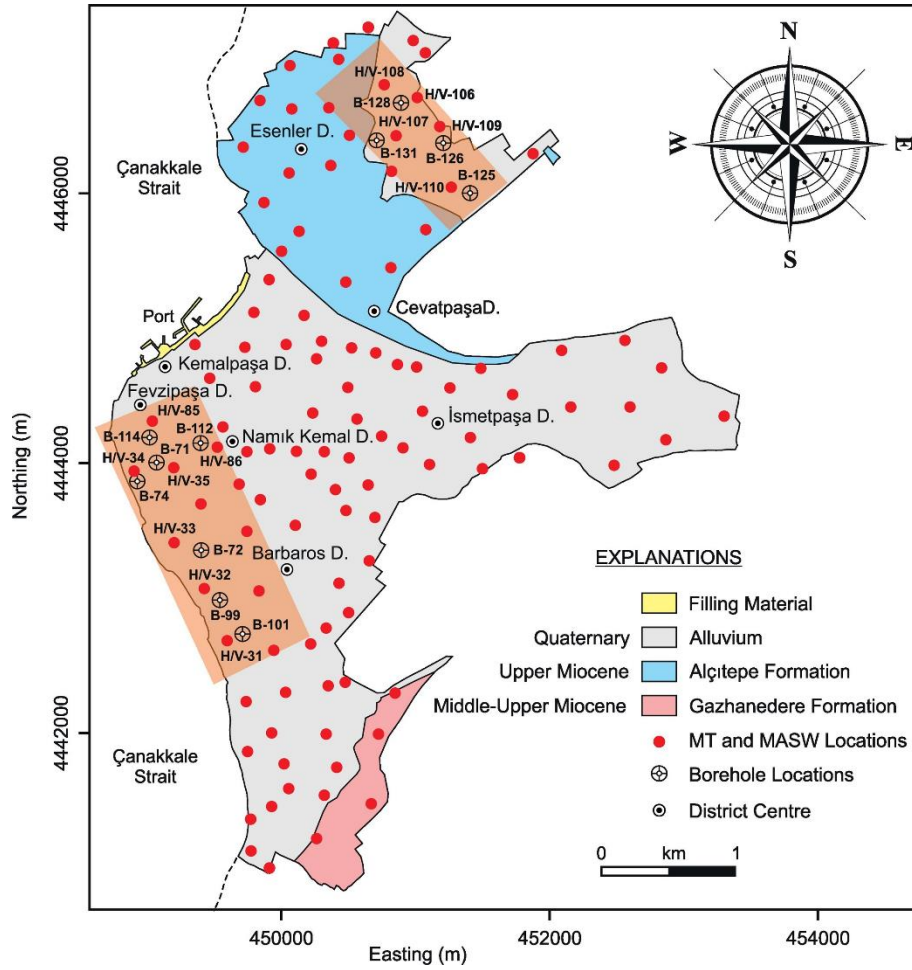
Figure 2.15. Geological framework of Çanakkale (Beklar, Demirci, Ekinci and Buyuksarac, 2019)

The multi-channel analysis of surface waves (MASW) is a geophysical method commonly used for site characterization. It utilizes phase-velocity variations of surface waves at different frequencies to determine shear wave properties and investigate variations in one-dimensional S-wave velocity. In this study, a 12-channel MASW system was employed to record data. Seismic waves were generated by five impacts from a 10 kg sledgehammer, and the resulting signals were recorded. The offset distance of 6 meters was used to acquire an effective dispersion curve, representing the relationship between phase velocity and frequency. The study focused on the variations in one-dimensional S-wave velocity within the area of investigation. The S-wave velocity ranged from 80 m/s to 1000 m/s, and it was observed that lower velocities occurred at depths of around 10 meters. Interestingly, the presence of water did not significantly affect the shear velocity at greater depths. One notable finding was the amplification of low S-wave earthquakes, which could be up to 10 times

greater than high S-wave earthquakes. This highlights the importance of understanding seismic waves' frequency-dependent behavior in evaluating earthquakes' potential impact. By utilizing MASW and analyzing the resulting data, this study provided valuable insights into the variations of shear wave properties and S-wave velocity in the study area. Such information is crucial for accurately characterizing the subsurface conditions, assessing the seismic hazard, and designing appropriate engineering measures to mitigate potential risks (Beklar, Demirci, Ekinci and Buyuksarac, 2019).

2.3.2 Previous Research on Geotechnical Earthquake Engineering in Jordan

2.3.2.1 Amman-Irbid-Jerash Highway Landslides

In Jordan, the Amman-Irbid-Jerash highway has been experiencing numerous landslides. A study was conducted using the Transient Electromagnetic (TEM) geophysical method to understand better the soil and surface characteristics contributing to these landslides. The study area was divided into four units, each with distinct properties. The first unit, with a thickness of up to 25 meters, exhibited high resistivity of up to 100 Ohm.m. It primarily consisted of colluvial deposits. Moving to the second unit, located beneath the surface, clayey and chalky marl were identified. The resistivity of this unit decreased to around 15 Ohm.m, and it had a thickness of up to 4 meters. As we approached the surface, the resistivity was further reduced in the third subsurface unit within the study area. However, the resistivity increased significantly in the fourth unit, surpassing 200 Ohm.m. Borehole logs were used to establish a correlation with this unit, which was interpreted as consisting of extensively fractured and densely compacted limestone. Based on the findings, the second subsurface unit is believed to be the most vulnerable to landslides. These results provide insights into the soil composition and subsurface characteristics, shedding light on the factors contributing to the landslides along the Amman-Irbid-Jerash highway (Al-Amoush, 2016).

The geological formations of the study area, as depicted in the figure, are believed to belong to the Upper Cretaceous age. These formations can be summarized from the oldest to the most recent. The Na'ur formations include limestone with a thickness of up to 200m, followed by formations of bituminous marly limestone and dark greenish-grey dolomitic limestone. The Fuhays limestone, with a thickness of 80m, consists of thin-bedded nodular limestone, marly limestone, and dark shale. The

Hummar Formation, which belongs to the Upper Cenomanian, is characterized by extensive marly, micritic, and dolomitic limestone. It forms a prominent cliff and is relatively resistant to the surrounding layers. The Shu'ayb formation, with a thickness of 60m, extends from the upper Cenomanian to the lower Turonian and is composed of chalky limestone and dolomitic layers. Moving to Wadi El-Sir, which dates back to the Turonian age, the formations have a thickness of up to 120m and include fossiliferous horizons, dolomitic limestone, and carbonate lithofacies (Al-Amoush, 2016).
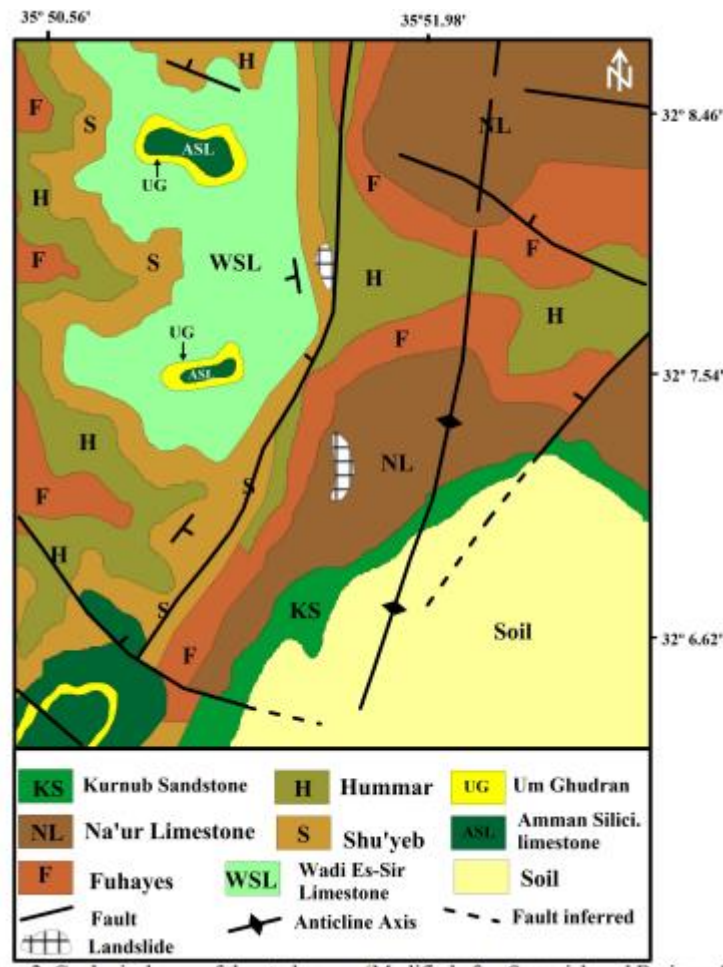
Figure 2.16. Geological map of Amman-Irbid-Jerash (Al-Amoush, 2016)

2.3.2.2 Karamah Dam Slope Stability

The Karamah Dam was constructed in Jordan to store fresh water from the King Abdullah Canal. The dam has a height of 45 meters and stretches 2150 meters. However, it is essential to note the presence of the Lisan Formation, which contains saline groundwater that migrates at a depth of 25 meters. The study highlights the need

for caution due to the active central Jordan Valley Fault near the dam area. The stability of the slopes around the dam was investigated, particularly under wet conditions. The study revealed that the slopes are unstable when subjected to moisture, indicating potential instability and the need for appropriate measures to ensure the dam's and surrounding areas' safety. Given the importance of the Karamah dam in storing freshwater resources, it is essential to address the challenges posed by the migration of saline groundwater and the proximity of the active fault. These findings emphasize the significance of comprehensive geological and geotechnical assessments to mitigate risks and maintain the stability of the dam structure, primarily since Jordan is known for its arid location and lack of rain. The primary objective behind the dam's construction was to create a reservoir with a capacity of 55 million cubic meters. It was designed to receive excess water from the Abdullah King canal during winter. The dam covers an area of approximately 4 square kilometers. A network of pipes measuring 3.6 kilometers was installed to establish a connection between the canal and the dam. These pipes have a pumping capacity of 4 cubic meters per second, facilitating water transfer to the reservoir. To ensure the stability and reliability of the dam's foundations, extensive geophysical and geological data was collected through field mapping, drilling, and laboratory testing. These investigations were crucial in the design process, providing valuable insights into the subsurface conditions and helping to make informed decisions regarding the dam's construction and foundation design (Abderahman and Darwish, 2001). The table shows the results of the tests.

Table 2.7 Karamah dam's tests result (Abderahman and Darwish, 2001)

Parameter	Value
Plasticity	Up to 47
Organic Matter Content	Up to 8.8%
Permeability (Lugeons)	Low (below middle and left shoulder), high up to 70 Lugeons (right shoulder)
Natural Water Content	15% - 55%
Maximum Dry Density	1.52 - 1.64 g/cm^3
Optimum Moisture Content	24.4% - 29.4%
% Passing Sieve No. 200	Approximately 95%
Unit Weight	24 - 26.3 KN/m^3
Cohesion	75.4 KPa - 240.3 KPa
Internal Friction Angle	10° - 22°

The dam is situated in an area characterized by three discontinuities, which increases the risk of wedge failure along both abutments. Additionally, the presence of water further enhances the potential for sliding (Abderahman and Darwish, 2001).

2.3.2.3 Al-Aqaba City Liquefaction

Al-Aqaba city, located in Jordan, is situated in a seismic region along the active plate boundary of the Dead Sea Transform. The area experiences active tectonic subsidence. The investigation reveals that the stratigraphic sequence in Al-Aqaba is composed of liquefaction-susceptible sediments, including alluvial silt, gravel, and aeolian sand in the shallow subsurface. The objective of this study is to assess the liquefaction potential in Al-Aqaba. Seed's cyclic stress ratio method was employed to achieve this, utilizing the standard penetration test with an overburden pressure of 100 KPa and a peak ground acceleration of up to 0.3g. The study area has experienced earthquakes larger than M 6.5 at least three times, resulting in significant damage due to the absence of a suitable earthquake-resistant design. For instance, during the Nuwiba earthquake in 1995, settlements reached 10-20 cm. The area is known for its exposure to strike-slip faults. Regarding liquefaction analysis, the stress reduction factor decreases from 1 to 0.9 at a depth of 35 feet. The study evaluated liquefaction

susceptibility under different peak ground motions: 0.1g, 0.2g, and 0.3g. It was found that when the peak acceleration of ground motion reaches 0.2g, liquefaction hazards may occur in thin coastal areas. At 0.3g, the coastal regions would face severe liquefaction damage. These coastal areas predominantly comprise poorly consolidated, younger deposits, including aeolian sand with thin beds of silty clay, sand gravel, and silt. These deposits originated from the erosion of granitic rocks located north and east of Aqaba. Additionally, the study identified the main reasons for liquefaction in the area: younger (Holocene) sediments and shallow groundwater, which lies between two to three meters below the surface in coastal areas. The saturation of the sediments further decreases the normal effective stress. The study recommends improving liquefaction analysis in the area by considering seasonal fluctuations in groundwater levels. It also highlights the importance of recognizing Aqaba as a highly seismically hazardous region (Mansoor, Niemi and Misra, 2001).

CHAPTER 3

3. EARTHQUAKE HISTORY FOR JORDAN AND TURKEY

This chapter examines significant and well-known earthquakes that have impacted Turkey and Jordan from a geotechnical earthquake perspective. It aims to understand the influence of faults, quantify the magnitude and intensity of the earthquakes, and analyze the response of soils during these events. By studying the outcomes and behavior of the soil, the chapter aims to identify areas for improvement in the respective country's standards and enhance earthquake mitigation measures. The comparison of past earthquakes between Turkey and Jordan is also a focal point of this chapter. This comparative analysis allows us to identify the weaknesses in current standards and regulations in both countries. By evaluating and contrasting the earthquake experiences, valuable insights can be gained to enhance the understanding of seismic hazards and improve the effectiveness of future standards. The chapter discusses these earthquakes, their impact, and the lessons learned. The analysis aims to contribute to advancing geotechnical earthquake engineering practices and developing more resilient structures and infrastructure in Turkey and Jordan.

3.1 Overview of Seismic Activity in Turkey and Jordan

3.1.1 Overview of Seismic Activity in Turkey

The North Anatolian Fault System (NAFS) and East Anatolian Fault System (EAFS) play a crucial role in Turkey's geology, facilitating the movement and interaction of tectonic plates. These fault systems are characterized by their ability to

accommodate horizontal displacement, known as strike-slip faulting. They are prominent fault belts in Turkey. In particular, the NAFS and EAFS enable the Anatolian micro-plate to escape westward between the Eurasian and African Plate. They span significant distances across northern Turkey, showcasing their regional importance. On the other hand, western and central Anatolia experience a different type of faulting. This area is dominated by normal fault systems, reflecting the extensional forces associated with the tectonic activity in the Aegean region (Tan, Tapirdamaz, Yoruk, 2008).

The map depicts the earthquakes in Turkey from 2100 BC to 2004 AD. The red points on the map indicate earthquakes between 2100 BC and 1963 AD, while the white points represent earthquakes between 1964 AD and 2004 AD. The map provides a visual representation of the spatial distribution of earthquakes throughout the specified period.
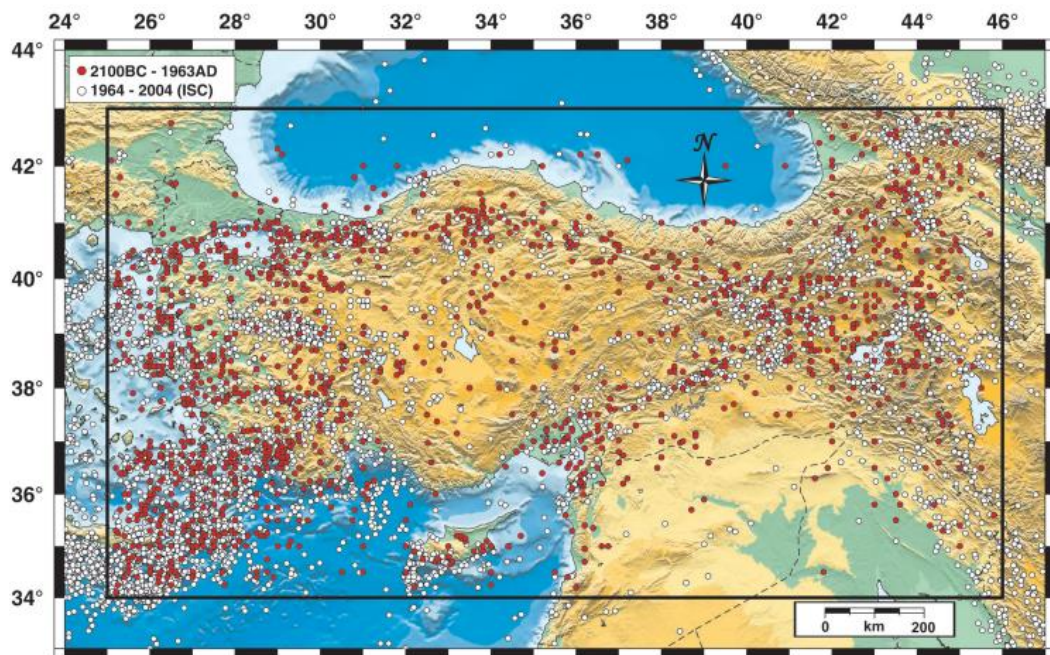
Figure 3.1. Seismicity map of Turkey (Tan, Tapirdamaz, Yoruk, 2008).

In the past four decades, Turkey has experienced less than 30 earthquakes with a magnitude larger than 6.0. When we consider more minor earthquakes with a magnitude of 4.0 or higher, we observe that they tend to cluster in the western and eastern regions of Anatolia. This indicates that seismic activity is more concentrated in these areas than in other parts of Turkey. The distribution of these smaller events

provides insight into the spatial patterns of seismicity within the country (Tan, Tapirdamaz, Yoruk, 2008).

3.1.1.1 Turkey-Syria Earthquake

As a student residing and studying in Turkey, it is essential to commence this chapter by addressing the Turkey-Syria earthquake, given the profound impact and distressing consequences we have encountered and observed, encompassing the substantial toll on physical infrastructure and human well-being.

The earthquake in February 2023 in Turkey and Syria was a catastrophic event caused by multiple factors. Firstly, the magnitude of the earthquakes was significant, with the first seismic event measuring 7.8 and the second measuring 7.5 on the Richter scale. Additionally, the poor quality of buildings played a crucial role in the extent of the disaster, as approximately 40,000 buildings collapsed or became uninhabitable, according to statistics. Another contributing factor to the high losses was the timing of the earthquake, which struck at 4:17 AM when many people were asleep and unprepared. Furthermore, the adverse weather conditions, including winter storms, freezing temperatures, and heavy snowfall, also contributed to the challenges faced during this time. The absence of steel reinforcement in certain multi-story buildings, particularly in the masonry infill walls, significantly compromises their ability to withstand lateral stresses effectively. It is crucial to combine the properties of concrete, which excels in compression, with steel, which excels in tension. Properly mixing concrete with the appropriate proportions of cement, sand, aggregate, and water is essential to achieve the desired strength and durability. In the design code, it is necessary to consider "base isolation" as a method to isolate the building from the foundation, providing flexibility during an earthquake. This technique incorporates sufficient steel reinforcement to enhance the building's resilience and structural integrity (Ahmad, 2023).

The building code in Turkey was recently updated in 2018 to mitigate earthquake damage. It is believed that buildings that collapsed during the recent earthquake may have been either older or not constructed in compliance with the updated building code. However, the situation regarding Syria's building code and conditions is not clear now. The earthquake is recent, and detailed information regarding whether the collapsed buildings were old or did not adhere to the building code is unavailable. In

Antakya, there were instances where newly constructed buildings collapsed, while in Erzin, new buildings built according to the code remained standing. Reports have also suggested that certain old buildings have remained intact (Ahmad, 2023).

Turkey is considered one of the most seismically active regions in the world, primarily due to collision tectonics occurring on the Anatolian plate. The Anatolian plate occupies a significant portion of the northern part of the Arabian plate. As the Arabian plate moves northwards along the southern boundary of Eurasia, it applies pressure on the Anatolian plate. This pressure leads to a westward escape process known as extrusion. The extrusion predominantly takes place along two major fault lines within Turkey: The North Anatolian Fault (NAF), which exhibits a right-lateral strike-slip movement, and the East Anatolian Fault (EAF), located in the southern region of the country. The northwestern Arabian plate also experiences a left-lateral strike-slip motion along the Dead Sea Transform Fault (DSF), which intersects with the EAF in southern Turkey (Chadha, 2023). The figure illustrates the Anatolian plate and the region of the earthquake.
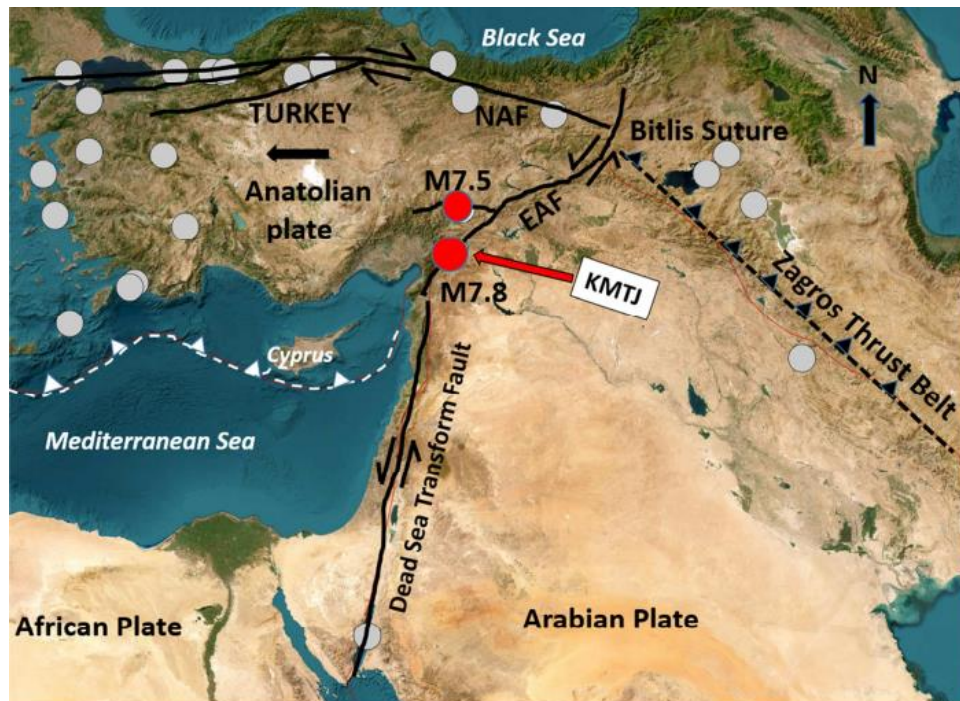
Figure 3.2. Anatolian plate and the region of the earthquake (Chadha, 2023)

The earthquake occurred along the East Anatolian Fault (EAF) near the Kahramanmaraş Triple Junction (KMTJ), which is believed to connect with the Dead Sea Transform fault. The North Anatolian Fault (NAF) extends approximately 1500

km from the Bitlis Suture zone in the east to the Sea of Marmara in the west. It is a major right-lateral strike-slip fault in northern Turkey. As the Arabian plate moves northward, most of the motion is accommodated between the Anatolian and Eurasian plates, resulting in westward movement. The earthquake at the boundaries of the Amanos and Pazarcik segments on the East Anatolian Fault (EAF) was centered at the Kahramanmaras Triple Junction (KMTJ). This earthquake, with a magnitude of Mw 7.8, was highly destructive. The epicenter was located 32 km to the West-Northwest (WNW) of Gaziantep. It occurred at a depth of 18 km. It involved a left-lateral strike-slip motion, rupturing a nearly vertical fault segment of the East Anatolian Fault (EAF) oriented in the Northeast-Southwest direction. The second earthquake, with a magnitude of Mw 7.5, occurred on the Surgu Fault, situated west of Celikhan, and ran in an east-west direction from the East Anatolian Fault. Before this main earthquake, thirty-six aftershocks, ranging in magnitude from Mw 4 to 6.7, occurred within nine hours. This indicates a bidirectional fault rupture spanning approximately 300 km in the NorthEast-SouthWest direction. Over ten days, a total of two hundred and twenty-two aftershocks were recorded, primarily confined to the three segments of the East Anatolian Fault and the Surgu Fault (Chadha, 2023). The figure illustrates the earthquake's location on EAF, SUF, and KMTJ.
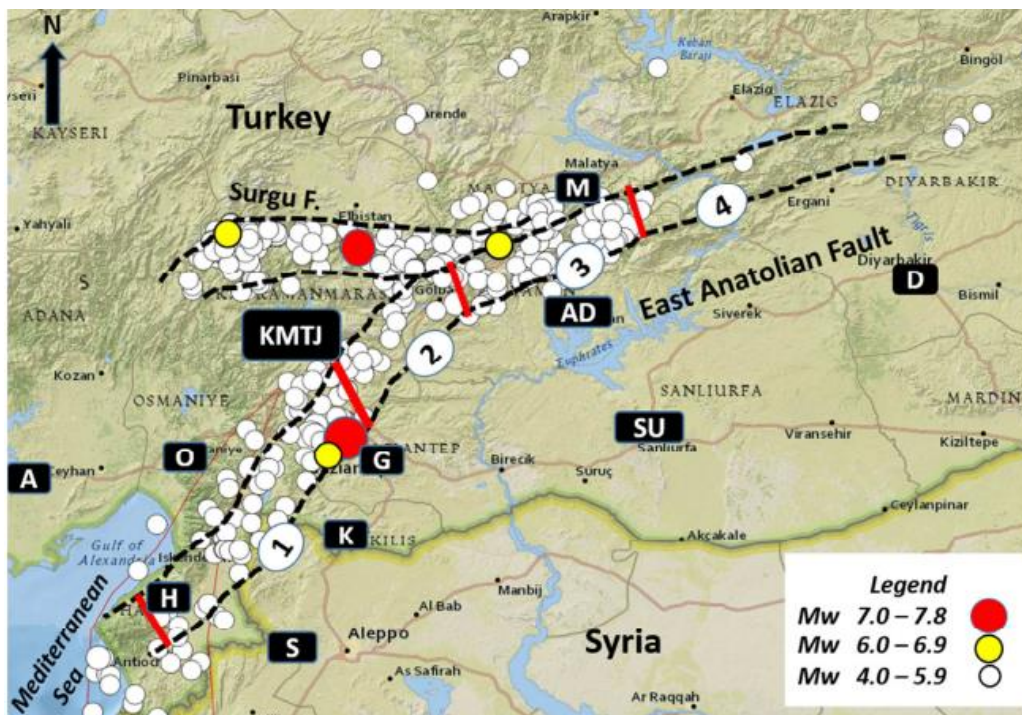
Figure 3.3. Location of earthquake on EAF, SUF, and KMTJ (Chadha, 2023)

40

Earthquakes are rare due to their high magnitude and significant acceleration. The acceleration recorded during the earthquake was exceptionally high, surpassing the lowest reference period. Comparing the earthquake's characteristics with the requirements of the Turkish seismic code, it was observed that the earthquake primarily affected the quiet period range. The maximum acceleration reached a staggering 2.4g, while the design acceleration specified by the code was 1.4g. This is depicted in the accompanying curves (a, b) (Papazafeiropoulos and Plevris, 2023).
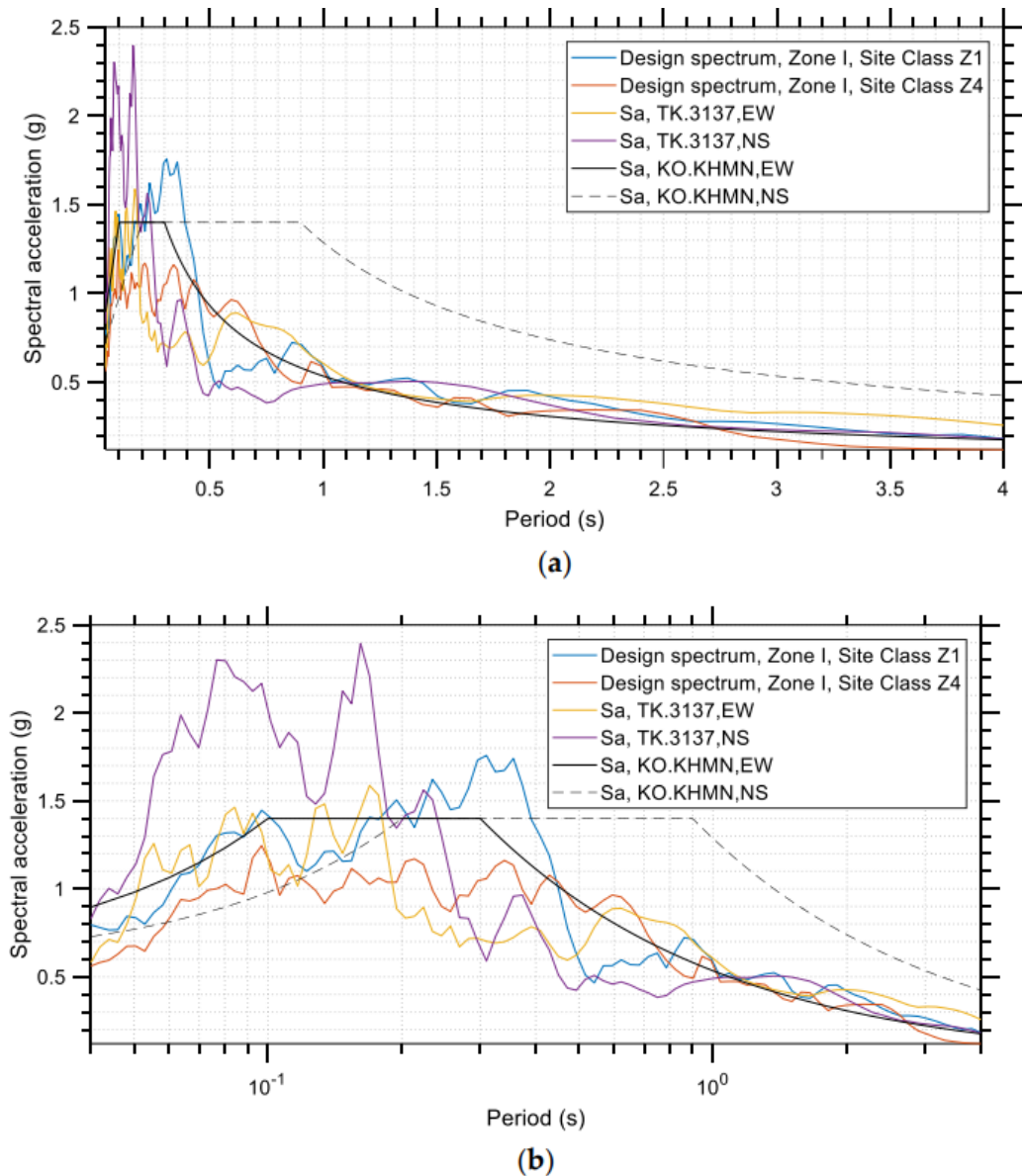
Figure 3.4. Turkish seismic code comparing with the actual acceleration, linear scale (a), Logarithmic scale (b) (Papazafeiropoulos and Plevris, 2023)

3.1.1.2 Van City Earthquake

On October 23, 2011, a powerful earthquake with a moment magnitude (Mw) of 7.2 struck the city of Van, Turkey. The quake was believed to have occurred at a depth of 20 km, triggered by fault movement along a 50 km long and 20 km broad fault segment running east-west from Erçek Lake to Van Lake. The earthquake's impact was particularly severe in the Ercis region, where 52 buildings collapsed, and in the center of Van, where six buildings were destroyed. The central villages in the area also suffered extensive damage, with some villages nearly wiped out and their populations, totaling approximately one million, greatly affected. The earthquake resulted in the tragic loss of 604 lives and left more than 2000 people injured. The event highlighted the urgent need for improved seismic resilience measures, building standards, and disaster response strategies in earthquake-prone regions of Turkey. Following the initial earthquake, seismic activity continued in the area. On November 9, another earthquake with a magnitude of Mw 5.7 struck Edremit. This subsequent event resulted in the loss of 10 lives out of 40 individuals and the collapse of 25 buildings, primarily affecting the city center. The occurrence of multiple earthquakes in a short period further compounded the challenges faced by the affected communities. Van City has significant tectonic activity in the East Anatolian region. It lies east of two major faults within the Anatolian plate, namely the North Anatolian Fault and the East Anatolian Fault. The area experiences a complex network of strike-slip faults, with movements occurring in various directions (Taskin, Sezen, Tugsal and Erken, 2013). The following table provides an overview of the central fault systems and their associated directions of motion in the region.

Table 3.1 Strike-Slip Faults in Van Earthquake area (Taskin, Sezen, Tugsal and Erken, 2013)

Tectonic Features	Direction
Left-Lateral Strike-Slip	Northeast to Southwest
Right-Lateral Strike-Slip	Northwest to southeast
Thrust Faulting	East to west
Oblique Faulting	North to south

The earthquake resulted in various geotechnical issues in the region, particularly in the high plateaus of eastern Anatolia, where Lake Van is located. These issues include soil amplification, liquefaction, rockfalls, lateral spreading, and sand boils caused by liquefaction. The damage resulting from these phenomena extended up to a radius of 30 km from the earthquake's epicenter. Lake Van is situated in an area consisting of Pliocene-Quaternary deposits, lacustrine sediments, ophiolitic melange series, and fluvial deposits of varying sizes and heterogeneity, with a depth of 150 m. The city most affected by the earthquake was Ercis, where the fluvial sediments reach a depth of 240 m. These sedimentary units make up around 80% of the settlements in Van and Ercis, exhibiting differences in age and thickness. The region's diverse geological composition and the specific characteristics of the sedimentary deposits played a significant role in the geotechnical challenges experienced during the earthquake. The damage caused by liquefaction and its associated phenomena was particularly substantial in villages built with adobe houses on alluvial settlements. From a structural perspective, these buildings had reinforced concrete frames, but the non-structural partition walls were made of briquette material. It is important to note that these buildings lacked adequate engineering measures, and many of the villages were constructed without cement or mud mortar, relying solely on briquette materials. The combination of adobe construction, non-structural partition walls, and the absence of proper engineering techniques rendered these buildings vulnerable to liquefaction. The structural integrity of the structures was compromised, leading to significant damage and collapse during the earthquake (Taskin, Sezen, Tugsal and Erken, 2013).

The lessons learned from this earthquake emphasize the importance of adhering to building codes to ensure the safety and cost-effectiveness of construction. It is crucial to follow proper design procedures in both geotechnical and structural aspects, using high-quality materials in construction. Additionally, site conditions should be thoroughly considered to mitigate potential risks. It is advisable to avoid constructing tall buildings in areas with high seismic activity. By implementing these measures, the resilience of structures can be significantly enhanced, reducing the impact of future earthquakes and protecting lives and property. Engineers, architects, and construction professionals must stay updated with the latest building codes, guidelines, and best practices to create safer and more sustainable built environments. Furthermore, raising awareness among the general public about the importance of safe construction

practices can contribute to a more resilient society (Taskin, Sezen, Tugsal and Erken, 2013).

3.1.1.3 Kocaeli City Earthquake

One of the most significant earthquakes in Turkey's history occurred in Kocaeli Mw 7.4 Kocaeli, Northwestern Anatolia 1999. This devastating earthquake caused widespread damage over an area of approximately 300 km^2. More than 77,342 buildings were severely damaged or completely collapsed, while around 77,169 structures sustained moderate damage. The loss of human life was substantial, with 15,845 people confirmed dead and tens of thousands more reported missing. The earthquake's economic impact was also significant, as the affected area accounted for 35% of Turkey's industrial output. The seismic stations in Izmit recorded high amplification in a short period, reaching up to 0.25 seconds. On the other hand, the records in Düzce and Yarimca showed more extended amplification periods, lasting up to 3 seconds. This earthquake highlighted the urgent need for improved seismic preparedness and building standards in Turkey. It catalyzed significant advancements in earthquake engineering and disaster management practices in the country (Elnashai, 2000).

The Kocaeli earthquake, which occurred in August 1999, significantly impacted highway bridges in the region. It was followed by another earthquake in Düzce in November 1999, with a magnitude of 7.2. The Düzce earthquake resulted in the collapse of the Arifiye highway bridge, which was a part of the Trans European Motorway (TEM) connecting Istanbul and Ankara. The bridge was located approximately 50 km away from the epicenter of the Kocaeli earthquake. The Arifiye bridge, built in the 1980s according to ASHTO standards, consisted of four spans and was about 100m long (Pamuk, Kalkan and Ling, 2005.

It suffered damage to its structural and geotechnical elements due to the surface rupture caused by the Düzce earthquake. The Sakarya station (SKR) near the bridge recorded a horizontal ground acceleration of 0.4g and a peak vertical ground acceleration of 0.26g. One of the problems identified was the failure of the shear key, which was not designed adequately to withstand the sizeable transverse movement. Additionally, the bridge's skewed geometry was not considered during its design. From a geotechnical perspective, the Arifiye Overpass utilized a mechanically stabilized

earth wall (MSEW) system but did not undergo any subsoil remediation. The presence of undesirable alluvial soil prone to seismic hazards led to settlement issues, with the ramp experiencing up to 60 cm of settlement. Further geotechnical investigations revealed the existence of very soft soil layers extending up to 22m beneath the southern abutment, followed by a dense layer of sedimentary deposits consisting of silty sand with gravel (N_{30}=100). At a depth of 34m, the layers became thicker, including silty sand and clay, which experienced liquefaction during the earthquake. It should be noted that groundwater was present at a depth of less than 5m from the ground surface. These geotechnical and structural issues highlighted the importance of considering soil conditions, proper design techniques, and subsoil remediation to ensure the stability and resilience of highway bridges in seismic areas (Pamuk, Kalkan and Ling, 2005).

3.1.1.4 Çay-Eber City Earthquake

The Çay-Eber Earthquake occurred in 2002 in the Afyon province in western Turkey. It had a magnitude of 6.0 on the Richter scale. The earthquake resulted in the loss of 42 lives and left 325 people injured. More than 10,000 buildings suffered significant damage, some collapsing due to poor construction quality and resonance phenomena. The affected area is situated on the eastern boundary of Western Anatolia. Historically, this region was not considered seismically dangerous until the 2002 earthquake. Studies indicate that a normal fault caused the seismic activity. Following the main shock, three aftershocks with magnitudes ranging from 5 to 5.3 occurred within 4.5 hours. However, the surface rupture associated with this earthquake was minor compared to the Kocaeli and Düzce earthquakes, spanning a length of 60 meters to 5 kilometers. The geological composition of the area consists of a brownish alluvial fan material with limited groundwater presence. This geological makeup affects the S and P velocities, leading to variations in seismic wave travel times at shallow depths. The soil composition includes clayey silt and layers or bands of silty clay (Ulusay, Aydan, Erken, Tuncay, kumsar and Kaya, 2004).

Standard Penetration Test (SPT) results indicate a significant presence of gravel in the soil. Boreholes drilled in liquefaction-prone areas revealed silty sand layers extending to a depth of 4 meters, followed by layers of silty clay, gravel, and silty gravel down to 15 meters. The SPT results indicate moderate to dense soil at greater depths. The tests near the damaged buildings revealed very thick gravelly sands below

8 meters, with a thin layer of sand covering the surface. Sand volcanoes were observed near the villages of Maltepe and Kadıköy, with heights and diameters reaching up to 50 cm. The lateral spreading of these sand volcanoes, resulting from liquefaction settlements, was measured to be between 5-10 cm. The soil in this area primarily consisted of fine to medium sand with a light brown color. Liquefaction was observed at a depth of 2 meters, indicating a high groundwater level. Some boreholes revealed liquefied sand covered by sandy clay at a depth of 0.8 meters, which was believed to contribute to the liquefaction near Kadıköy (Ulusay, Aydan, Erken, Tuncay, kumsar and Kaya, 2004).

Areas with thick layers and low permeability surface soils, composed of fine-grained alluvial deposits and exhibiting high relative density (N1)60, did not experience liquefaction. The sand layers required a peak ground acceleration of 0.21g to trigger liquefaction. This earthquake highlighted the importance of improving the Turkish Seismic Codes to mitigate amplification effects that may occur in areas prone to resonance phenomena. It also emphasized the need for effective urban regional planning to ensure proper design and construction practices in such areas (Ulusay, Aydan, Erken, Tuncay, kumsar and Kaya, 2004).

3.1.1.5 Sivrice City Earthquake

In 2020, an earthquake occurred in the eastern part of Anatolia due to the movement along the East Anatolian Fault (EAF), with a magnitude of 6.8. The earthquake caused significant damage in the region of Sivrice, where the Arabian plate moved northward, followed by the westward movement of the Anatolian plate. The motion of the fault lines can be observed in the accompanying figure. The initial impact of the earthquake resulted in the loss of approximately 41 lives and left hundreds of people injured.
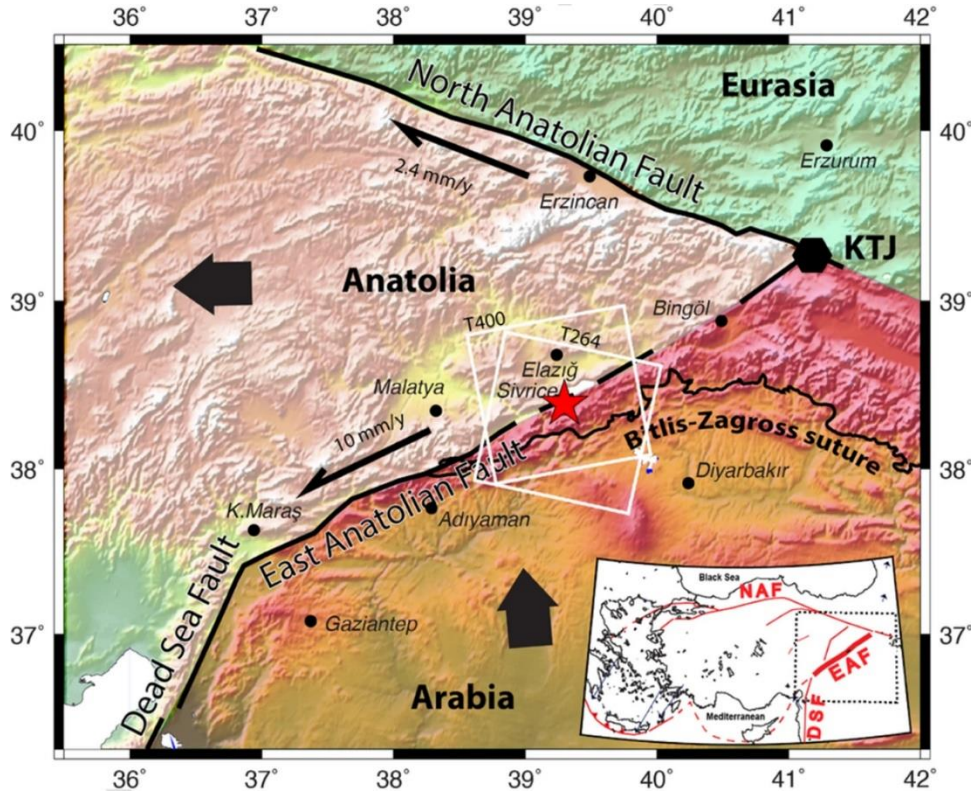
Figure 3.5. The movement of the faults causing the Sivrice earthquake (Sayın, Yön, Onat, Gör, Öncü, Tunç, Bakır, Karaton and Calayır, 2021)

The values of the peak ground acceleration of Sivrice and Elazığ city for East-West and Nort-South direction are illustrated in the table.

Table 3.2 Peak ground acceleration values (Sayın, Yön, Onat, Gör, Öncü, Tunç, Bakır, Karaton and Calayır, 2021)

Station	PGA (E-W Direction)	PGA (N-S Direction)
Sivrice	0.292g	0.238g
Elazığ City Center	0.141g	0.119g

Additionally, a comparison of the spectra provided by the Turkish Building Earthquake codes for 2007 and 2018 revealed that the recent code is safer. The 2007 code classified the soil in the area as (Z3), while the current code considers it soft soil (ZC). It is worth mentioning that the Sivrice-Elazığ earthquake occurred after a 145-year gap since the last devastating earthquake on the same fault segment. The earthquake's aftershocks continued for up to 32 days, with a maximum of 488

aftershocks recorded in one day, measuring Mw 5.1. The lowest number of aftershocks per day was 20, with Mw 2.1. Although classified as a moderate earthquake, the event caused significant damage to numerous buildings. 8,519 buildings were classified as heavily damaged or collapsed, 1,540 buildings were categorized as moderately damaged, and 4,688 buildings suffered low damage. The earthquake mainly affected Seven specific areas, exhibiting soil deformation, which caused cracks in the asphalt pavements up to 2 cm, lateral spreading with an inclination of up to 3 degrees, and soil displacement of up to 6 cm, as depicted in the figure. The occurrence of sandy soil, soil liquefaction, and rockfalls that have a 20 - 110 cm size was also observed (Sayın, Yön, Onat, Gör, Öncü, Tunç, Bakır, Karaton and Calayır, 2021).

Figure 3.6. Lateral spreading displacement (Sayın, Yön, Onat, Gör, Öncü, Tunç, Bakır, Karaton and Calayır, 2021)

Failures observed in reinforced concrete (RC) buildings during earthquakes include insufficient steel reinforcement, the use of short walls, heavy loading of columns from beams, and the use of poor-quality materials. Another common failure is observed in infill walls. These failures have been noticed in previous earthquakes, such as the Kocaeli earthquake in 1999, the Van earthquake in 2011, and the Simav earthquake. Incorrect implementation of reinforcement led to buckling of the bars,

resulting in reduced shear strength and loss of load-carrying capacity in the columns. The bars were deformed at a 90-degree angle, whereas in a proper design, they should be able to withstand deformation and bending up to 135 degrees (Sayın, Yön, Onat, Gör, Öncü, Tunç, Bakır, Karaton and Calayır, 2021).

The investigation of the collapsed buildings revealed that the concrete compressive strength was only 7-10 MPa, significantly lower than the previous building code (TSC-2007) requirement of 20 MPa and the current code (TBEC-2018) requirement of at least 25 MPa. It is crucial to ensure the correct mixing of concrete and the proper placement of concrete cover for reinforcement bars, especially considering the age of the buildings. The conclusion emphasizes the importance of adhering to building standards, using shear walls that meet performance criteria, staying updated with advancements in seismology and engineering practices, and ensuring that deformations and torsion of columns are appropriately accounted for and controlled by engineers (Sayın, Yön, Onat, Gör, Öncü, Tunç, Bakır, Karaton and Calayır, 2021).

3.1.2 Overview of Seismic Activity in Jordan

According to seismic records in Jordan, the country can be divided into two regions: areas with high seismic activity and areas with no significant seismic activity. The region with active seismicity includes the Jordan Rift Valley, the Dead Sea area, and the Gulf of Aqaba. These areas are known for experiencing frequent seismic events, including seismic storms. It is important to note that Jordan is not prone to devastating earthquakes alone. Instead, most of the earthquakes in Jordan are moderate in magnitude, and some of them are aftershocks from more significant earthquakes that occur in neighboring countries. The seismic activity in Jordan is mainly associated with the tectonic features of the region, such as the movement along the Jordan Rift Valley and the Dead Sea Transform Fault. These geological factors contribute to the occurrence of seismic events in the country. However, Jordan's overall seismic hazard is relatively lower than that of other seismically active regions (Jimenez, Al-Nimry, and Khasawneh, 2008).

The region south of the Dead Sea and the south of the Gulf of Aqaba in Jordan are well-known for their relatively high seismic activity. In the event of an earthquake in Jordan, this area is considered the most likely epicenter. Jordan is situated in the

northwestern part of the Arabian plate. The Dead Sea Fault, which extends along the western boundaries of Jordan, is the most significant in the region. The average seismic cycle for this fault is approximately 380 years, indicating that devastating earthquakes are rare. The maximum magnitude recorded on this fault is Mw 6.4 (Jimenez, Al-Nimry and Khasawneh, 2008).

3.1.2.1 Dead Sea Region Seismicity

The Dead Sea Fault is a well-known left-lateral strike-slip fault. It extends from the northern tip of the Red Sea to the southern part of Turkey. The Wadi Araba stretches southward from the Dead Sea fault to the Gulf of Aqaba. The Wadi Araba has experienced four significant seismic events in the past thousand years, with magnitudes below Mw 7.3. The Dead Sea fault is a transform boundary between the Arabian Plate and the Sinai microplate, facilitating horizontal movement between the plates. This movement has significantly shaped the Jordan Rift Valley, which encompasses the Dead Sea, a remarkable low-lying saline lake. The Dead Sea Fault's left-lateral strike-slip motion contributes to the tectonic activity in the region (Klinger, Avouac, Dorbath, Abou Karaki and Tisnerat, 2008).

3.1.2.2 Gulf of Aqaba City Earthquake

One of the most significant earthquakes in Jordan occurred in the Gulf of Aqaba in 1995. It had a moment magnitude of 7.1. Following the main event, a series of aftershocks were recorded until 1997, totaling 2,089 earthquakes with local magnitudes ranging from 2 to 6.2. The earthquake's impact was particularly notable in coastal cities due to shaking intensity, geological characteristics, and local conditions. The effects also extended to neighboring countries such as Egypt, Palestine, and Saudi Arabia, as depicted in the accompanying figure with the seismic swarm (Al-Tarazi, 2000).
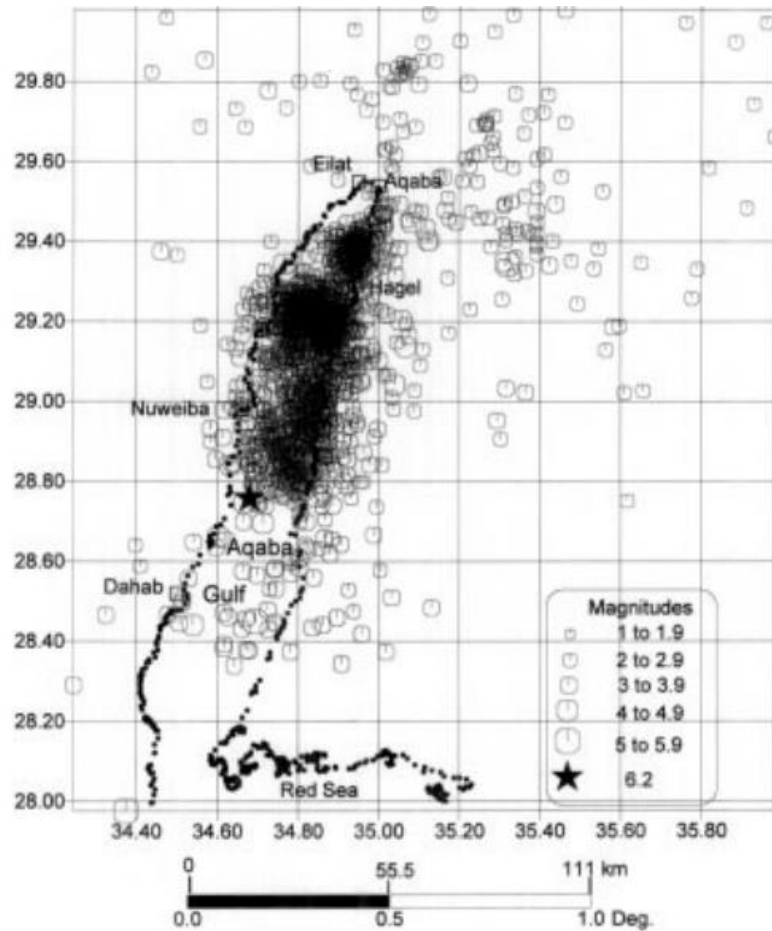
Figure 3.7. The seismic swarm from 1995 (The major one) to 1997 (Al-Tarazi, 2000)

The table illustrates the losses from the earthquake.

Table 3.3 Losses of Gulf of Aqaba earthquake 1995 (Al-Tarazi, 2000)

City	Fatalities	Injuries	Damage Description
Aqaba, Jordan	11	47	Deaths and injuries, damage reported in the city
Nuweiba, Egypt	5	11	Deaths and injuries, damage reported, including Cairo
Haqel, Saudi Arabia	1	2	1 fatality, 2 slight injuries
Eilat, Palestine	1	Several	1 fatality, several injuries

Additionally, the earthquake was felt in neighboring countries such as Syria, Sudan, and Lebanon. In Eilat, significant damage was reported, including power

breakdowns and instances of liquefaction. Furthermore, the coastal areas of Aqaba experienced high waves due to the earthquake (Al-Tarazi, 2000).

Three distinct surface sediment types characterize Aqaba City. The first sediment type comprises alluvial gravel and sand, containing silty claystone, poorly cemented coarse-grained sandstone, and scattered boulders. The second sediment type includes coral formations embedded in calcreted sand. Lastly, the third sediment type comprises Wadi sediments from the Holocene period, consisting of sand, gravel, and rocks composed of granite and granodiorite. It was noted that buildings constructed on sand and gravel foundations were more vulnerable to damage and experienced higher seismic intensity levels. Conversely, structures built on hard or soft rock foundations were less affected and sustained less damage, as shown in the figure. Furthermore, it was observed that buildings located in flat areas and near the shore were particularly exposed to higher intensity levels. The peak ground acceleration in these areas was approximately three times greater than in other regions (Al-Tarazi, 2000).
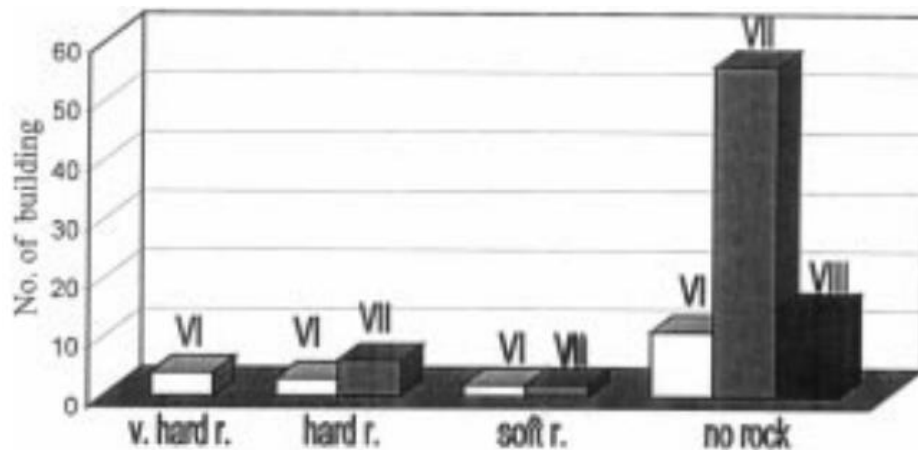
Figure 3.8. The correlation between the geological foundation and the intensity in Aqaba city was examined (Al-Tarazi, 2000).

The construction of buildings in Aqaba city is believed to have been done effectively, which helped mitigate the damage. However, this also highlights the significance of studying the liquefaction phenomenon in the area, as it is an essential consideration for future construction projects and risk assessment.

3.1.2.3 Dead Sea City Earthquake

In 2004, the Dead Sea area in Jordan experienced a moderate earthquake with a magnitude of 5.28. This earthquake occurred along the Dead Sea Fault System

(DSFS), a central geological fault system running through the Middle East. The DSFS is a transform fault where the Arabian Plate and the Sinai microplate slide horizontally past each other. It is known for its significant tectonic activity and has been responsible for numerous regional earthquakes throughout history.

The earthquake had its epicenter near the DSFS, resulting in high waves reaching up to 1 meter in height along the eastern to western shoreline of the Dead Sea. The impact of the earthquake was felt in Jordan, Syria, Palestine, and the occupied Palestinian territories, with about ten people injured in Jordan and similar effects observed in Palestine.

Although classified as a moderate earthquake, it was considered the most significant event in the area in the last half-century, particularly in the southern part and Gulf of Aqaba. Some older buildings made of masonry in the region experienced low levels of damage. However, an old concrete wall in Amman collapsed, indicating a higher peak ground acceleration (PGA) of 108 cm/s². In Hamamat Ma'en, near the Dead Sea, the PGA was even higher at 154 cm/s², and landslides were observed. This event highlighted the importance of raising awareness about earthquakes and knowing how to act during their occurrence. Cases of overcrowding in schools and other public areas were reported due to a lack of knowledge of proper safety measures. The earthquake served as a reminder of the need to educate the public on earthquake preparedness and response (Al-Tarazi, Sandvol and Gomez, 2008).

3.1.2.4 Jericho City Earthquake

The devastating 1927 Jericho earthquake struck the Jordan Valley, registering a magnitude of 6.2 on the Richter scale. Around a hundred stations recorded this seismic event extensively, shedding light on its destructive impact. The earthquake resulted in a tragic loss of life, claiming a total of 285 lives and injuring around 1,000 individuals in both Jordan and Palestine. In Jordan, the capital city of Amman suffered significant damage, resulting in the loss of 11 lives. The town of A-Salt was severely affected, with 32 fatalities and numerous injuries reported. Irbid also experienced the impact of the earthquake, resulting in 15 casualties. The Jordan River witnessed landslides and slumping, while the nearby Dead Sea witnessed a significant wave measuring 1 meter in height. The earthquake's effects were felt in various cities in the Palestinian territories. Jericho, Lydda, Nablus, Jerusalem, and Ramleh were particularly affected

(Avni, Bowman, Shapira and Nur, 2002). The table illustrates the losses on the Palestine side.

Table 3.4 The losses in Palestine side (1927 earthquake) (Avni, Bowman, Shapira and Nur, 2002)

City	Deaths	Injuries
Nablus	60	500
Ramleh & Lydda	50	160

Jerusalem, fortunately, experienced fewer casualties, with only a few deaths and a limited number of injuries. Numerous buildings collapsed due to the powerful seismic forces unleashed by the earthquake (Avni, Bowman, Shapira and Nur, 2002).

3.2 Comparison and Analysis of Historical Earthquakes in Both Countries

In the previous section of this chapter, we searched to identify the most important earthquakes in Turkey and Jordan. Now, we can compare these earthquakes and their implications. This comparison involves examining the geographical locations of the countries about fault lines and considering the consequences of fault movement. Additionally, we can assess the damage caused by these earthquakes, which provides valuable insights for evaluating building standards and earthquake preparedness in both countries. It is also crucial to consider the behavior of the soil in each country when subjected to seismic activity. By analyzing these factors, we can better understand the earthquake risks faced by each country and make informed assessments of their respective building standards and measures for earthquake resilience.

3.2.1   Tectonic Plates of Turkey and Jordan

Several major fault zones at the boundary between the Eurasian and Arabian tectonic plates characterize Turkey. The North Anatolian Fault (NAF) is the most prominent, a right-lateral strike-slip fault extending across the country's northern part. The NAF has been responsible for numerous historical earthquakes, including the devastating 1999 Izmit and Düzce earthquakes. Other important faults in Turkey include the East Anatolian Fault, a right-lateral strike-slip fault that accommodates the eastward motion of the Anatolian Plate relative to the Eurasian Plate. It is one of the

major fault systems in Turkey and has been responsible for significant earthquakes throughout history, including the devastating 2023 kahramanmaraş. Also the West Anatolian Fault and the North Aegean Fault. On the other hand, Jordan is located in the complex tectonic region of the Dead Sea Transform (DST), which is part of the boundary between the Arabian Plate and the Sinai microplate. The Dead Sea Fault System (DSFS) is the central fault system in Jordan, running along the country's western boundary. It is a left-lateral strike-slip fault and is associated with significant tectonic activity. The DSFS has been responsible for several historical earthquakes, including the 1927 Jericho earthquake. When comparing the fault systems of Turkey and Jordan, it is notable that the North Anatolian Fault in Turkey is longer and has a higher activity level than the Dead Sea Fault System in Jordan. The North Anatolian Fault has experienced several large earthquakes in recent history and poses a significant seismic hazard to the densely populated regions of Turkey along its path.

3.2.2   Frequency and Magnitude of Earthquakes

Several notable differences arise when comparing Turkey and Jordan regarding earthquakes' frequency, magnitude, and peak ground acceleration.

Frequency and Magnitude and Peak Ground Acceleration:

Turkey experiences a higher frequency of earthquakes compared to Jordan. Because it is in a seismically active region, its major fault systems, such as the North Anatolian Fault, exhibit regular seismic activity.

On the other hand, Jordan has a lower frequency of earthquakes. While it is located along the Dead Sea Fault System, associated with tectonic activity, significant earthquakes in Jordan are less frequent when the Arabian Plate and the Sinai microplate slide past each other horizontally. This faulting allows gradual strain release over time through frequent, more minor earthquakes, known as seismic creep. This reduces the buildup of stress and the occurrence of large, destructive earthquakes. However, notable earthquakes have occurred in Jordan, such as the 1927 Jericho earthquake and the 1995 Gulf of Aqaba earthquake.

Magnitude-wise, Turkey has witnessed some of the largest earthquakes globally. It has experienced several earthquakes with magnitudes above 7.0, causing significant damage and loss of life. Jordan, while also having experienced notable earthquakes, generally has lower-magnitude events in comparison.

Peak Ground Acceleration:

Turkey is known for its high PGA values due to the occurrence of large-magnitude earthquakes. Areas along the North and East Anatolian Fault have recorded substantial PGA values during past earthquakes. In contrast, Jordan typically has lower PGA values compared to Turkey. However, localized areas near active faults, such as the Dead Sea Fault System, may experience higher PGA values during significant earthquakes.

Table 3.5 Comparison between earthquakes of Turkey and Jordan

Turkey			
Earthquake	Magnitude (Mw)	Buildings Damage	PGA (g)
Kahramanmaraş (2023)	7.8 7.5	40000	2.4
Van (October, 2011)	7.2	15000	0.17
Edremit (November, 2011)	5.7	25	0.09
Kocaeli (August, 1999)	7.4	77342	0.4
Düzce (November, 1999)	7.2	33000	0.3
Çay-Eber (2002)	6	10000	0.113
Sivrice (2020)	6.8	14747	0.292
Jordan			
Earthquake	Magnitude (Mw)	Buildings Damage	PGA (g)
Gulf of Aqaba (1995)	7.1	Eilat = 57, Cairo = 8, Jordan = 1, all most the building cracks	0.113
Dead Sea (2004)	5.28	Some of the old buildings were damaged	0.157
Jericho (1927)	6.2	Jerusalem = 300, Nablus = 700, Jordan = 500, Ramla & Lod = 100	-

3.2.3 Comparison Between the Number of Earthquakes That Occurred on Turkey and Jordan from 2000AD to Date

Comparing the number of earthquakes in Turkey and Jordan from 2000 AD to the present can provide insights into the seismic activity and earthquake risks in both countries. This comparison allows us to assess the frequency of earthquakes in each region and understand the relative level of seismicity. We can identify patterns and trends in seismic activity by examining and comparing the earthquake data, including the number of recorded earthquakes, their magnitudes, and their locations. This information is valuable for assessing the overall earthquake hazard in each country, evaluating the effectiveness of seismic monitoring and reporting systems, and understanding the potential impact on infrastructure and communities. Furthermore, comparing the earthquake activity between Turkey and Jordan can help identify similarities and differences in the tectonic settings, fault systems, and geological conditions contributing to seismic events. It can also aid in developing earthquake preparedness and mitigation strategies tailored to the specific needs of each country. According to the Disaster and Emergency Management Authority (AFAD) under the Prime Ministry, Turkey experiences at least one earthquake annually with a magnitude of 5. This places Turkey as the third most earthquake-prone country in losses caused by earthquakes and eighth in the total number of people affected. These statistics highlight the significant earthquake risk in Turkey and emphasize the need for stringent geotechnical and building requirements. The graph depicts the frequency of earthquakes that have occurred in Turkey since the year 2000 AD.
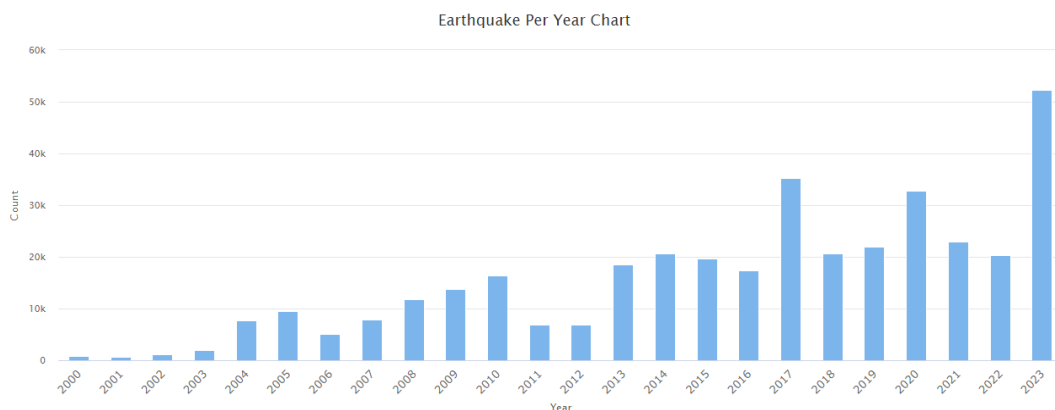
Figure 3.9. Number of earthquakes that occurred in Turkey from 2000 AD (AFAD)

In 2023, Turkey experienced the highest number of earthquakes, including the devastating earthquake in Kahramanmaraş in February, with a magnitude of Mw 7.8. The total number of earthquakes recorded that year reached 52,218. Conversely 2001, the lowest number of earthquakes was observed, with 599 earthquakes recorded. In addition, the figure illustrates the magnitude range of earthquakes where equal to 4.
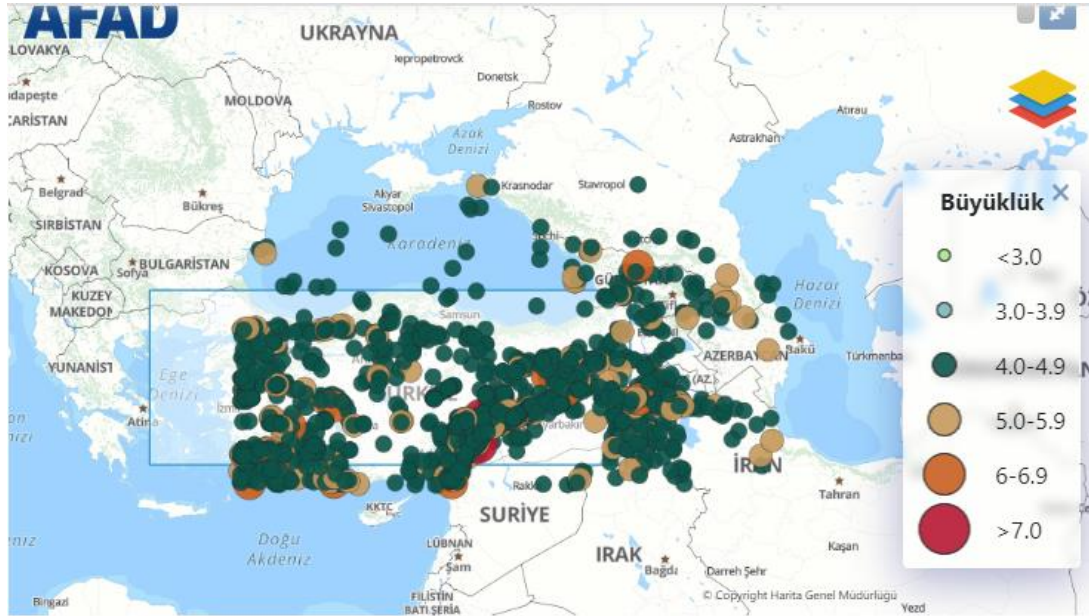
Figure 3.10. Distribution of the Turkey's earthquakes from 2000 AD (AFAD)

It is worth noting that significant earthquakes have occurred in Turkey in recent years. In 1992, Otlukbeli (Erzincan) was struck by an earthquake with a magnitude of Mw 7. In 2021, the Akdeniz (Antalya) region experienced an earthquake with a magnitude of Mw 6; in 2022, another earthquake with a magnitude of Mw 6.4.

Turkey's high seismic activity can be attributed to its geographical location and tectonic setting. Situated at the convergence of several major tectonic plates, the country experiences significant seismic activity. The collision between the Eurasian Plate and the Arabian Plate, which form its boundaries, leads to crustal deformation and compression, accumulating stress and subsequent earthquakes. The North Anatolian Fault (NAF), a prominent fault line across northern Turkey, plays a significant role in the country's seismicity by accommodating the movement between the Anatolian Plate and the Eurasian Plate. Additionally, Turkey is located near the junction of other tectonic features, including the East Anatolian Fault and the West Anatolian Fault, further contributing to its overall seismic activity (Tan, Tapirdamaz and Toruk, 2008).

Three areas exposing for earthquake in Jordan, Wadi Araba, Dead Sea, Gulf of Aqaba.

According to the Jordan Seismological Observatory, Jordan experiences an average of 150 earthquakes annually, with a typical magnitude of 2.5. The minimum recorded number of earthquakes in a year is 60 (MEMR). Detailed data or charts about earthquakes in Jordan are not readily available. It is generally believed that Jordan experiences relatively low seismic activity, with only three specific areas mentioned earlier being prone to earthquakes of low to moderate magnitudes due to faults.

When comparing Turkey and Jordan, significant differences in their exposure to ground motion and seismic activity are evident. Turkey experiences a much higher frequency of earthquakes, with thousands occurring annually, whereas Jordan experiences a relatively lower number, typically in the hundreds. Additionally, the average magnitude of earthquakes in Turkey is at least 4, with several areas experiencing magnitudes of 5 or higher. In contrast, Jordan has an average earthquake magnitude of 2.5, occasionally reaching 3.5, and rarely experiencing earthquakes of magnitude 5 or greater. The impact of earthquakes on casualties and building damage is also notable. Turkey has experienced a higher number of fatalities and significant damage to buildings, primarily due to the higher magnitude and occurrence of devastating earthquakes. On the other hand, Jordan's lower frequency of earthquakes, mainly concentrated at the country's edges due to tectonic plate movements, results in fewer casualties and less damage to structures. However, this does not diminish the importance of reviewing building standards and earthquake mitigation measures in Jordan, as preparedness and safety remain essential considerations.

3.2.4 Soil Behavior That Observant According to Earthquakes of Turkey, and Jordan

In Turkey, several earthquakes have exhibited soil liquefaction phenomenon, showcasing different aspects of its effects:

İzmit Earthquake 1999: Yalova experienced liquefaction-induced settlement, site effects, and damage during this earthquake (Ozcep, Karabulut, Ozel, Ozcep, Imre and Zarif, 2014).

Kocaeli Earthquake 1999: Liquefaction caused damage to marine structures, such as quay walls, storage tanks, and buildings (Sumer, Kaya, Hansen, 2002).

Van Earthquake 2011: Liquefaction, particularly in sand boil locations, was observed during this earthquake (Akin, Ozvan, Akin. M. K, and Topal, 2013). Amplification and lateral spreading were also noted in the Edremit earthquake of 2011.

Sivrice Earthquake 2020: Liquefaction-induced sand boils were observed in this earthquake (Sayın, Yön, Onat, et al, 2020).

In Jordan, Aqaba City, located along the Gulf of Aqaba shore, exhibits susceptibility to liquefaction in some coastal regions. However, the eastern part of Aqaba is considered non-liquefiable (Mansoor, Niemi and Misra, 2004).

The Dead Sea area in Jordan experiences various soil deformations, including subsidence and landslides. Liquefaction occurs in the region during earthquakes with a magnitude of 6.0 or higher, often accompanied by lateral spreading (Abou Karaki, Closson and Salameh, et al, 2008).

Due to seismic activity, liquefaction is common in both countries, but amplification phenomena are more prevalent in Turkish earthquakes. Turkey has observed boiling sand phenomena more frequently than Jordan. On the other hand, Jordan's earthquakes are characterized by subsidence, lateral spreading (even in non-seismic areas due to water pressure), and occasional tsunamis caused by faults in the nearby sea, which are not noticed in Turkey.

CHAPTER 4

4. GEOTECHNICAL EARTHQUAKE ENGINEERING STANDARDS

In this chapter, a comparison will be made between the building standards in Turkey and Jordan concerning geotechnical earthquake engineering. Where will review previous studies conducted on building standards, while several studies have examined the comparison of building standards in Turkey with those of other countries, there is a notable absence of research comparing Turkey's building standards with those of Jordan. Furthermore, there is a lack of comprehensive studies explicitly investigating the building standards in Jordan. Therefore, this study aims to fill this gap by providing the first comparative analysis of building standards between Turkey and Jordan, particularly on geotechnical earthquake engineering.

4.1 Review of the Current Geotechnical Earthquake Engineering Standards in Turkey and Jordan

4.1.1 A Comparative Study Between American Standard ASCE 7-16 and The Turkish Building Earthquake Code (TBEC-2018) and Turkish Earthquake Code (TEC-2007)

A comparative study evaluated the seismic design standards between the American standard ASCE 7-16 and the Turkish Building Earthquake Code (TBEC-2018) and Turkish Earthquake Code (TEC-2007) for reinforced concrete buildings. While the American standard is regularly updated every three to five years, the Turkish standards have undergone revisions in 1975, 1998, 2007, and 2018. The study aimed to compare the calculation of seismic loads between these standards using

61

the ETABS program. Various performance parameters, such as shear force, relative story displacement, and top displacement, were analyzed for reinforced concrete buildings of different heights. The study found that the maximum base shear force was observed in 3-5 story buildings according to TEC-2007, whereas TBEC-2018 yielded higher base shear forces for 7-9 story buildings in most soil classes. Furthermore, crack sections exhibited lower spectral acceleration and more extended vibration periods, resulting in approximately 34% higher displacements and periods in TBEC-2018 compared to TEC-2007 and 45% higher displacements and periods in ASCE 7-16 compared to TEC-2007 (Aksoylo, Mobark, Arslan and Erkan, 2020).

Regarding displacement demands, all standards showed similar results for structures built on soft ground. However, ASCE 7-16 had lower demanding displacement values compared to TBEC-2018, while TEC-2007 had the highest demanding displacement values for high-rise buildings when compared to TBEC-2018. The TBEC-2018 (Turkish Building Earthquake Code) has more detailed soil classification and soil profile requirements than the TEC-2007 (Turkish Earthquake Code). This is similar to the approach followed in ASCE-7-16 (American Society of Civil Engineers), where the site class and soil profile are combined in a single table (A to F) to determine the acceleration coefficients for design. However, there are still some differences in the specific details between the codes. When comparing the building's period, which represents the time needed to complete one entire oscillation cycle during an earthquake, the TBEC-2018 generally results in more extended periods than TEC-2007. This means that the building's response to earthquake shaking is slower under the 2018 standard, with an increase of about 20% -25 % in the periods (Aksoylo, Mobark, Arslan and Erkan, 2020).

One of the significant changes in TBEC-2018 is related to the values of acceleration used in seismic load calculations. These calculations depend on the values of SS (short period) and S1 (1 second period) obtained from the new seismic hazard map. In TEC-2007, these values were fixed at 0.2 and 1, respectively, based on the zones. However, the new standard introduces two coefficients (Fs and F1) representing the soil characteristics, like the approach followed in ASCE 7. TBEC-2018 incorporates a more refined method than TEC-2007, considering site class, design category, occupancy category, building height, and seismic design category. Specific building categories such as army barracks, schools, and museums are more important in TBEC-2018 than in TEC-2007. Additionally, TBEC-2018 introduces new design

parameters, including an overstrength (D) system alongside the seismic structure behavior factor (R). The overstrength system ensures that elements with brittle characteristics remain within elastic limits. The value of (D) ranges from 1.5 to 3.5, depending on the type of structure. These additions further enhance the design provisions and considerations for seismic resistance in TBEC-2018. In the (TEC-2007), the calculation of the spectral acceleration coefficient A(T) involves the effective ground acceleration coefficient (A_0), which varies between 0.4 and 0.1 for each seismic zone, the importance factor (I) that reflects the significance of the structure, and the spectral response acceleration factor (S(T)) which describes the structure's response to ground motion at a specific period T. These parameters are dependent on the characteristics of the ground motion and the structural properties. In contrast, (TBEC-2018) introduces a different approach. The spectral acceleration coefficient A(T) is now determined based on the design spectral response acceleration (SD_S) at a specific period (TD_S), which depends on the spectral response acceleration (S_1) of the ground motion at the same period. This represents the response of the ground motion without any amplification due to site conditions. The site amplification factor (F_1) is also considered, accounting for the effects of local site conditions on the ground motion (Aksoylo, Mobark, Arslan and Erkan, 2020).

To calculate the response spectrum amplification factor for a specific period, the design spectral response acceleration at a reference period (SD_1) is divided by the spectral response acceleration at the same period (SD_1) but for a specific ground motion (SD_S). In summary, while TEC-2007 relies on the effective ground acceleration coefficient, importance factor, and spectral response acceleration factor, TBEC-2018 utilizes design spectral response acceleration, spectral response acceleration of the ground motion, and site amplification factor to determine the spectral acceleration coefficient (Aksoylo, Mobark, Arslan and Erkan, 2020).

The equation that used in (TEC-2007) for determining the spectral curve:

$$A_T = A_\circ \times I \times S_T \tag{4.1}$$

Where that used in (TBEC-2018) is (Aksoylo, Mobark, Arslan and Erkan, 2020):

$$SD_S = S_S \times FSSD_1 = S_1 \times F_1 \tag{4.2}$$

$$T_A = 0.2 \times \frac{SD_1}{SD_S} \tag{4.3}$$

$$T_B = \frac{SD_1}{SD_S} \tag{4.4}$$

Regarding soil type C, there are notable differences between (TBEC-2018), (TEC-2007), and (ASCE 7-16) in terms of seismic design parameters. TBEC-2018 introduces a 50% increase in the spectral acceleration coefficient for seismic zones compared to TEC-2007 and ASCE 7-16. Another significant distinction lies in the allowable relative displacement between floors in buildings. TBEC-2018 sets a slightly smaller limit of 0.016 mm, indicating stricter requirements for deformation control during earthquakes, whereas TEC-2007 and ASCE 7-16 allow for a slightly higher relative displacement of 0.02 mm. Furthermore, TBEC-2018 considers the effective section rigidities, which are taken into account in ASCE-7-16 as well. However, TEC-2007 does not account for this factor. Consequently, when evaluating the base shear force for 3 and 5-story buildings, TEC-2007 tends to yield higher values than ASCE-7-16 and TBEC-2018, particularly for weak soil conditions. Conversely, for 7 and 9-story buildings, only TBEC-2018 achieves the maximum base shear force, specifically in solid soil conditions (Aksoylo, Mobark, Arslan and Erkan, 2020).

There are differences in the rigidity of buildings between TEC-2007, ASCE 7-16, and TBEC-2018, particularly in terms of different soil types. It was observed that TEC-2007 achieved higher rigidity values compared to ASCE 7-16 and TBEC-2018 in Z3 (ZD, D) soil type. However, in Z4 (ZE, E) soil classes, TBEC-2018 exhibited higher rigidity due to lower displacement. Despite these differences, none of the standards provided sufficient rigidity for Z4 (ZE, E) soil classes in 7-story and 9-story buildings. However, in the case of solid soil conditions, TEC-2007 demonstrated adequate rigidity for the structures (Aksoylo, Mobark, Arslan and Erkan, 2020).

4.1.2 Seismic Design Codes of Turkey

This study focuses on the building standards implemented in Turkey and explores the reasons behind building collapses. The researchers argue that the problem lies not solely in the building codes followed but also in the low quality of materials used and the lack of control and inspection systems during construction. Despite seismic design codes and requirements reflecting modern knowledge in seismic science, Turkey has experienced catastrophic consequences following earthquakes. The authors highlight significant earthquakes such as Erzincan (1992), Kocaeli (1999), and Düzce (1999). To fully understand the catastrophic impact of earthquakes, it is crucial to consider the engineering aspects of building codes and their comprehensive

alignment with culture, economic development, and social factors. Until 2000, approximately 46.2% of buildings constructed were one-story, while only 1.5% comprised seven-story structures out of 7,838,675 buildings. Among them, 74.9% were residential buildings. Past earthquakes have revealed several problems, including inadequate reinforcement, low concrete strength, insufficient lateral stiffness, poor ductility, and inadequate column strength. These issues have contributed to the vulnerability of buildings during seismic events. Turkey's seismic hazard map was published in 1972 and updated in 1996. The map divides the country into five distinct zones based on the level of seismic risk. The first zone represents areas with a higher risk of seismic activity, while the fifth zone indicates areas with lower exposure to seismicity (Ilki, Celep, 2012).

For a visual representation of these zones, please refer to the accompanying figure (Figure up to 2012).
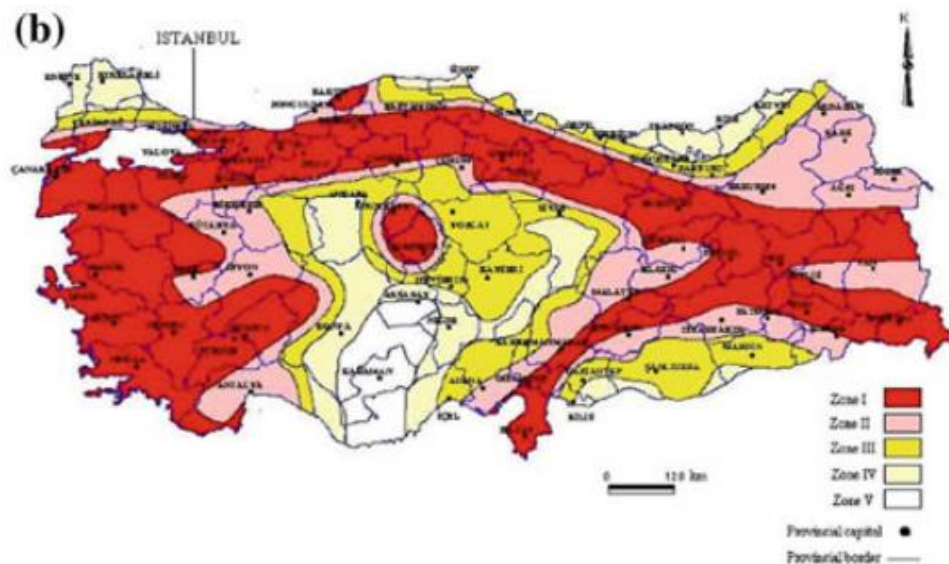
Figure 4.13. Distribution of the seismic hazard of Turkey up to 2012 (Ilki, Celep, 2012).

The study reveals that over 80% of the population resides in the first three zones of the hazard map, indicating a significant concentration of people in areas with higher seismic risk. Following the devastating earthquake in Erzincan in 1939, which claimed the lives of 33,000 people and resulted in the loss of 140,000 buildings, the focus on earthquake-resistant design and improvement of building codes became a top priority in Turkey. As a response, the first seismic regulation was established in 1940, which introduced a fundamental base shear coefficient of 0.1 for calculating lateral seismic

loads. This coefficient was added to half of the wind load, half of the live load, and the dead load, as depicted in the equation (Ilki, Celep, 2012).

$$H = 0.10 \times \left(G + \frac{P}{2}\right) + \frac{W}{2} \tag{4.5}$$

Until the 1944 seismic regulation, the geotechnical conditions of construction sites and the distribution of lateral loads along the height of buildings were not adequately considered. The regulation established a hazard map with two seismic zones. In the 1960s, many buildings were demolished by the 1961 seismic regulation, making way for new multi-story structures. This regulation introduced parameters such as ground conditions, seismic zones, and structural system types to determine the base shear coefficient. It also required all building members to resist lateral seismic loads. However, the regulations did not address how to handle structural torsion. The code did not adequately account for the higher seismic demand on lower buildings, especially those constructed on stiff soil conditions. Due to their relatively higher stiffness, lower buildings may experience higher levels of seismic forces during earthquakes. This oversight could lead to unnecessarily high seismic design loads for rather tall structures while potentially posing safety risks for low-rise buildings. Significant improvements were made in the seismic regulation of 1948. Minimum dimensions for columns, beams, and shear walls were defined, reinforcement requirements for beam-column joints were added, and a building importance factor was introduced. The code also considered the dynamic characteristics of the building (Ilki, Celep, 2012).

In 1972, the hazard map was divided into five seismic hazard areas. A seismic regulation was established in 1975, which continued until 1998. During this period, many buildings were constructed. The concept of "ductility" was introduced for the first time in the code, and several significant additions were made, including requirements for confinement, quantitative shear design for beam-column joints, and an explicit definition of irregular buildings. The code also reduced the allowable stresses of concrete and steel from 50% to 33% and transitioned to ultimate strength design instead of the permissible stress approach in 1984. The seismic hazard map was also reviewed (Ilki, Celep, 2012).

The 1998 seismic regulation was perceived as a safer code for buildings, with more detailed provisions for confinement, reinforcement detailing, capacity design, and performance evaluation of structures under seismic design. It included an elastic

design spectrum and detailed seismic and wind load guidelines. However, the code focused primarily on reinforced concrete structures and neglected steel constructions, resulting in fewer steel buildings being constructed. The 2007 seismic regulation addressed this gap by comprehensively covering reinforced concrete and steel constructions. The code was renamed "Regulation for Buildings in Seismic Areas" instead of "Regulation for Structures in Disaster Areas". It introduced rules for evaluating the seismic safety of buildings and guidelines for addressing deficiencies. However, some approaches used in building evaluation and analysis were considered inappropriate and non-standard in design. The code placed increased emphasis on seismic assessment and retrofitting, devoting an entire chapter to these topics (Ilki, Celep, 2012).

4.1.3 New Improvements in the 2018 Turkish Seismic Code

According to a study conducted by Sucuoğlu on TBEC-2018, significant improvements have been made compared to the 2007 code, particularly in designing high-rise buildings to withstand earthquakes, implementing base isolation systems, and utilizing pile foundations. Establishing an official public body to oversee non-standard practices has also been emphasized. The seismic hazard map of Turkey has been updated by AFAD, with the project initiated in 2000. This update includes revisions to the active fault map, now presented as a contour map based on geographical coordinates. The seismic hazard map expresses the hazard levels regarding spectral acceleration, whereas previous codes relied on Peak Ground Acceleration (PGA) values. TBEC-2018 categorizes earthquake ground motion levels based on return periods and associated probabilities of exceeding certain ground motion levels. Four different levels, DD-1, DD-2, DD-3, and DD-4 are specified to represent varying degrees of earthquake ground motion (Sucuoglu, 2018).

The following table provides an overview of these levels:

Table 4.1 Earthquake ground motion levels (TBEC-2018) (Sucuoglu, 2018)

Designation	Return Period	Probability of Exceedance	Description
DD-1	2475 years	2%	Maximum expected earthquake ground motion
DD-2	475 years	10%	Standard design earthquake ground motion
DD-3	72 years	50%	Frequently expected earthquake ground motion
DD-4	43 years	50%	Service level earthquake ground motion

The new building code in Turkey introduces several essential factors to consider during the design process, such as the importance of the building (BKS), seismic design category, and building height. The BKS is categorized into three levels: BKS 1, BKS 2, and BKS 3. For high-importance buildings like hospitals and schools (BKS 1), an importance factor (I) of 1.5 is applied. Normal buildings (BKS 3) have an importance factor of 1, while residential buildings (BKS 2) have an importance factor of 1.2. The code also addresses building performance levels, which are divided into four categories. The first level is "Continued Operation" (CO), where the structural damage is negligible, and the building can continue its normal operation. The second level is "Limited Damage" (LD), which refers to buildings that have experienced some limited inelastic behavior and minor damage. The third level is "Controlled Damage" (CD), where the structural damage is more significant but can be repaired; buildings that are not of considerable height are classified accordingly, whereas, in this scenario, the design approach employed is Force-Based Design (FBD.

The final level is "Collapse Prevention" (CP), which applies to buildings that have suffered severe damage but can still prevent complete or partial collapse (Sucuoglu, 2018).

4.1.4 Comparative Study Between (TEC-2007) and (TBEC-2018)

Three researchers conducted a study on the (TBEC-2018) and compared it with the previous code (TEC-2007). They designed a school in Gaziantep province of Turkey using SAP2000 software for their analysis. The study highlighted several important changes introduced in the new code. One significant improvement in (TBEC-2018) is the consideration of site conditions and the behavior of the ground during earthquakes. Unlike (TEC-2007), which only examined earthquake zones and assigned a single acceleration coefficient to each area, (TBEC-2018) incorporates different values for long and short-period coefficients, considering the specific characteristics of the ground. Moreover, the classification of ground conditions differs between the two codes. (TEC-2007) divided ground classes into Z1 to Z4, whereas (TBEC-2018) expands this division into five classes labeled ZA to ZF. The building importance coefficient in (TBEC-2018) has also increased from 1.4 to 1.5, emphasizing the significance of designing high-rise buildings with earthquake considerations. Including behavior coefficient and strength coefficient (D) adds a criterion for ensuring structural integrity. During the analysis, the researchers found that joint displacement, shear force, and base reaction values in (TBEC-2018) were higher than those in (TEC-2007). This indicates that additional measures may be required to ensure structural stability, affecting the design considerations for various building components and systems. Overall, the study suggests that (TBEC-2018) provides enhanced safety compared to (TEC-2007) (Atmaca, Atmaca, A. and Kilcik, 2019).

4.2 Comparison of Similarities and Differences Between the Standards in Both Countries

The seismic building standards in Jordan were updated in 2022, while the seismic building standards in Turkey were updated in 2018. Both codes address various aspects of seismic resistance, including soil classes, ground motion conditions, building importance, foundation design, and soil behavior during earthquakes.

4.2.1 Soil Investigation Report

The Turkish and Jordanian codes require a comprehensive geotechnical report that includes information about the soil profile and provides geotechnical design parameters for different soil layers. The report should present various options for foundation types and provide analyses and examinations of these options. Additionally, the report should offer design recommendations for the foundation, considering factors such as expected performance level, bearing capacity, short-term and long-term ground displacement-settlement, swelling behavior, net foundation pressures, and potential buoyancy forces. In cases where soil improvement is necessary, the report should outline the methods and parameters for design, including the bearing capacity and anticipated foundation displacement resulting from soil improvement operations. If structures are built on slopes, slope stability analyses should be conducted, and appropriate measures should be determined to prevent slippage, considering the excavation and construction processes. The building code incorporates parameters related to soil behavior in different loading and permeability conditions. Strength parameters are determined based on drained and undrained conditions, considering the site's loading speed and permeability characteristics. In cohesive soils, the undrained shear strength (C_u) is used in total stress analysis, considering the potential loss or softening of strength due to earthquake effects. For cohesionless soils, the undrained shear strength (τ_{cy}, u) is utilized in total stress analysis, considering the increase in pore water pressure and decrease in the internal friction angle caused by earthquake effects. If pore water pressures can be determined under earthquake conditions, effective stress parameters can also be used for analysis. Additionally, the code addresses the minimum uniaxial compressive strength (u_q) for rocks. It utilizes the geological strength index (GSI) as a parameter for rock mass classification to determine the strength characteristics. These considerations ensure that the strength parameters used in seismic design adequately account for the soil and rock conditions in the field.

The equation used to calculate the maximum shear modulus (G_{max}) is given by:

$$G_{max} = \rho \times V_s^2 \tag{4.6}$$

Where (ρ) represents the density of the soil, and V_S is the shear wave velocity. The shear wave velocity can be determined through various methods such as the

Standard Penetration Test (SPT), Cone Penetration Test (CPT), or geophysical techniques.

4.2.2 Local Ground Classes

Soil classes in TBEC 2018 are divided into six categories: ZA, ZB, ZC, ZD, ZE, and ZF. The ZF class represents soils that require site-specific investigation and evaluation due to their unique characteristics. The table below provides an overview of the characteristics associated with each soil class.

Table 4.2 Local ground classes (TBEC, 2018)

Local Ground Classes	Soil Type	Average in the Top 30 meters		
		$(V_s)_{30}$ [m/s]	$(N_{60})_{30}$ [pulse/30cm]	$(C_u)_{30}$ [kPa]
ZA	Solid, hard rocks	> 1500	-	-
ZB	Slightly weathered, medium-solid rocks	760 – 1500	-	-
ZC	Very dense layers of sand, gravel, and stiff clay or weathered, weak rocks with many cracks	360 – 760	> 50	> 250
ZD	Medium to firm layers of sand, gravel, or very solid clay	180 - 360	15 - 50	70 - 250
ZE	Profiles with layers of loose sand, gravel, or soft to solid clay or a total layer of soft clay (cu < 25 kPa) with a total thickness of more	< 180	< 15	< 70

	than 3 meters,	
	meeting the	
	conditions of PI > 20	
	and w > 40%	

Grounds that require site-specific research and evaluation:

<table>
<tr><td>ZF</td><td>

1. Soils that have the risk of collapse and potential collapse under the influence of earthquakes (liquefiable soils, highly sensitive clays, collapsible weak cemented soils, etc.),

2. Clays with a total thickness of more than 3 meters of peat and high organic content,

3. High plasticity (PI>50) clays with a total thickness of more than 8 meters,

4. Very thick (> 35 m) soft or medium solid clays

</td></tr>
</table>

The (JBEC-2022) also classifies the soil on the site into six classes based on soil type. The following table outlines the characteristics of each soil class as per the Jordanian classification.

Table 4.3 Local ground classes (JBEC, 2022)

Local Ground Classes	Soil Type	Average in the Top 30 meters		
		$(V_s)_{30}$ [m/s]	$(N_{60})_{30}$ [pulse /30cm]	$(C_u)_{30}$ [kPa]
SA	Hard rocks	> 1500	-	-
SB	Rock	$760 < V_s \leq 1500$	-	-
SC	Dense soil and soft rock	$360 < V_s \leq 760$	> 50	> 100
SD	Stiff soil section	$180 < V_s \leq 360$	$15 < N_{60} \leq 50$	$50 < C_u \leq 100$
SE	Soft soil section (cu < 25 kPa) with a total	< 180	< 15	< 50

	thickness of more than 3 meters, meeting the conditions of PI > 20 and moisture content > 40%
SF	Grounds that require site-specific research and evaluation: 1. Soils that have the risk of collapse and potential collapse under the influence of earthquakes (liquefiable soils, highly sensitive clays, collapsible weak cemented soils, etc.), 2. Clays with a total thickness of more than 3 meters of peat and/or high organic content, 3. High plasticity (PI>75) clays with a total thickness of more than 7.6 meters, 4. Very thick (> 65 m) soft or medium solid clays and (Cu) < 50 kPa.

The Turkish Building Earthquake Code (TBEC-2018) and the Jordan Building Code (JBC) differ in the symbols used to classify soil types. The TBEC-2018 utilizes symbols from ZA to ZF, while the JBC uses symbols from SA to SF. However, both codes classify soils based on similar characteristics.

One notable difference between the TBEC-2018 and JBC is the value of undrained shear strength $(C_u)_{30}$ for certain soil classes. Specifically, there are variations in undrained shear strength values for ZC - SC, ZD - SD, and ZE - SE soil classes.

The table below compares the undrained shear strength values for these soil classes in the TBEC-2018 and JBC.

Table 4.4 Comparison between local ground classes of (TBEC-2018 & JBEC-2022)

Soil Class	TBEC-2018 $(C_u)_{30}$ [kPa]	JBC $(C_u)_{30}$ [kPa]	Soil Type (TBEC-2018)	Soil Type (JBC)
ZC - SC	> 250	> 100	Very dense layers of sand, gravel, and stiff clay or weathered, weak rocks with many cracks	High-density soil and soft rock
ZD - SD	70 – 250	50 – 100	Medium to firm layers of sand, gravel, or very solid clay	Hard soil stratum
ZE - SE	< 70	< 50	Profiles with layers of loose sand, gravel, or soft to solid clay or a total layer of soft clay (cu < 25 kPa) with a total thickness of more than 3 meters, meeting the conditions of PI > 20 and w > 40%	Soft soil section (cu < 25 kPa) with a total thickness of more than 3 meters, meeting the conditions of PI > 20 and moisture content > 40%

TBEC-2018 and JBC generally classify soils in similar layers, although the TBEC-2018 provides more detailed information about soil characteristics than the JBC. However, there are differences in the values of undrained shear strength, as depicted in the table provided. The variation in undrained shear strength (C_u) values between the Turkish Building Earthquake Code and the Jordan Building Earthquake Code can be attributed to differences in geological and geotechnical conditions and the

geographic location of the two countries. The characteristics of soil can vary significantly across different regions and countries due to factors such as soil type, composition, and formation history. These variations in local geology and soil conditions between Turkey and Jordan result in differences in the assigned values of undrained shear strength in their respective building codes.

In both the Jordanian and Turkish building codes, if a soil layer with a depth greater than 3 meters exists between the surface of the rock and the bottom of the continuous base or mat foundation, the site-soil classification as (ZA-SA) or (ZB-SB) cannot be determined. In the Jordanian code, if detailed soil properties cannot be determined, the soil is of type (SD) unless the designing engineer has evidence that the soil falls within the site category (SE, SF). On the other hand, in the Turkish code, the soil in such cases may be classified as (ZC or ZD).

Both codes classify soils that require particular analysis underclass (ZF-SF), as these soils may be susceptible to failure or collapse under earthquake effects. Such soils include those prone to liquefaction, clay soil, quick clays, and weakly cemented soil. However, there are some differences in the classification criteria between the two codes:

1. In the Jordanian code, for the (SF) class, clay soil with high plasticity must have a depth greater than 7.5 meters and a plasticity index (PI) greater than 75. This implies that the liquid limit (LL) value can be higher than 75% to classify the clay soil as having high plasticity. On the other hand, in the Turkish code, the depth requirement is greater than 8 meters, and the plasticity index (PI) must be greater than 50. This means the Turkish standard classifies the clay soil as having high plasticity when the liquid limit (LL > 50%) indicates that the Turkish standard is more restrictive with clay soil.

2. For soft clay soils with intermediate strength and high depth, the Jordanian code requires the depth to be greater than 36 meters, while the Turkish code requires the depth to be greater than 35 meters. In this case, only the Jordanian code includes a requirement for undrained shear strength (Cu < 50 kPa), whereas the Turkish code does not mention it.

4.2.3 Building Importance Factors

The Turkish Building Earthquake Code 2018 (TBEC-2018) categorizes building importance into three levels, represented by Building Importance Factors (BKS) of 1, 2, and 3. For BKS=1, which includes facilities like hospitals, educational facilities, and military barracks, an importance factor (I) of 1.5 is assigned. Similarly, the Jordan Building Earthquake Code 2022 (JBEC-2022) also divides building importance into four categories, with the highest category (IV) posting an importance factor (I) of 1.5, which applies to facilities such as hospitals and fire brigade buildings. In TBEC-2018, BKS=2 represents buildings of moderate importance, including shopping malls, sports facilities, and places of worship, with an importance factor (I) of 1.2. In JBEC-2022, the corresponding category for moderate importance also has an importance factor (I) of 1.25. For buildings not falling under the BKS=1 or BKS=2 categories, such as houses, workplaces, hotels, and specific industrial structures, the importance factor (I) is assigned 1 in both TBEC-2018 and JBEC-2022. The table compares the building importance factors (BKS) and importance factors (I) between TBEC-2018 and JBEC-2022.

Table 4.5 Building importance factor (TBEC-2018, JBEC-2022)

Building Importance	TBEC-2018 (BKS)	TBEC-2018 (I)	JBEC-2022 (Importance Category)	JBEC-2022 (I)
High Importance	BKS = 1	I = 1.5	IV (Hospitals, Dispensaries, etc.)	I = 1.5
Moderate Importance	BKS = 2	I = 1.2	III (Shopping malls, Theatres, etc.)	I = 1.25
Other Buildings	BKS = 3	I = 1	I, II	I = 1

4.2.4 Local Ground Effect Coefficients

Both standards rely on seismic design criteria based on the forces generated by ground earthquake movements. The requirements consider a design period of 50 years with a 10% probability of exceeding the minimum ground earthquake force, considering a longer earthquake recurrence period of 475 years. Additionally, both standards include a seismic hazard map that illustrates the spectral acceleration coefficient for two specific periods: 0.2 second and 1.0 second, which are crucial for seismic design. In the map, (S_s) represents the short-period spectral acceleration coefficient for 0.2 second, and (S_1) represents the spectral acceleration coefficient for a period of 1.0 second, with a damping rate of 5% from critical damping. These coefficients represent the acceleration of the spectral response as a percentage of the gravitational acceleration (g).

The seismic hazard maps provide spectral acceleration coefficients for different periods, such as short periods (0.2 sec) and (1.0 sec), which are used to calculate the adjusted risk-targeted maximum considered earthquake (MCER) in both the TBEC-2018 and JBEC-2022. However, there are differences in the symbols used to represent these coefficients between the two standards in these equations (The TBEC-2018 symbols and the JBEC-2022 symbols, respectively):

$$SD_S - SM_S = S_S \times F_S - F_a \tag{4.7}$$
$$SD_1 - SM_1 = S_1 \times F_1 - F_V \tag{4.8}$$

The local ground effect coefficients for the short-period region (0.1 sec) are denoted as F_s and F_a in TBEC-2018 and JBEC-2022, respectively. Additionally, for the 1.0 second, the local ground effect coefficients are represented as F_1 and F_v.

In both standards, S_s refers to the short-period map spectral acceleration coefficient, while S_1 represents the map spectral acceleration coefficient for a period of 1.0 second.

4.2.5 Local Ground Effect Coefficients for The Short Period Region

There are variations in the values of the local ground effect coefficients for the short-period region (F_s - F_a) between TBEC-2018 and JBEC-2022, even for the same site classification. Notably, TBEC-2018 considers and provides the local ground effect coefficient values for the short period for spectral acceleration (S_s) larger than or equal to 1.50, whereas JBEC-2022 only includes spectral acceleration values for $S_s > 1.25$.

We observed that the local ground effect coefficient values for the short-period region (F_s and F_a) are consistent for all spectral acceleration coefficient values for soils available in site types (ZA-SA, ZD-SD) in both standards. However, for site type (ZF-SF), a site-specific soil behavior analysis is required. Furthermore, the two standards have differences in the site types (ZB-SB, ZC-SC, ZE-SE), as illustrated in the table below.

Table 4.6 Local ground effect coefficients for the short period region (TBEC-2018, JBEC-2022) (a)

| Local Ground Class | Local Ground Effect Coefficient (Fs – Fa) for Short Period | | | | | |
| | Ss ≤ 0.25 | | Ss = 0.50 | | Ss = 0.75 | |
	(TBEC)	(JBEC)	(TBEC)	(JBEC)	(TBEC)	(JBEC)
ZB-SB	0.9	1.0	0.9	1.0	0.9	1.0
ZC-SC	1.3	1.2	1.3	1.2	1.2	1.1
ZE-SE	2.4	2.5	1.7	1.7	1.3	1.2

Table 4.7 Local ground effect coefficients for the short period region (TBEC-2018, JBEC-2022) (b)

| Local Ground Class | Local Ground Effect Coefficient (Fs – Fa) for Short Period | | | | | |
| | Ss = 1.00 | | Ss = 1.25 | | Ss ≥ 1.50 | |
	(TBEC)	(JBEC)	(TBEC)	(JBEC)	(TBEC)	(JBEC)
ZB-SB	0.9	1.0	0.9	1.0	0.9	-
ZC-SC	1.2	1.0	1.2	1.0	1.2	-
ZE-SE	1.1	0.9	0.9	0.9	0.8	-

It is evident that the local ground effect coefficients for the short-period region values of the site (SB) in JBEC-2022 are higher than those of the site (ZB) in TBEC-2018. On the other hand, the local ground effect coefficients for the short-period region values of the site (ZC) in TBEC-2018 are higher than the values of the site (SC) in JBEC-2022.

As for the local ground class of (ZE-SE), the values of local ground effect coefficients for the short period region show some similarity between the two standards for certain spectral accelerations. However, for most cases, the values in

TBEC-2018 are higher, except for the value of S ≤ 0.25, which is higher in JBEC-2022. These differences in the local ground effect coefficients between TBEC-2018 and JBEC-2022 can influence the seismic design considerations and response of structures in each respective code.

4.2.6 Local Ground Effect Coefficients for the 1.0 Second

Furthermore, discrepancies exist in the local ground effect coefficients for the 1.0-second spectral acceleration coefficients between TBEC-2018 and JBEC-2022.

In TBEC-2018, the values of local ground effect coefficients for the 1.0 second are determined for spectral acceleration coefficients equal to or greater than $S_1 \geq 0.60$, whereas JBEC-2022 considers values for $S_1 \geq 0.50$.

Additionally, the values of local ground effect coefficients for the 1.0-second spectral acceleration coefficients are consistent between both standards only for site class (ZA-SA), where they remain constant at 0.8 for all spectral acceleration coefficients. However, as the table below shows, these values differ for other site classes.

Table 4.8 Local ground effect coefficients for the 1.0 second period (TBEC-2018, JBEC-2022) (a)

Local Ground Class	Local Ground Effect Coefficients for the 1.0 Second					
	$S_1 \leq 0.10$		$S_1 = 0.20$		$S_1 = 0.30$	
	(TBEC)	(JBEC)	(TBEC)	(JBEC)	(TBEC)	(JBEC)
ZB-SB	0.8	1.0	0.8	1.0	0.8	1.0
ZC-SC	1.5	1.7	1.5	1.6	1.5	1.5
ZD-SD	2.4	2.4	2.2	2.0	2.0	1.8
ZE-SE	4.2	3.5	3.3	3.2	2.8	2.8

Table 4.9 Local ground effect coefficients for the 1.0 second period (TBEC-2018, JBEC-2022) (b)

Local Ground Class	Local Ground Effect Coefficients for the 1.0 Second					
	$S_1 = 0.40$		$S_1 = 0.50$		$S_1 \geq 0.60$	
	(TBEC)	(JBEC)	(TBEC)	(JBEC)	(TBEC)	(JBEC)

ZB-SB	0.8	1.0	0.8	1.0	0.8	-
ZC-SC	1.5	1.4	1.5	1.3	1.4	-
ZD-SD	1.9	1.6	1.8	1.5	1.7	-
ZE-SE	2.4	2.4	2.2	2.4	2.0	-

Furthermore, TBEC-2018 and JBEC-2022 concur that sites classified as local ground class (ZF-SF) require a site-specific soil behavior analysis to determine the values of local ground effect coefficients for the 1.0 second.

Upon comparing the values of site coefficients for different spectral acceleration coefficients for local ground effect coefficients for the 1.0 second between TBEC-2018 and JBEC-2022, several observations can be made:

1. For site class (ZB-SB), the values in JBEC-2022 are generally higher compared to TBEC-2018.
2. For site class (ZC-SC), the values vary, with some being higher in JBEC-2022 and some higher in TBEC-2018.
3. For site class (ZD-SD), the values are generally higher in TBEC-2018, except for values of spectral acceleration $S \leq 0.10$.
4. For site class (ZE-SE), the values for the first two spectral acceleration coefficients are higher in TBEC-2018 than in JBEC-2022, while the value of the site coefficient for $S \geq 0.50$ is higher in JBEC-2022.

4.2.7   Defining Earthquake Design Classes

Defining earthquake design class based on spectral acceleration coefficients for a short period (SD_S) is a crucial aspect of earthquake design. The (TBEC-2018) and the (JBEC-2022) consider various factors in determining the seismic hazard level, such as soil type, occupancy class, building use, and seismic response acceleration variables. The Jordanian code is influenced by standards like ASCE/SEI 7-10 and IBC 2012 to establish its rules and criteria.

While both codes consider the design based on spectral acceleration coefficients for a short period (SD_S), the JBEC-2022 also considers spectral acceleration coefficients for a 1.0-second period (SD_1) to assess the most dangerous conditions. As seen in the table below, there are differences between TBEC-2018 and JBEC-2022 in

how they determine the earthquake design classes according to spectral acceleration coefficients for a short period (SD_S).

Table 4.10 Earthquake design classes (TBEC-2018, JBEC-2022)

Spectral Acceleration Coefficients Values for Short Period (SD_S)		Danger Category			
		TBEC		JBEC	
TBEC (2018)	JBEC (2022)	BKS =1	BKS= 2,3	I, II, III	IV
$SD_S < 0.33$	$SD_S < 0.167$	4a	4	A	A
$0.33 \leq SD_S < 0.50$	$0.167 \leq SD_S < 0.33$	3a	3	B	C
$0.50 \leq SD_S < 0.75$	$0.33 \leq SD_S < 0.50$	2a	2	C	D
$0.75 \leq SD_S$	$0.50 \leq SD_S$	1a	1	D	D

It is evident that there are noticeable differences between the (JBEC-2022) and the (TBEC-2018) in their categorization of values for spectral acceleration coefficient (SD_S) for short periods.

In JBEC-2022, the code includes categories for values of SD_S less than 0.167, while TBEC-2018 starts its classification from SD_S values less than 0.33. This means that JBEC-2022 considers lower spectral acceleration levels in its seismic design criteria than TBEC-2018.

Additionally, the two codes differ in terms of the consideration of high spectral acceleration values. TBEC-2018 considers SD_S values greater than or equal to 0.75 for the short period (0.2 second). On the other hand, JBEC-2022 considers SD_1 values greater than or equal 0.75 for the more extended period of 1.0 second. This indicates that JBEC-2022 identifies higher spectral acceleration values in the more extended period as more dangerous.

Based on these differences, JBEC-2022 classifies structures under "E" for the danger category (I, II, III) and "F" for the danger category (IV), for ($0.75 \leq SD_1$).

The discrepancies in classification and criteria between the two codes arise from variations in the geotechnical conditions and seismicity of the respective regions.

Furthermore, it is worth noting that the (JBEC-2022) introduces a requirement for amplifying the building importance factor when the spectral acceleration coefficient (SDs) for a short period exceeds 0.65. In such cases, the building importance factor (I) is multiplied by an amplification factor of 1.5. On the other hand, the (TBEC-2018) adopts a fixed value of 1.5 for the building importance factor (I) as an essential design parameter for ($0.50 \leq SD_S$). This difference stems from the different risk assessment and safety considerations employed in each code. JBEC-2022 emphasizes increased protection for structures in regions where the spectral acceleration exceeds a certain threshold, hence the need for amplification. In contrast, TBEC-2018 adopts a more conservative approach by maintaining a constant building importance factor of 1.5 for essential structures, regardless of the spectral acceleration coefficient value.

4.2.8 Determining the Dominant Natural Vibration Period of the Building

The determination of the dominant natural vibration period of the building is crucial for calculating the base shear strength. To achieve this, an empirical approach is often employed. Notably, there are differences between (TBEC-2018) and (JBEC-2022) in the equations used for this purpose and the coefficients' values.

In (TBEC-2018):

$$T_{PA} = C_t \times H_N^{\frac{3}{4}} \tag{4.9}$$

Where in (JBEC-2022):

$$T_a = C_t \times h_n^x \tag{4.10}$$

In (JBEC-2022), the coefficient (x) is determined based on the (C_t) coefficient, which is determined according to the building type. However, in (TBEC-2018), the coefficient (x) is fixed at ($\frac{3}{4}$), and the (C_t) coefficient is determined using the following equation:

$$C_t = \frac{0.1}{A_t^{.5}} \tag{4.11}$$

Where C_t must be less than 0.07.

However, specific values are fixed in both codes but differ between them. For instance, the coefficient (C_t) values for steel-framed buildings differ. In (TBEC-2018), it is set at 0.08; in (JBEC-2022), it is 0.0724. Similarly, for buildings consisting solely

of reinforced concrete frames, the coefficient (C_t) is 0.1 in (TBEC-2018) and 0.0466 in (JBEC-2022), representing a significant difference. For other types of buildings, (TBEC-2018) sets (C_t) at 0.07, whereas (JBEC-2022) uses 0.0488, again indicating a substantial variation. The provided table below depicts this information:

Table 4.11 The differences in (C_t) coefficient between (TBEC-2018) and (JBEC-2022)

Building Type	Coefficient (C_t) - TBEC-2018	Coefficient (C_t) - JBEC-2022
Steel-Framed Building	0.08	0.0724
Reinforced Concrete-Framed Building	0.1	0.0466
Other Building Types (e.g., mixed)	0.07	0.0488

4.2.9 Accidental Torsion

Both codes have variations in the application of accidental torsion for lateral force. Apart from the inherent torsion, they consider accidental torsion arising from member eccentricity. This occurs when a building member is displaced by 5% in all directions due to horizontal irregularities. To account for this, the torsion amplification factor is applied.

There is a discrepancy between the two codes regarding this factor. The (JBEC-2022) specifies that the factor must be greater than 1.0 and equal to or less than 3.0. Conversely, the (TBEC-2018) states that the factor should be greater than 1.2 and equal to or less than 2. However, both codes utilize the same equation for calculation.

4.2.10 Deep Foundation Ties

"Deep Foundation Ties" are structural elements that secure deep foundation systems to a building's superstructure. These systems, like piles or drilled shafts, are employed when surface soil can't effectively bear a building's weight. Deep foundation ties efficiently transfer loads from the superstructure to these deep elements. They

include connectors, brackets, or reinforcements, ensuring a robust link between the foundation and structure. This improves stability and load-bearing capacity.

In (JBEC-2022), deep foundation ties apply to seismic design classes (C, E, D, F), excluding (A, B). Conversely, (TBEC-2018) restricts tie beams in foundation soils only to local soil class ZA. Both codes agree that ties should be designed to withstand tension and compression, not less than (0.10 SD_S) multiplied by the largest sum of dead and live loads on the wedge or column cap.

4.2.11 Base Shear Force

There are differences in the equations used to calculate the base shear force for seismic design between (JBEC-2022) and (TBEC-2018):

In (JBEC-2022), the equation for base shear force (V) is as follows:

$$V = \frac{F \times SD_S}{R} \times W \tag{4.12}$$

While in (TBEC-2018), the equation is:

$$V = \frac{SD_S \times W}{R_a} \tag{4.13}$$

Notably, the Jordanian code (JBEC-2022) introduces the coefficient (F), which varies based on the number of stories:

F = 1.0 for one-story buildings

F = 1.1 for two-story buildings

F = 1.2 for three-story buildings

However, (TBEC-2018) does not include these distinctions or specify values of (F). Additionally, (TBEC-2018) uses a constant value of (R_a) equal to 4 in their equation. Moreover, (JBEC-2022) accounts for the earthquake load reduction coefficient (R), which varies based on the type of building and falls within the range of 1.5 to 8.

The differences in these equations highlight variations in the approach taken by each code to calculate the base shear force for seismic design, considering factors such as the number of stories and the type of building.

4.2.12 Shallow Foundations

The codes (TBEC-2018 and JBEC-2022) agree that shallow foundations can be used when the soil's bearing capacity at shallow depths is sufficient to support the loads imposed by the building. This is especially applicable when bedrock is present.

Shallow foundations are typically employed when the width of the foundation (measured in meters) is more significant than the foundation depth (also measured in meters). It's important to note that the foundation depth should generally be less than 3 meters. Additionally, consideration should be given to groundwater conditions.

The bearing capacity of shallow foundations can be calculated using analysis methods outlined in both codes.

The formula employed to determine the bearing capacity of shallow foundations in TBEC-2018 is as follows Hansen's equation:

$$q_k = cN_c s_c d_c i_c g_c b_c + qN_q s_q d_q i_q g_q b_q + 0.5\,\gamma \grave{B} N_\gamma s_\gamma d_\gamma i_\gamma g_\gamma b_\gamma \tag{4.14}$$

In contrast, the Jordanian building code employs a different equation for calculating the bearing capacity of shallow foundations, which can be summarized as follows in Meyerhof's equation:

$$q_u = cN_c F_{cs} F_{cd} F_{ci} + qN_q F_{qs} F_{qd} F_{qi} + 0.5\,\gamma_2 B N_\gamma F_{\gamma s} F_{\gamma d} F_{\gamma i} \tag{4.15}$$

In both codes, soil bearing capacity can be determined using standard geotechnical tests such as the Standard Penetration Test and the Cone Penetration Test.

4.2.13 Correction Factors to SPT

We can observe a difference in the equation used for correction factors in the Standard Penetration Test (SPT) between (TBEC-2018) and (JBEC-2022). Where the equation that used in (TBEC-2018):

$$N_{1,60} = NC_N C_R C_S C_B C_E \tag{4.16}$$

$N_{1,60}$ indicates that the blow count "N" has been normalized or corrected to a standard energy level of 60% of the theoretical energy transferred from the hammer to the sampler.

Also, C_N is the geological stress (depth) correction coefficient applied in cohesionless soils and determined using the following equation:

$$C_N = 9.78 \times \left(\frac{1}{\acute{\sigma}_{vo}}\right)^{0.5} \tag{4.17}$$

where C_N must be less than or equal to 1.70.

The effective vertical stress $(\acute{\sigma}_{vo})$ (kN/m²) at the testing depth is computed based on the field conditions during the Standard Penetration Test (SPT). This calculation will not consider any alterations in effective stress due to subsequent fill placement, foundation loading, excavation, or similar factors.

Furthermore, there are correction coefficients involved in this calculation, each serving a specific purpose:

CR represents the rod length correction coefficient.

CS stands for the sampler type correction coefficient.

CB signifies the drilling drill diameter correction coefficient.

CE denotes the energy ratio correction coefficient.

These correction coefficients can be obtained from a table in the code for reference.

In contrast, the correction factor applied to the SPT test in the Jordanian code is outlined as follows:

$$N = C_N N_F \tag{4.18}$$

Where C_N is the geological stress (depth) correction coefficient applied in cohesionless soils and determined using the following equation:

$$C_N = \left(\frac{98.1}{\acute{\sigma}_v}\right) \tag{4.19}$$

Where N_F is the field value of a number of blows (without correction).

The Standard Penetration Test (SPT) is recognized as a method for assessing ground liquefaction in both codes.

4.2.14 Calculation of Liquefaction Resistance

Resistanceology employed in TBEC-2018 for computing liquefaction resistance necessitates the determination of liquefaction resistance (τ_R) followed by calculating the shear stress induced in the ground during an earthquake event. The equation used to compute liquefaction resistance is based on the cyclic resistance ratio (CRR$_{M7.5}$) against an earthquake with a moment magnitude of 7.5, along with the design earthquake moment magnitude correction coefficient (C_M) and the effective vertical stress (σ'_{vo}), as depicted in the equation:

$$\tau_R = CRR_{M7.5} C_M \sigma'_{Vo} \tag{4.20}$$

Where $CRR_{M7.5} = \frac{1}{34 - N_{1,60f}} + \frac{N_{1,60f}}{135} + \frac{50}{(10 N_{1,60f} + 45)^2} - \frac{1}{200}$ $\qquad$ (4.21)

where $N_{1,60f}$ means SPT hit count corrected for fines content, as Idriss & Seed's, 1997 equations illustrate.

$$C_M = \frac{10^{2.24}}{M_W^{2.56}} \tag{4.22}$$

Furthermore, the shear stress experienced by the ground during an earthquake can be determined based on several factors. These factors include the total vertical stress (σ_{Vo}) at the depth where liquefaction is being assessed, the short-period design spectral acceleration coefficient (SDs), and the stress reduction coefficient (rd) specific to that depth. The equation below provides a representation of this calculation:

$$\tau_{\text{earthquake}} = 0.65\sigma_{Vo}(0.45SD_S)rd \tag{4.23}$$

In Jordanian code, the calculation of liquefaction resistance (F_L) depends on resulting from dividing the ratio of stresses necessary to cause liquefaction (R_F) by knowing the magnitude of the earthquake strength and the number of corrected blows (N) from the standard in-situ penetration experiment, divided by the equivalent average shear stress (R_i).

$$R_i = 0.65 \left(\frac{a_{max}}{g}\right)\left(\frac{\sigma_v}{\acute{\sigma}_v}\right)rd \tag{4.24}$$

So, the liquefaction resistance $F_L = \left(\frac{R_F}{R_i}\right)$ \hfill (4.25)

In summary, there are notable distinctions between the two codes. (TBEC-2018) places a greater emphasis on calculating liquefaction resistance by considering factors such as (CRR$_{M7.5}$), the design earthquake moment magnitude, short-period design spectral acceleration, and stress reduction coefficients. In contrast, the Jordanian code (JBEC-2022) focuses primarily on factors like effective stress, total effective stress, peak horizontal acceleration at the ground surface, and gravitational acceleration. Furthermore, it's worth noting that in (TBEC-2018), the safety factor against liquefaction must be greater than or equal to 1.10, while in (JBEC-2022), it must be greater than or equal to 1.0. This variance can be attributed to the differences in soil characteristics between Turkey and Jordan. Turkey's soil has the lowest resistance to liquefaction compared to Jordan's. Additionally, the variation in the number and magnitude of earthquakes experienced by each country has also influenced these differing safety factor requirements.

4.2.15 Overturning of Retaining Walls

Table 4.12 Factor of safety against overturning of retaining walls in (TBEC-2018 & JBEC-2022)

Aspect	Jordanian Code	Turkish Code
Incohesive Soil	≥ 1.5	≥ 1.3

Cohesive Soil	≥ 2	≥ 1.3

Both codes stress the critical importance of incorporating a safety factor to forestall any potential overturning of retaining walls. Nonetheless, a discernible discrepancy emerges when scrutinizing their distinct requisites. The Jordanian code prescribes a safety factor of 1.5 or higher for incohesive soils and 2 or higher for cohesive soils. Conversely, the Turkish code dictates a safety factor of 1.3 or higher. This contrast can be ascribed to disparities in geotechnical conditions, levels of seismicity, and engineering protocols observed in the two regions. Furthermore, given Turkey's heightened vulnerability to seismic activity relative to Jordan and its geological characteristics, one might anticipate a more stringent safety factor in the Turkish code. Nonetheless, the inverse is observed, signifying that the Jordanian code adopts a more cautious approach, necessitating more significant safety factors to account for specific soil behaviors and seismic risks endemic to Jordan.

4.2.16 Horizontal and Vertical Static-Equivalent Earthquake Coefficients

Differences in determining horizontal and vertical static-equivalent earthquake coefficients between the Turkish and Jordanian codes are apparent. The Jordanian code calculates the horizontal static-equivalent earthquake coefficient by dividing the country into different areas based on local ground motion characteristics. Specific values of the horizontal static-equivalent earthquake coefficient, ranging from 0.05 to 0.25, are assigned to these areas. On the other hand, the Turkish code calculates the horizontal static-equivalent earthquake coefficient based on the area's spectral acceleration coefficient (SD_S) and the coefficients for retaining structures (r), which depend on the amount of displacement. The equation represents this:

$$k_h = \frac{0.4SD_S}{r} \tag{4.26}$$

The Jordanian code simplifies its approach by providing region-specific values, which may suit regions with relatively low seismic activity. In contrast, the Turkish code adopts a more detailed approach, considering factors such as seismic levels and soil characteristics to provide precise values for each region. By tailoring values to specific areas based on their unique seismic and geological characteristics, it aims to enhance the accuracy of seismic design and structural safety. This approach can be particularly valuable in Turkey, which experiences a broad spectrum of seismic

activity. Furthermore, it's worth noting that the Jordanian code assigns a zero value to the vertical static-equivalent earthquake coefficient. In contrast, the Turkish code gives a value of $0.5k_h$ to this coefficient. This difference in approach stems from how each code considers seismic inertial forces. The Jordanian code assumes that these forces can manifest in any direction but primarily focuses on the horizontal direction. In contrast, given Turkey's higher seismicity, the Turkish code incorporates a vertical coefficient as an additional safety measure, recognizing the potential for significant vertical seismic forces. This reflects the Turkish code's commitment to ensuring structural safety in a region prone to substantial seismic activity.

4.2.17 The Resultant of the Total Earth Pressure

Both building codes emphasize the significance of considering the resultant of the total earth pressure, especially in the context of seismic effects. Understanding and calculating this force is a crucial initial step when designing retaining walls. It necessitates a comprehensive grasp of soil mechanics, geotechnical engineering principles, and familiarity with site-specific conditions and parameters. These site-specific conditions can encompass seismic activity in the area, which plays a pivotal role in the structural analysis. Furthermore, these calculations must consider various factors to ensure the retaining wall's structural integrity. These factors include the soil type, the wall's geometry, the coefficient of wall friction, and any additional loads acting upon the wall. Calculations typically involve determining active and passive earth pressures to design the wall adequately. The importance of comprehending and accurately calculating the resultant of the total earth pressure cannot be overstated, as it directly impacts the stability and safety of retaining walls, particularly when subjected to seismic forces.

The equation used to calculate the coefficient of active earth pressure (K_a) in both codes is as follows:

$$K_a = \frac{\sin^2(\Psi + \acute{\phi}_d - \theta)}{\cos\theta \sin^2\Psi \sin(\Psi - \theta - \delta_d)\left[1 + \sqrt{\frac{\sin(\phi_d + \delta_d)\sin(\phi_d - \beta - \theta)}{\sin(\Psi - \theta - \delta_d)\sin(\Psi + \beta)}}\right]^2} \qquad (4.27)$$

The equation of the passive earthquake is as follows:

$$K_p = \frac{\sin^2(\Psi + \acute{\phi}_d - \theta)}{\cos\theta \sin^2\Psi \sin(\Psi + \theta)\left[1 - \sqrt{\frac{\sin(\phi_d)\sin(\phi_d + \beta - \theta)}{\sin(\Psi + \theta)\sin(\Psi + \beta)}}\right]^2} \qquad (4.28)$$

A distinction in dynamic water pressure calculation was observed due to water beneath a wall during an earthquake. The equation specified in the Turkish code is as follows:

$$\triangle P_{su} = \frac{7}{12}(0.4SD_S)\gamma_{su}d_{su}^2 \tag{4.29}$$

The equation utilized in the Jordanian code is as follows:

$$P_Z = K_h\gamma_W Z \tag{4.30}$$

A significant disparity between the Turkish and Jordanian codes is observed in their treatment of dynamic water pressure induced by seismic activity. The Turkish code incorporates a comprehensive approach, resulting in a substantially larger calculation than the Jordanian code. Specifically, the Turkish code doubles the height of the wall below the water level (z, d_{su}) and multiplies the equation by a factor of (7/12). This method demonstrates a higher level of precision in accounting for the dynamic effects of earthquakes. This variation can be attributed to Turkey's susceptibility to frequent seismic events and the necessity to safeguard structures from lateral forces, changes in pore pressure, and the stability of retaining walls regarding sliding and overturning. Given these considerations, the Turkish code emphasizes addressing dynamic water pressure to enhance structural resilience. In contrast, Jordan faces fewer seismic risks, reducing the urgency of accounting for dynamic water pressure in their code. In essence, the difference in how these two codes handle dynamic water pressure reflects each region's varying seismic conditions and priorities.

CHAPTER 5

5. CASE STUDIES

In this chapter, earthquake analyses are performed using PLAXIS 3D, incorporating seismic events from both Turkey and Jordan for the presented analysis. The chapter delves explicitly into examining mesh deformation, foundation deformation, and pile deformation attributed to earthquakes in Turkey and Jordan.

PLAXIS operates as a finite element method, breaking down elements into a series of nodes. The software's capability to analyze dynamic behavior is a crucial feature of the software. This dynamic analysis hinges on matrices, including the mass matrix with acceleration, damping matrix with velocity, and stiffness matrix with displacement, as illustrated in the equation:

$$m\ddot{u} + C\dot{u} + Ku = F \tag{5.1}$$

This equation encapsulates the interplay of mass, damping, and stiffness matrices in the dynamic analysis, providing valuable insights into the seismic response of the system (Kramer, 1996).

In analyzing dynamic behavior, incorporating time integration is crucial for obtaining accurate calculation results. The implicit method emerges as a more acceptable and accurate approach. It is expressed in equations that determine displacement and velocity at the end of the time step based on their values at the beginning of the time step and the displacement increment (Sluys, 1992). The equation representing this process is as follows:

$$m\ddot{u}^{t+\triangle t} + C\dot{u}^{t+\triangle t} + Ku^{t+\triangle t} = F^{t+\triangle t} \tag{5.2}$$

To determine the absolute maximum displacement response, the time history of seismic waves can be input into PLAXIS for a specified period. This involves defining the pseudo-spectral acceleration of the soil and observing the resulting displacement

of the soil elements. This process provides valuable insights into the behavior of the soil when subjected to seismic forces.

In this study, two models have been established to compare earthquakes in Turkey and Jordan and their respective standards. The first model represents Turkey, while the second represents Jordan, each constructed based on recorded ground motion data from their respective regions. Several constraints were enforced to ensure similarity between the models. These included uniformity in soil profile, soil parameters, and groundwater level, as well as consistency in foundation loads, geometry, properties, and the specifications of piles in terms of geometry and properties.

5.1 Constraints of Models

5.1.1 Soil Profile and Parameters

Identical soil properties have been assumed to ensure an accurate comparison between the models. These properties encompass factors such as the soil profile, layer types, unit weight, friction angle, cohesion, elastic modulus, and Poisson's ratio. The details are outlined in the table below.

Table 5.1 Soil properties used during PLAXIS analysis

Depth (m) From	Depth (m) To	Soil Layer	γ_b kN/m^3	$\varphi°$	C kN/m^2	E50 kN/m^2	μ
0	2.00	Sandy Fill	17.5	31	0	25000	0.3
2.00	5.00	Medium Dense Sand	18	33	0	35000	0.28
5.00	15.0	dense sand	19.5	36	0	45000	0.25

The properties of sandy soil used in the models were selected to be within the range values of sand soil properties mentioned in geotechnical books, such as the Geotechnical Engineering Handbook (Das, 2011); they also checked according to the Jordanian standard that mentioned it according to (FHWA, 2003).

5.1.2 Ground Water Table

One of the critical considerations in analyzing soil behavior, especially in seismic conditions, is the existence of groundwater. This element can give rise to significant challenges, including liquefaction, affecting seismic forces, and potentially amplifying their effects. In these instances, the assumption is made regarding groundwater beneath the soil surface, positioned at a depth of 3 meters. The accompanying figure provides a visual representation of the depths of soil layers in conjunction with the groundwater level.

| Layers | | Borehole_1 | |
#	Material	Top	Bottom
1	Sandy fill	0.000	-2.000
2	medium dense sand	-2.000	-5.000
3	Dense sand	-5.000	-15.00
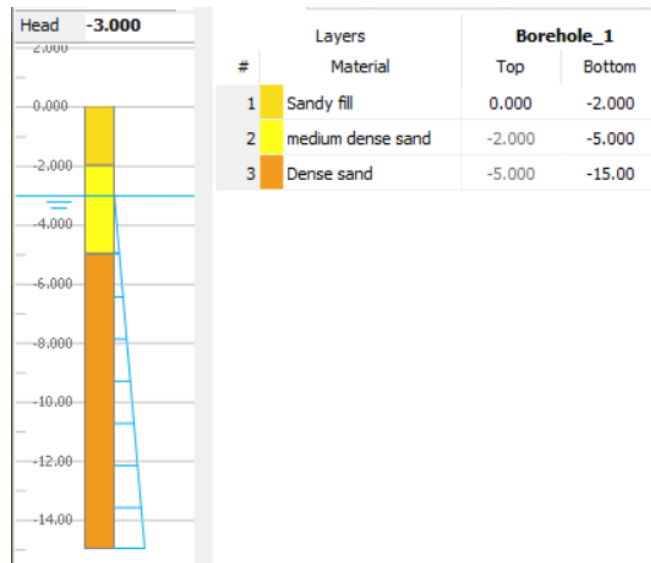
Figure 5.1. Ground water level used during PLAXIS analysis

5.1.3 Foundation Design

The selected foundation design is a circular piled raft foundation, integrating both raft and pile components. This configuration is commonly employed in geotechnical engineering, particularly in regions prone to seismic activity or areas with weak soil conditions. The circular raft is instrumental in providing stability and uniformly distributing loads, while the piles play a crucial role in anchoring the foundation to deeper, more stable soil layers. To achieve this, the number of piles is carefully chosen to encircle the entire raft, ensuring even load distribution. This strategic placement enhances the foundation's stability, especially in seismic conditions. The decision to use piles with a diameter of 0.6 m is a critical factor in achieving this equilibrium—the accompanying table for detailed specifications.

Table 5.2 Foundation and pile specifications

Property	Specification
Foundation Type	Circular Piled Raft Foundations
Foundation Thickness	70 cm
Raft Foundation Diameter	16 m
Pile Diameter	60 cm
Pile Length	8.0 m
Number of Piles	44 piles

The figures below depict a 3D model of the circular piled raft foundation, showcasing the arrangement of piles within the raft foundation.
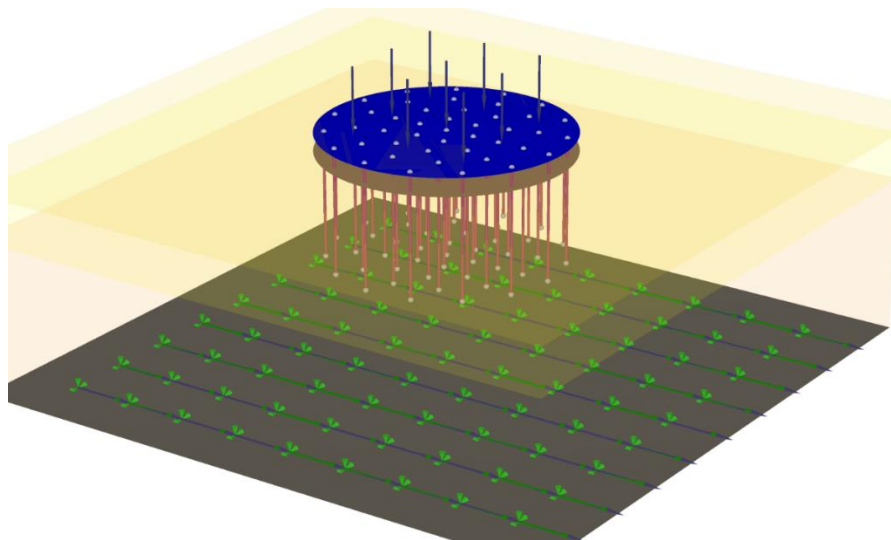
Figure 5.2. 3D model of circular piled raft foundation

In the design of piles, a pile with a diameter of 60 cm is chosen and distributed within the inner area of the circular foundation. The total number of piles is 44.
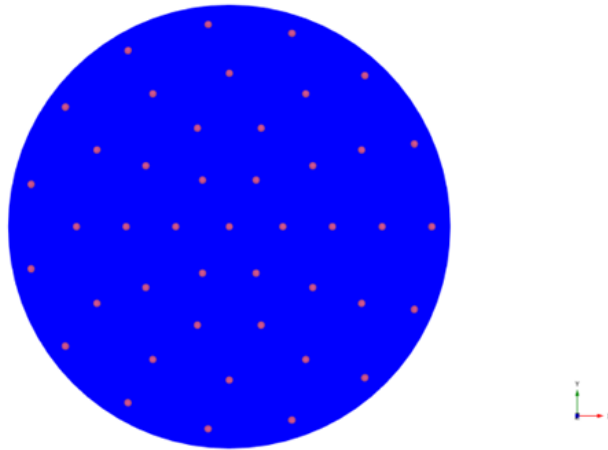
Figure 5.3. Distribution of piles within the raft foundation

The figure illustrates the 3D modeling boundary of the soil layers with a circular raft foundation with piles.
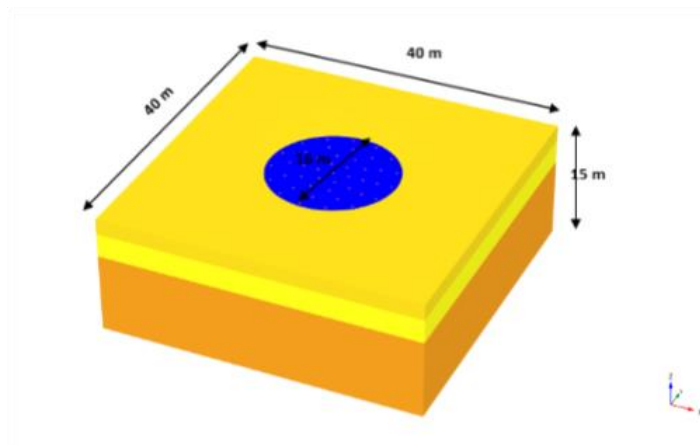
Figure 5.4. The 3D model boundary

5.2 Models

Two models are created in this section as suggested case studies. The first model represents the conditions in Turkey, while the second one represents the conditions in Jordan. Both models adhere to the constraints specified in the first part of the chapter.

5.2.1   Model of Turkey

In the presented structural model, the circular raft pile foundation undergoes a surface loading of 150 kN/m², concurrently experiencing seismic forces. Ground

motion data sourced from seismic activity in Turkey is selected for earthquake analysis. The PLAXIS software is employed for the analysis, adhering to constraints delineated in the preceding section of this chapter. The analysis is conducted to evaluate the influence of ground motion on the mesh, foundation, and piles, scrutinizing parameters including deformation, displacement, and bending moments. The seismic event chosen for examination is the Düzce earthquake.

In this case study, seismic data pertinent to the Düzce earthquake, including acceleration values over time, was sourced from the ground motion database provided by the Pacific Earthquake Engineering Research Center (PEER).

This data was subsequently utilized to perform a time history analysis using the PLAXIS software. The seismic characteristics of the Düzce earthquake were determined, revealing a moment magnitude of 7.14 and a Peak Ground Acceleration (PGA) of 0.3g, according to station IRIGM 487. The earthquake data is uniquely identified through Record Sequence Numbers (RSN), with the specific RSN for the Düzce earthquake being 8164. Using RSN facilitates the database's clear identification and distinction of each earthquake event.
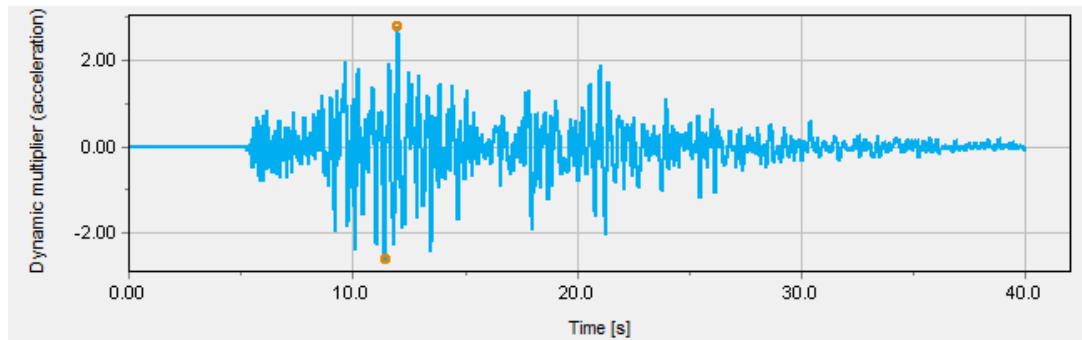
Figure 5.5. Düzce earthquake time history analysis

In our case in the Düzce earthquake that had a moment magnitude 7.14, indicates to substantial strength and potential for causing damage. Where the epicentral distance, measuring 2.7 km from the earthquake's epicenter, signifies its proximity to the specified location. Further, the hypocentral distance, spanning 26.72 km from the earthquake's focus, and the shear wave velocity in the upper 30 meters of soil (Vs30), is measured at 338.6 m/s. This Vs30 value, according to TBEC-2018, suggests that the soil type in the site can be medium to firm layers of sand, gravel, or very solid clay, which can classify the soil (ZD).

Incorporating acceleration values over time is pivotal for dynamic analysis, particularly when assessing how structures respond to seismic loads, as seen during an earthquake. Within the framework of PLAXIS software, a tool widely employed for geotechnical finite element analysis, this approach facilitates a more precise and realistic simulation of a foundation's behavior under seismic forces.
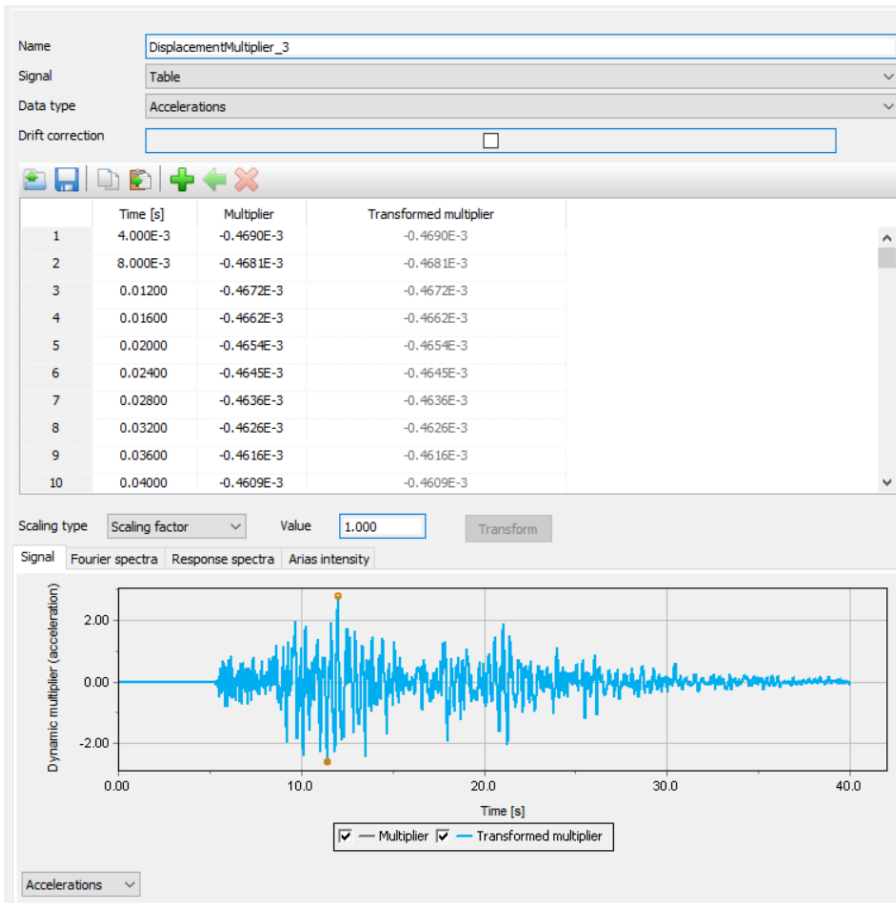
Figure 5.6. Time history analysis by PLAXIS (Düzce earthquake)

5.2.1.1 Deformation of Mesh (Düzce Earthquake)

In this analysis, a surface loading of 150 kN/m² was applied to the model, and it was subjected to an earthquake event with a magnitude of 7.12. The simulation revealed noticeable deformation in the mesh and consequential displacement. The deformed mesh scaled up 100 times to note that, with the maximum deformation reaching 0.03490 m at node 212. Additionally, the maximum displacement observed was 0.03257 m, occurring at element 10586 and node 422. Simultaneously, the minimum displacement was noted at 0.0497 m, corresponding to element 1190 and node 703.

Furthermore, a horizontal movement of 34 mm was recorded during the analysis. These findings highlight the dynamic response of the model to both surface loading and seismic events, providing insights into the deformation and displacement characteristics at specific time intervals. The details are organized in the following table for clarity.

Table 5.3 Deformed mesh and total displacements values (Düzce earthquake)

Parameter	Maximum Value (m)	Element	Node
Deformed Mesh	0.03490	-	212
Total Displacements	0.03257	10586	422

The following figures illustrate the mesh's deformation and the soil's total displacement by the values corresponding to the Düzce earthquake.

Deformed mesh |u| (scaled up 100 times) (Time 3.456*10^6 s)
Maximum value = 0.03490 m (at Node 212)
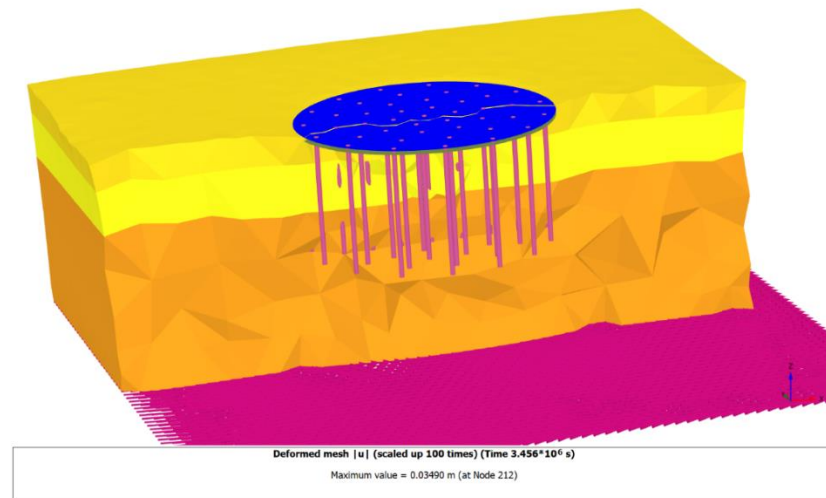
Figure 5.7. Deformed mesh (Düzce earthquake)
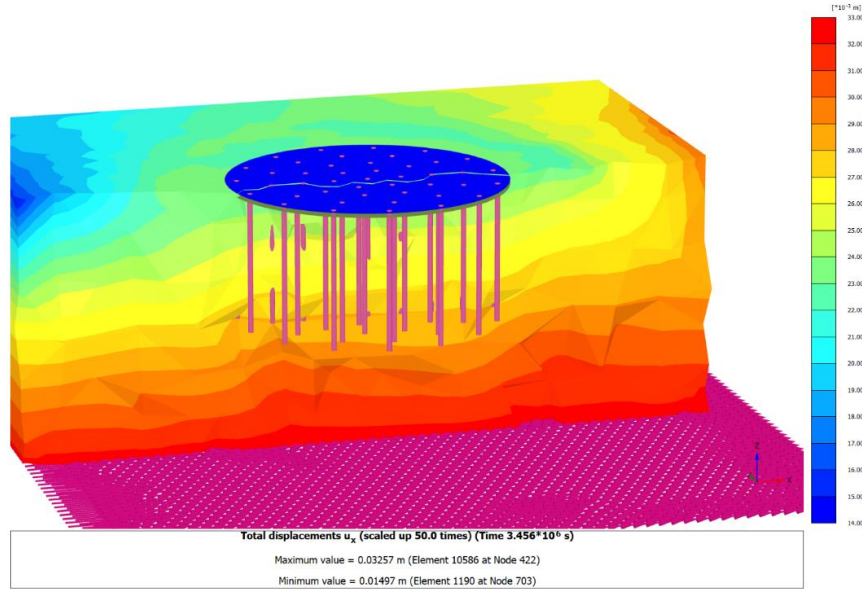
Figure 5.8. Total displacement of mesh (Düzce earthquake)

5.2.1.2 Bending Moment of Foundation (Düzce Earthquake)

The results of analyzing the Düzce earthquake's impact on the foundation revealed varying magnitudes of bending moments across different areas. The maximum bending moment (M_{11}) reached 161.8 kN.m/m, affecting element 231 at node 150, while the minimum value was -93.71, observed on element 5 at node 9637.

The bending moment (M_{11}) signifies the moment resulting from bending around the horizontal axis. This axis is typically associated with the direction in which significant bending moments predominantly occur.

Table 5.4 Bending moment (M_{11}) values of foundation (Düzce earthquake)

Parameters	Bending Moment Value (kN.m/m)	Element, Node
Maximum Value	161.8	231, 150
Minimum Value	-93.71	5, 9637

Similarly, the analysis of bending moment (M_{22}) indicated elevated bending moments in certain foundation areas. The maximum bending moment value was 142.8 kN.m/m, occurring at element 207 and node 140, while the minimum value was -109.7

99

kN.m/m, recorded at element 104 and node 9635. The bending moment (M_{22}) signifies the moment resulting from bending around the vertical axis.

Table 5.5 Bending moment (M_{22}) values of foundation (Düzce earthquake)

Parameters	Bending Moment Value (kN.m/m)	Element, Node
Maximum Value	142.8	207, 140
Minimum Value	-109.7	104, 9635

The following figures represent these findings for bending moment values of the foundation.
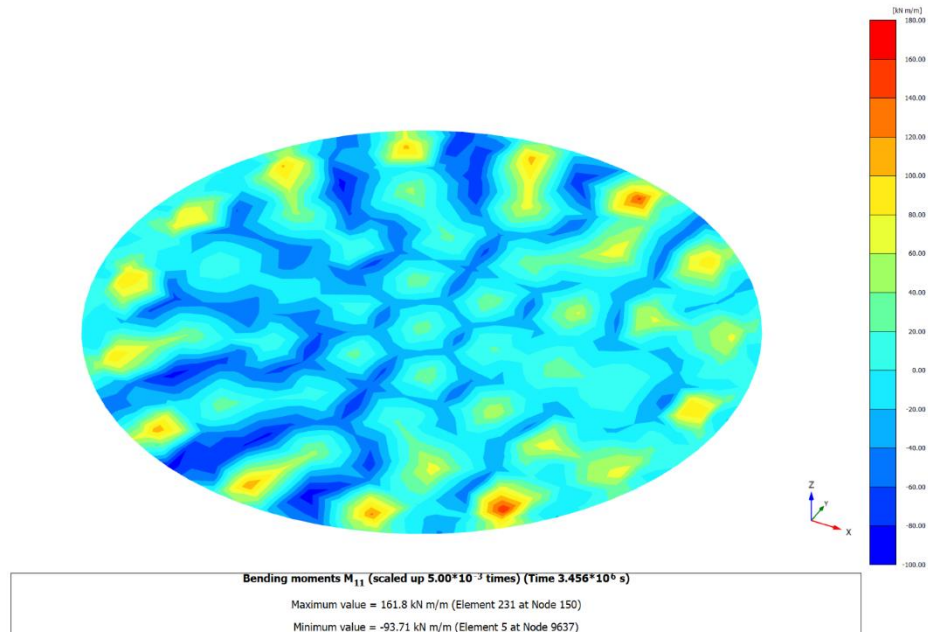
Figure 5.9. Bending moments (M_{11}) of foundation (Düzce earthquake)

Bending moments M₂₂ (scaled up 5.00*10⁻³ times) (Time 3.456*10⁶ s)

Maximum value = 142.8 kN m/m (Element 207 at Node 140)

Minimum value = -109.7 kN m/m (Element 104 at Node 9635)
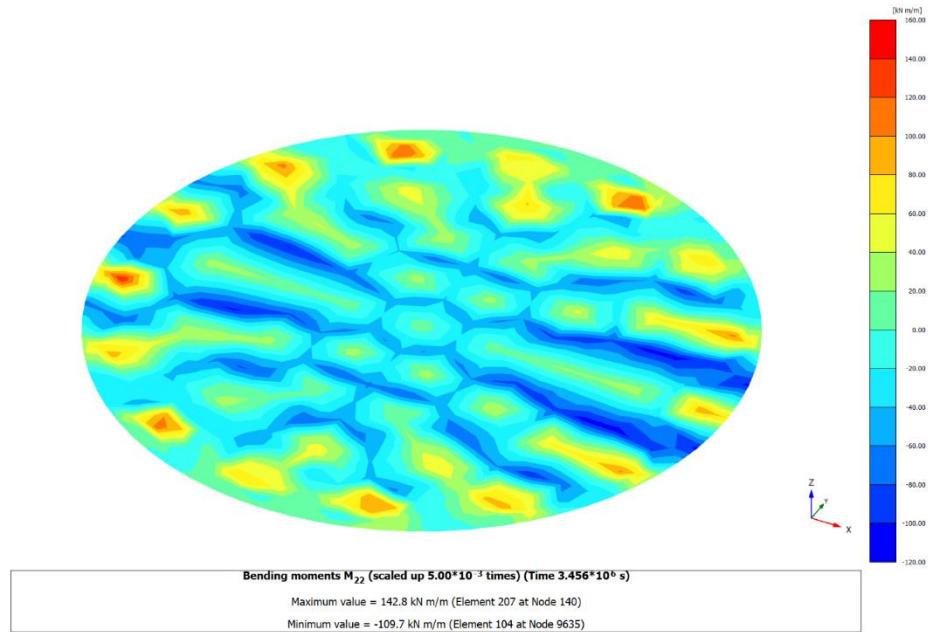
Figure 5.10. Bending moments (M_{22}) of foundation (Düzce earthquake)

5.2.1.3 Deformation of Piles (Düzce Earthquake)

This segment can observe the deformations elicited in pile elements due to seismic activity, influencing both displacements and bending moments. The analysis facilitates the determination of axial force values that impact the piles.

The total displacements experienced by piles, resulting from both applied loads and seismic activity. The maximum displacement reached 0.02822 m, affecting element 205 at node 22456, while the minimum displacement was recorded at 0.02319 m, impacting element 280 at node 22282.

Simultaneously, the axial forces acting on the piles were examined. The maximum axial force was -252.5 kN, observed on element 219 at node 22648, while the minimum axial force was registered at element 390 and node 22322, measuring -920.5 kN.

Table 5.6 Total displacement and axial forces of piles (Düzce earthquake)

Parameter	Maximum Value	Element, Node	Minimum Value	Element, Node
Total Displacements	0.02822 m	205, 22456	0.02319 m	280, 22282
Axial Forces	-252.5 kN	219, 22648	-920.5 kN	390, 22322

It is essential to exercise caution when interpreting the values presented in the table above. When determining maximum or minimum values, it is crucial to consider the magnitude alone, disregarding the associated sign. As mentioned earlier, the sign indicates whether the force is in tension or compression. Therefore, careful attention to the numeric magnitude without incorporating the sign is necessary when selecting maximum or minimum values.

In the analysis of piles, bending moments (M_2 and M_3) were scrutinized, where (M_2) represents the bending moment around the second axis (bending moment around the x-axis), and (M_3) represents the bending moment around the third axis (bending around the z-axis).

The bending moment values (M_2) exhibited a maximum of 209.7 kN.m, identified at element 464, node 22786, and a minimum of -211.6 kN.m, detected at element 1, node 22813. Similarly, the bending moment values (M_3) showed a maximum of 160.3 kN.m at element 270, node 23255, and a minimum of -177.3 kN.m at element 175, node 22305.

It's worth noting that while the PLAXIS software provides values with signs indicating concavity (upward or downward), it is imperative to focus on the magnitudes for determining maximum or minimum values, independent of the sign, by engineering concepts.

Table 5.7 Bending moment (M_2) values of piles (Düzce earthquake)

Bending Moment (M_2)	Value kN.m	Element, Node
Maximum Value	209.7	464, 22786
Minimum Value	-211.6	1, 22813

Table 5.8 Bending moment (M_3) values of piles (Düzce earthquake)

Bending Moment (M_3)	Value kN.m	Element, Node
Maximum Value	160.3	270, 23255
Minimum Value	-177.3	175, 22305

Bending moments M_2 (scaled up $5.00*10^{-3}$ times) (Time $3.456*10^6$ s)

Maximum value = 209.7 kN m (Element 463 at Node 22786)

Minimum value = -211.6 kN m (Element 1 at Node 22813)
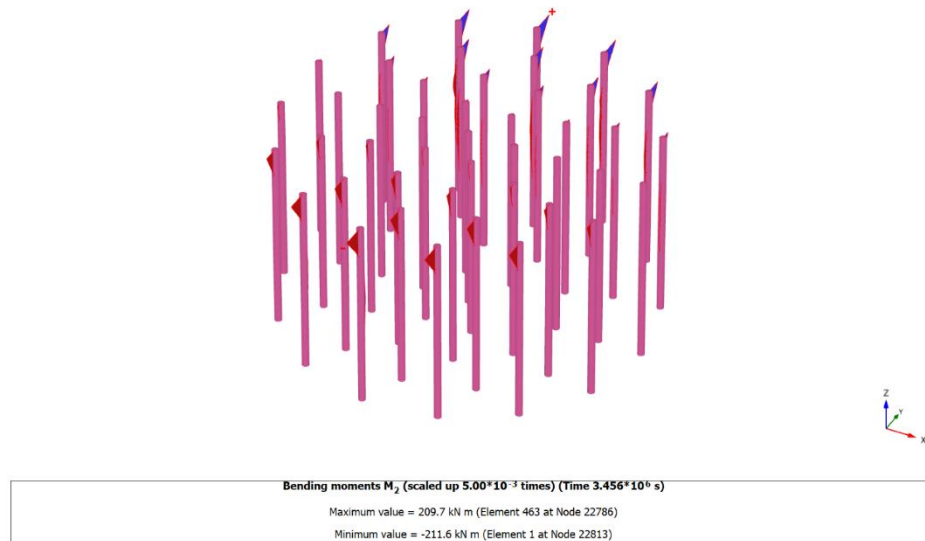
Figure 5.11. Bending moment (M_2) of piles (Düzce earthquake)

Bending moments M$_3$ (scaled up 5.00*10^{-3} times) (Time 3.456*10^6 s)

Maximum value = 160.3 kN m (Element 270 at Node 23255)

Minimum value = -177.3 kN m (Element 175 at Node 22305)
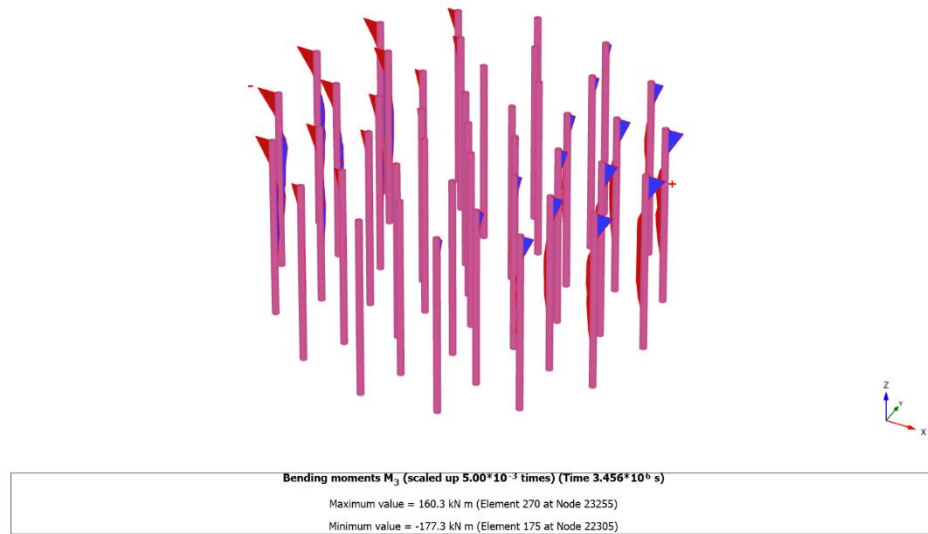
Figure 5.12. Bending moment (M$_3$) of piles (Düzce earthquake)

5.2.1.4 Analyzing Earthquake Characteristics Based on (TBEC-2018) Constraints

In this section, the study examines the spectral acceleration resulting from the Düzce earthquake to compare it with the constraints outlined in TBEC-2018. This evaluation aims to determine if the code successfully meets the necessary conditions for accommodating the acceleration spectrum induced by ground motion. The subsequent figure illustrates the spectral acceleration derived from the Düzce earthquake.
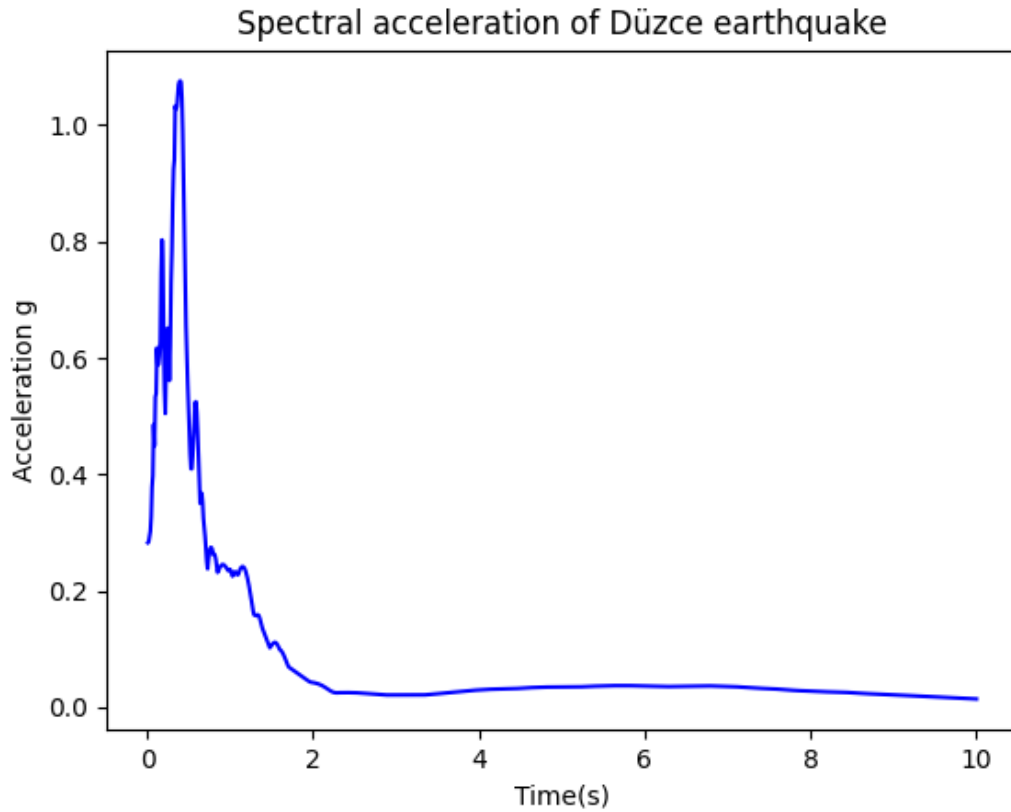
Figure 5.13. Spectral acceleration (Düzce earthquake)

To draw the design spectral acceleration by TBEC-2018 requirements, it is imperative to first identify the soil class assumed to be impacted by the earthquake. Subsequently, based on the determined soil class, the short spectral acceleration coefficient must be established following TBEC-2018 guidelines and the Turkish seismic hazard map. Moreover, it is essential to ascertain the corner period of the horizontal elastic design acceleration spectrum using the TBEC-2018 equation (T_A, T_B). Simultaneously, by the specified equation, the spectral acceleration at the time period (T_L).
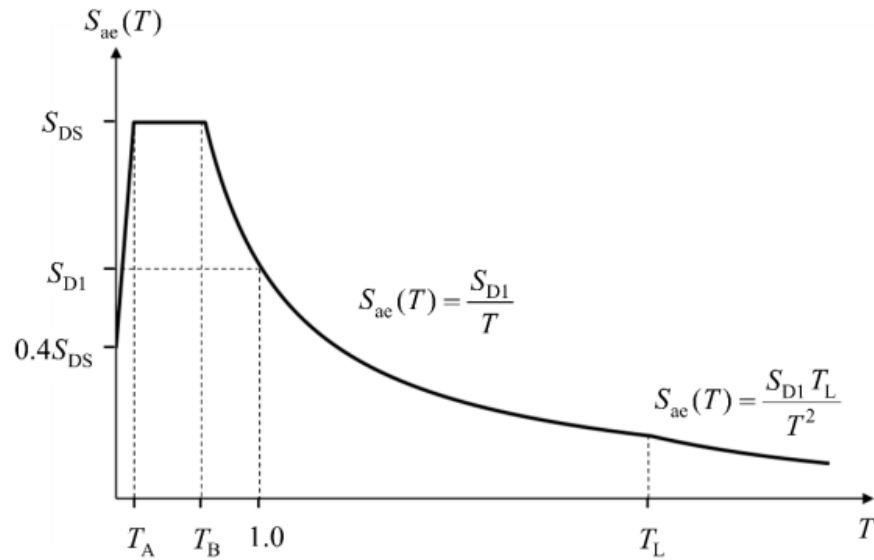
Figure 5.14. Design spectral acceleration according to Turkey Code (TBEC-2018)

In the modeled scenario, the soil under examination is characterized as dense, thus classifying it as Soil Class C according to TBEC-2018. As per TBEC-2018 (DD-2), the adopted design approach involves a 5% damping ratio. Referring to Turkey's seismic hazard map, the short spectral acceleration of Düzce (S_S) is determined as 1.333g. The corresponding coefficient for short spectral acceleration (f_s) is 1.12. The spectral acceleration for a 1.0-second period (S_1) is also determined as 0.362g, with a coefficient (f_1) of 1.5.
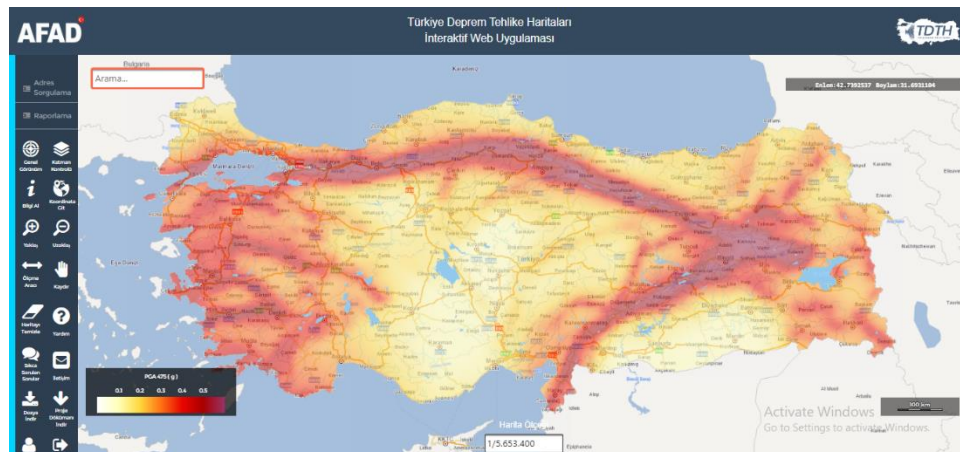
Figure 5.15. Seismic hazard map of Turkey (AFAD)

Consequently, the short-period design spectral acceleration coefficient for the Düzce earthquake (SD_S) is determined as 1.6g, and the design spectral acceleration coefficient for a 1.0-second period (SD_1) is calculated as 0.543g. The calculated values

for T_A and T_B are 0.0679 sec and 0.3394 sec, respectively. According to the code, the long period T_L is established at 6 seconds. The ensuing figure visually presents these values in a diagrammatic representation.
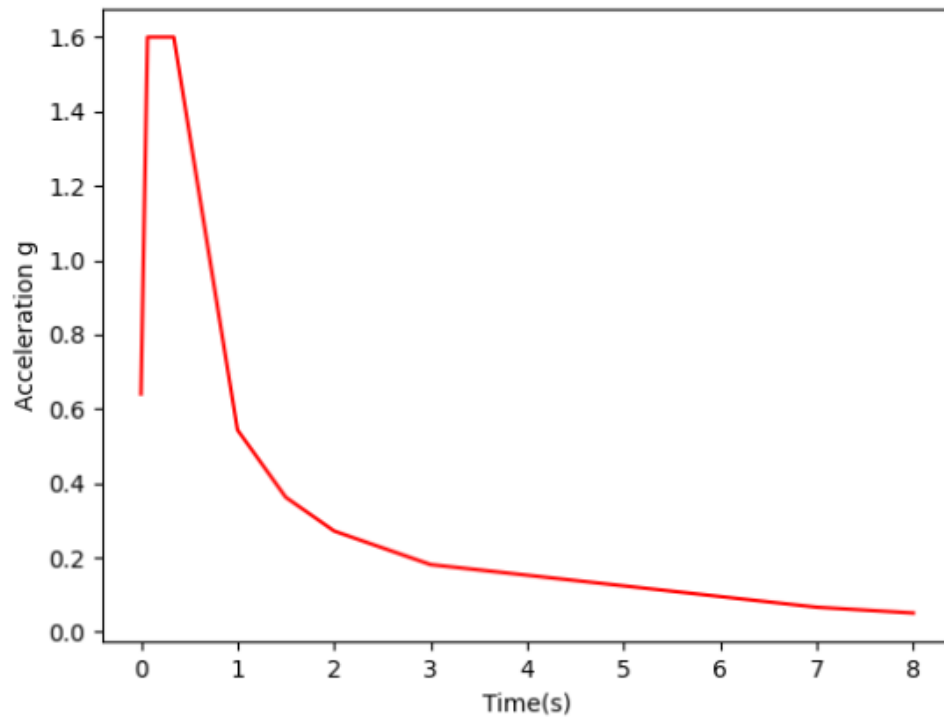
Figure 5.16. Design spectral acceleration of Düzce

When comparing the two graphs -depicting the acceleration spectrum for the Düzce earthquake and the design acceleration spectrum for Düzce- it becomes evident that the constraints and requirements outlined in TBEC-2018 are sufficient to encompass the values of earthquake acceleration, both those that have occurred and those that may potentially occur. This is visually demonstrated in the accompanying figure.
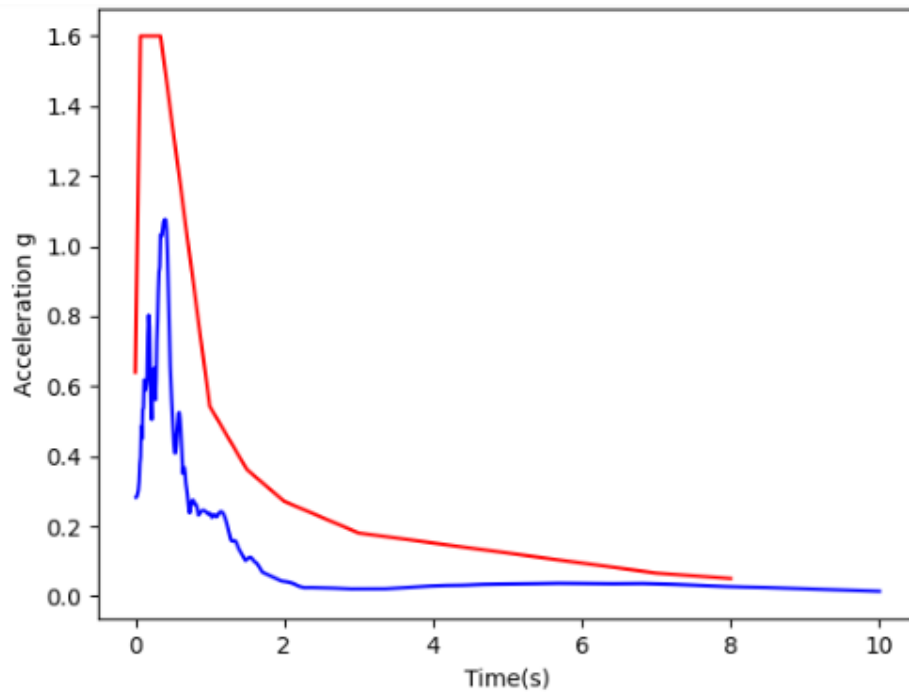
Figure 5.17. Correlation between design spectral acceleration in the Düzce area (red color) and the spectral acceleration of the Düzce Earthquake (blue color).

5.2.2 Model of Jordan

This case study explored the seismic influence on a circular raft pile foundation, specifically focusing on its response to earthquake occurrences in the Dead Sea region of Jordan. The study adhered to consistent soil structure and conditions outlined in the introductory section of this chapter. The seismic event under examination is the 2004 Dead Sea earthquake, distinguished by a moment magnitude of 5.28 and a Peak Ground Acceleration (PGA) of 0.12, as documented by the Ministry of Energy and Mineral Resources of Jordan.
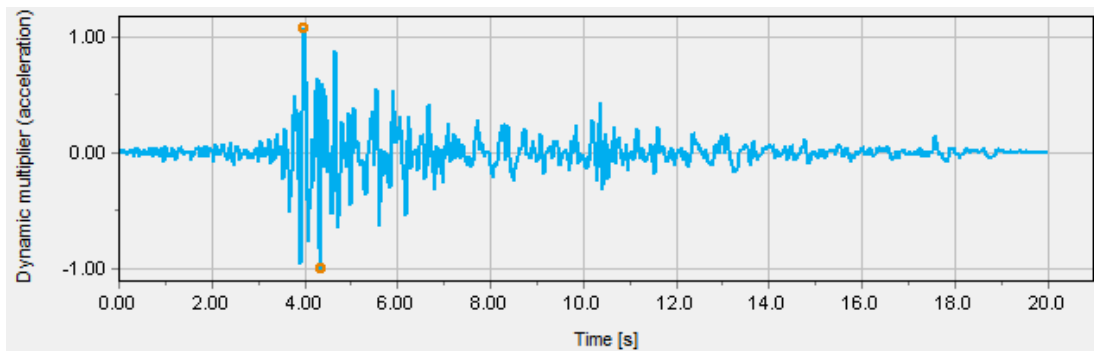
Figure 5.18. Dead Sea earthquake time history analysis

In our case, the Dead Sea earthquake, which had a moment magnitude of 5.28, denotes a moderate seismic event. Situated at a closest distance of 11.6 km from the epicenter. The hypo central distance, spanning 14 km from the earthquake's focal point, provides valuable information about the depth of the seismic source. Notably, the shear wave velocity in the upper 30 meters of soil (Vs30) is measured at 390 m/s. This Vs30 value, according to JBEC-2022, suggests that the soil type in the site can be dense soil and soft rock, which can classify the soil (SC).

The mesh, foundation, and piles were analyzed using PLAXIS 3D, wherein deformations, bending moments, and axial forces were determined.
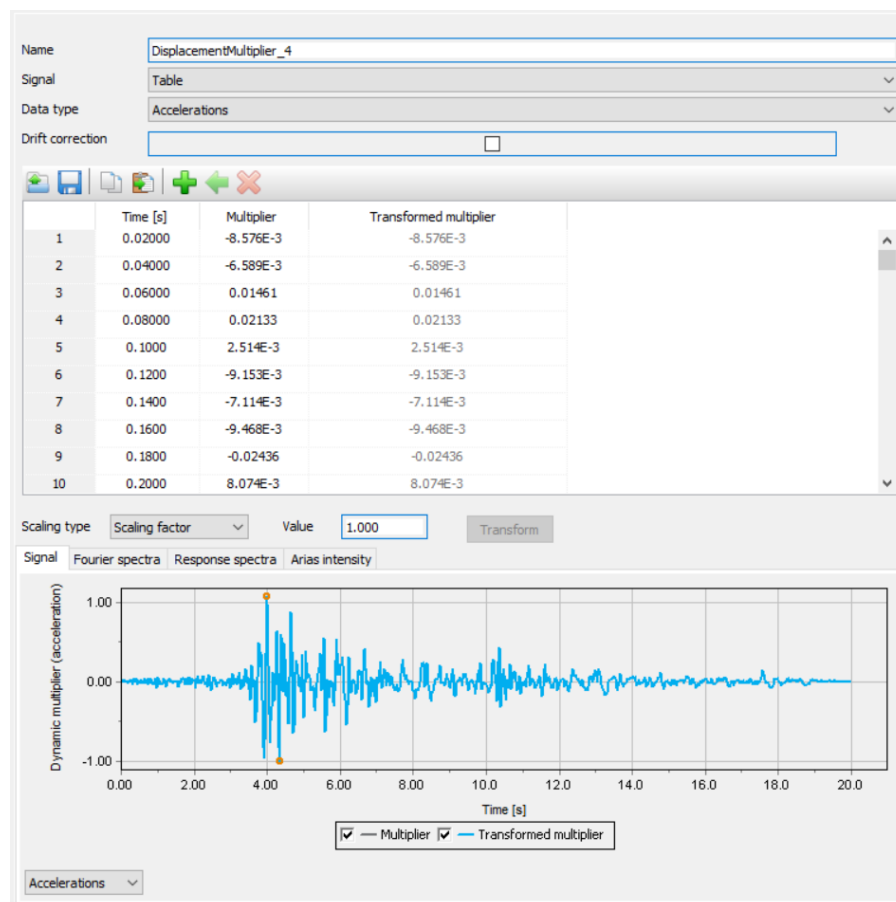
Figure 5.19. Time history analysis by PLAXIS (Dead Sea earthquake)

5.2.2.1 Deformation of Mesh

When subjecting the soil structure to surface loading (150 kN/m²) and seismic forces, the mesh experienced deformation. The maximum deformation, reaching a value of 0.01163 m, specifically at node 671. A normal displacement corresponding

to the mesh deformation was also noted, occurring with precision at element 1197 and node 671. Also, a horizontal displacement of 11 mm was recorded.
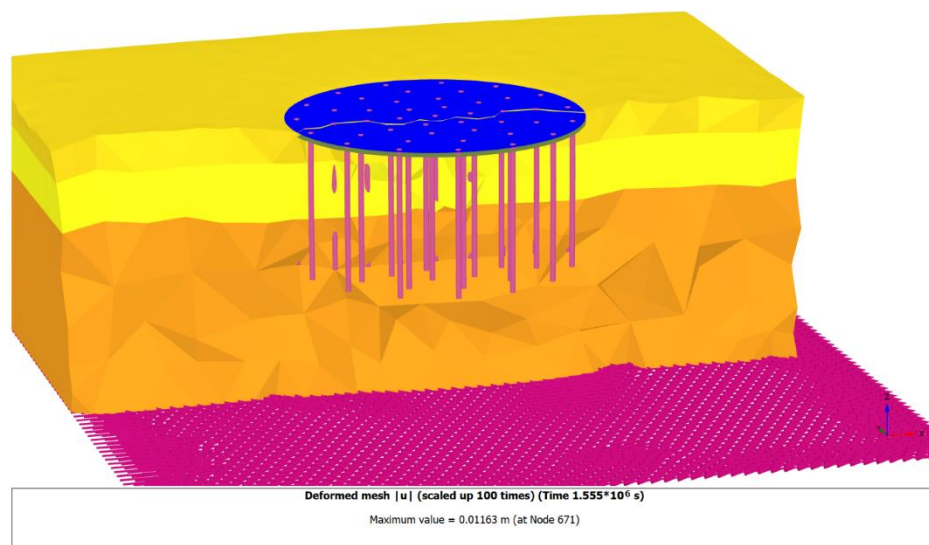
Figure 5.20. Deformation mesh (Dead Sea earthquake)

Total displacements |u| (scaled up 200 times) (Time 1.555*10^6 s)

Maximum value = 0.01163 m (Element 1197 at Node 671)
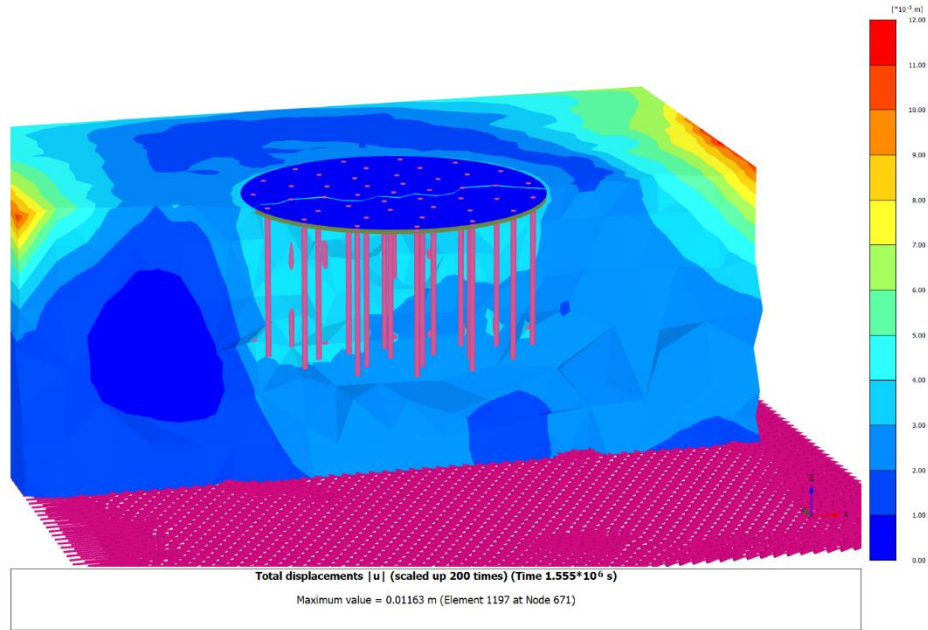
Figure 5.21. Total displacement of mesh (Dead Sea earthquake)

5.2.2.2 Bending Moments of Foundation (Dead Sea Earthquake)

The earthquake analysis scrutinized the bending moments (M11, M22) affecting the foundation. The maximum M_{11} bending moment reached 161.8 kN.m/m at element 231 (node 150), while the minimum M_{11} was -93.21 kN.m/m at element 5 (node 9637). Concurrently, the M_{22} bending moment exhibited a maximum of 142.4 kN.m/m at element 207 (node 140) and a minimum of -109.6 kN.m/m at element 104 (node 9635). These results underscore the dynamic response of the foundation under seismic forces.

Table 5.9 Bending Moment (M_{11}, M_{22}) Values of Foundation (Dead Sea Earthquake)

Moment Type	Maximum Value (kN.m/m)	Location (Element, Node)	Minimum Value (kN.m/m)	Location (Element, Node)
M_{11}	161.8	231, 150	-93.21	5, 9637
M_{22}	142.4	207, 140	-109.6	104, 9635

Bending moments M₁₁ (scaled up 5.00*10⁻³ times) (Time 1.555*10⁶ s)

Maximum value = 161.8 kN m/m (Element 231 at Node 150)

Minimum value = -93.21 kN m/m (Element 5 at Node 9637)
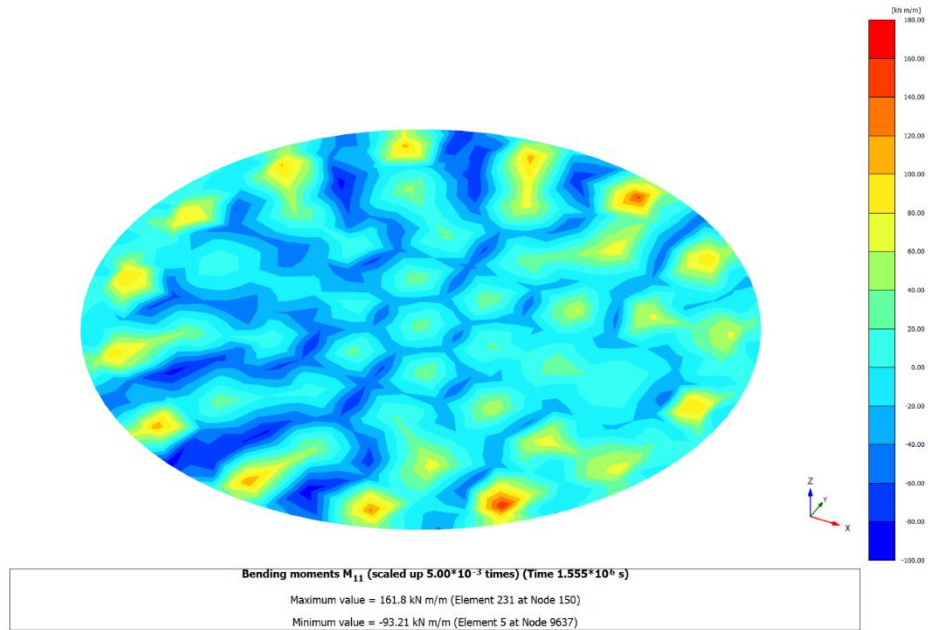
Figure 5.22. Bending moments (M_{11}) of foundation (Dead Sea earthquake

Bending moments M₂₂ (scaled up 5.00*10⁻³ times) (Time 1.555*10⁶ s)

Maximum value = 142.4 kN m/m (Element 207 at Node 140)

Minimum value = -109.6 kN m/m (Element 104 at Node 9635)
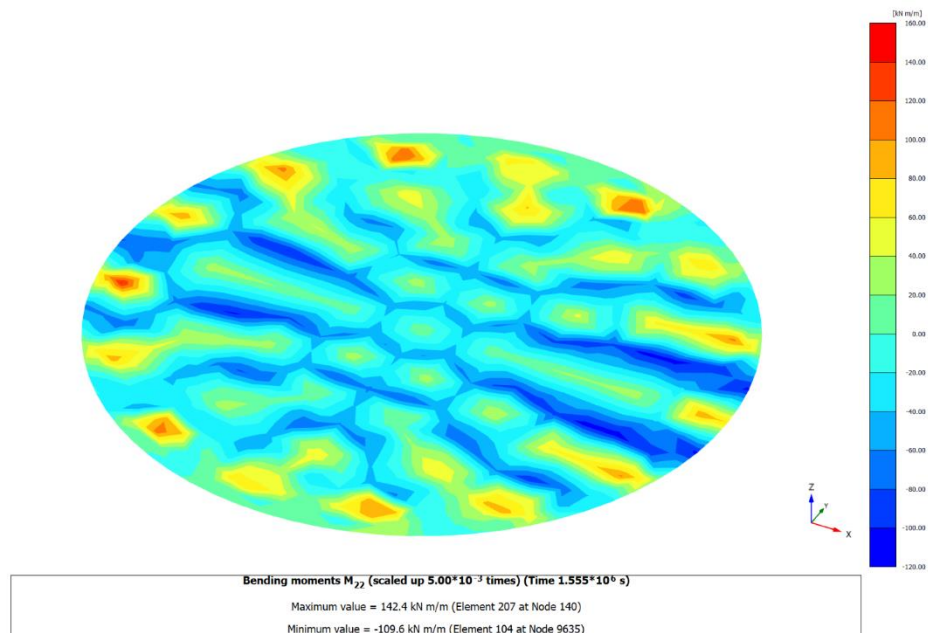
Figure 5.23. Bending moments (M_{22}) of foundation (Dead Sea earthquake)

112

5.2.2.3 Deformation of Piles (Dead Sea Earthquake)

The impact on the piles was scrutinized in analyzing the dynamic behavior induced by the earthquake. This examination encompassed observations of displacement, axial forces acting on the piles, and the values of bending moments.

The outcomes depict a displacement scenario where the maximum value, measuring 3.741×10^{-3} m, was identified at element 182 and node 22320.

Furthermore, the axial forces were scrutinized at the same timestamp. The examination revealed a maximum force of -253 kN exerted on element 219 at node 22648, while the minimum force was observed at element 390 and node 22322, registering at -918.1 kN.

Table 5.10 Axial force values of piles (Dead Sea earthquake)

Parameter	Maximum Value (kN)	Location (Element, Node)	Minimum Value (kN)	Location (Element, Node)
Axial Forces	-253	219, 22648	-918.1	390, 22322

The analysis of bending moments impacting the piles revealed distinct characteristics. Specifically, the bending moment (M_2) exhibited a peak value of 209.3 kN.m on element 463 at node 22786, while the lowest value of -211.2 kN.m was observed on element 1 at node 22813. The bending moments (M3) were also observed, with a maximum value of 159 kN.m affecting element 270 at node 23255 and a minimum value of -176.8 kN.m impacting element 175 at node 22305.

Table 5.11 Bending moment value (M_2, M_3) of piles (Dead Sea earthquake)

Moment Type	Maximum Value (kN.m)	Location (Element, Node)	Minimum Value (kN.m)	Location (Element, Node)
M_2	209.3	463, 22786	-211.2	1, 22813
M_3	159	270, 23255	-176.8	175, 22305

Bending moments M$_2$ (scaled up 5.00*10^{-3} times) (Time 1.555*10^6 s)

Maximum value = 209.3 kN m (Element 463 at Node 22786)

Minimum value = -211.2 kN m (Element 1 at Node 22813)
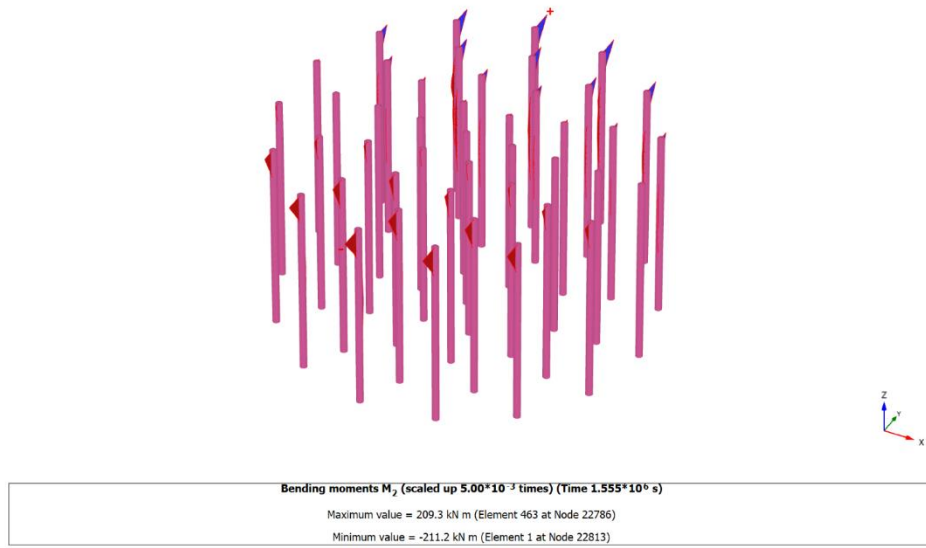
Figure 5.24. Bending moment (M$_2$) values of piles (Dead Sead earthquake)

Bending moments M$_3$ (scaled up 5.00*10^{-3} times) (Time 1.555*10^6 s)

Maximum value = 159.0 kN m (Element 270 at Node 23255)

Minimum value = -176.8 kN m (Element 175 at Node 22305)
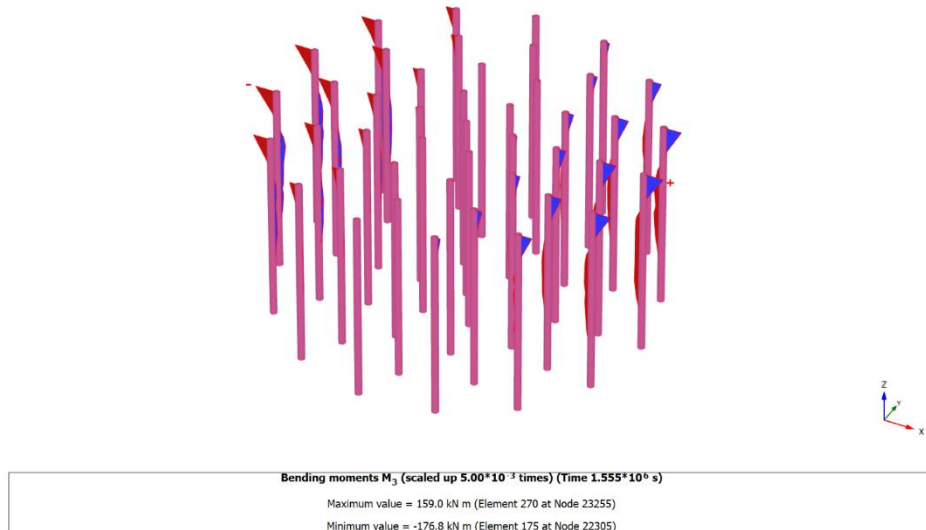
Figure 5.25. Bending moment (M$_3$) of piles (Dead Sea earthquake)

5.2.2.4 Analyzing Earthquake Characteristics Based on (JBEC-2022) Constraints

As in the previous section, examine the spectral acceleration resulting from the Dead Sea earthquake to compare it with the constraints outlined in JBEC-2022. This

evaluation aims to determine if the code successfully meets the necessary conditions for accommodating the acceleration spectrum induced by ground motion. The subsequent figure illustrates the spectral acceleration derived from the Dead Sea earthquake.
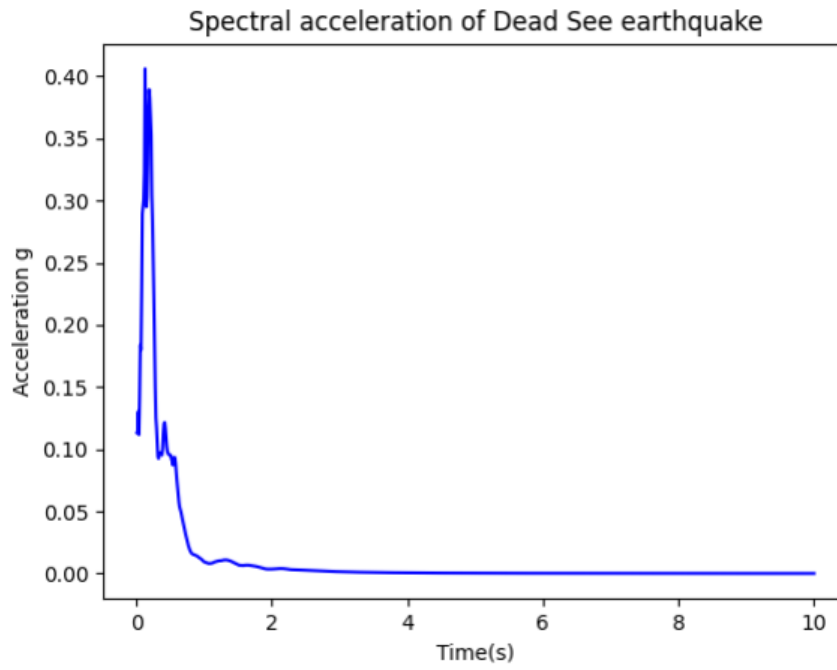
Figure 5.26. Spectral acceleration (Dead Sea earthquake)

Also, to draw design spectral acceleration by JBEC-2022 requirements, it is imperative to first identify the soil class assumed to be impacted by the earthquake. Subsequently, based on the determined soil class, the short spectral acceleration coefficient must be established following JBEC-20202 guidelines and the Jordanian seismic hazard map. Moreover, it is essential to ascertain the corner period of the horizontal elastic design acceleration spectrum using the JBEC-2022 equation (T_0, T_s). Simultaneously, the spectral acceleration at the time period (T_L) is by the specified equation.
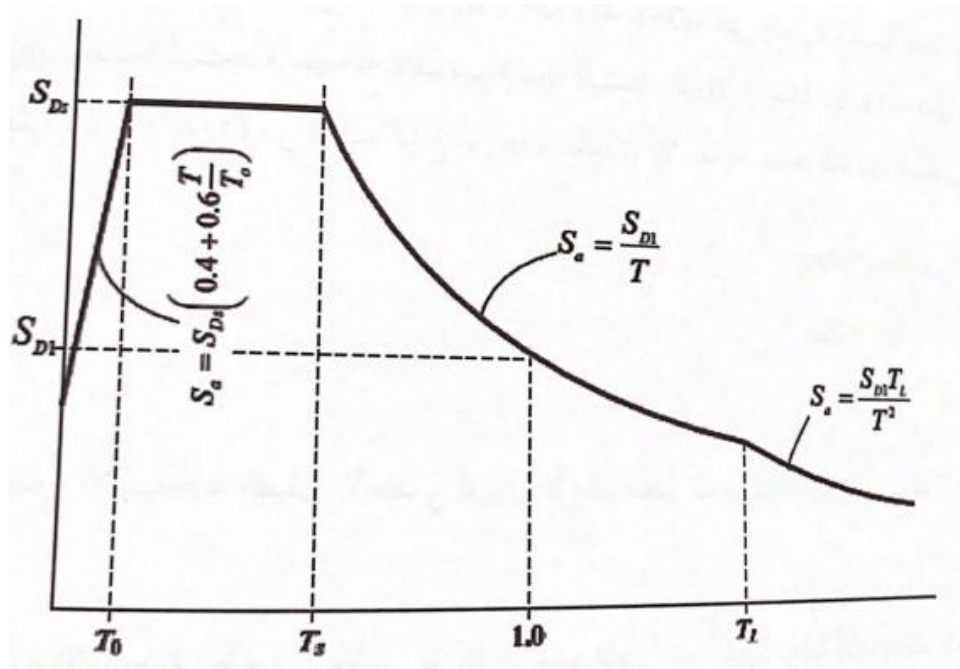
Figure 5.27. Design spectral acceleration according to Jordan Code (JBEC-2022)

Like the previous model, the soil under examination is characterized as dense, thus classifying it as Soil Class C according to JBEC-2022. As per JBEC-2022 (DD-2), the adopted design approach involves a 5% damping ratio. Referring to the seismic hazard map of Jordan, the short spectral acceleration of the Dead Sea (S_S) is determined as 0.702g. The corresponding coefficient for short spectral acceleration (f_a) is 1.15. Additionally, the spectral acceleration for a 1.0-second period (S_1) is determined as 0.257g, with a coefficient (f_v) of 1.55.
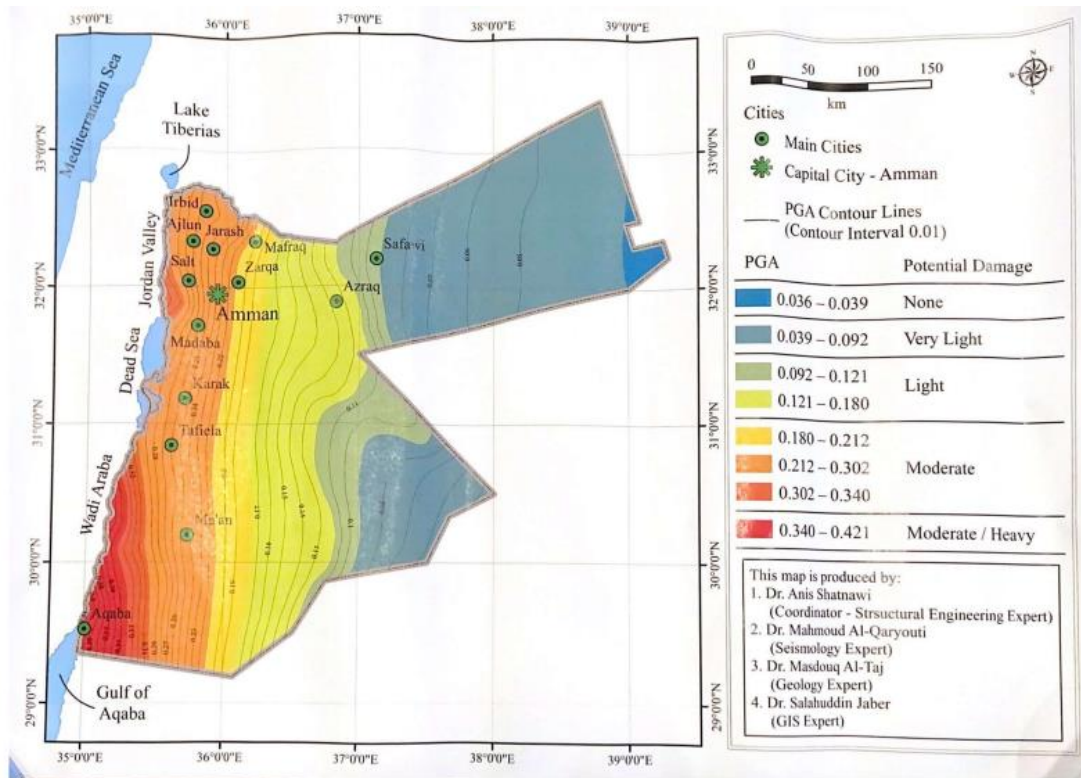
Figure 5.28. Seismic hazard map of Jordan (JBEC-2022)

The short-period design spectral acceleration coefficient for the Dead Sea earthquake (SM_S) is determined as 0.8073g, and the design spectral acceleration coefficient for a 1.0-second period (SD_1) is calculated as 0.39835. The calculated values for T_0 and T_s are 0.0986 sec and 0.493 sec, respectively. According to the code, the long period T_L is established at 6 seconds. The ensuing figure visually presents these values in a diagrammatic representation.
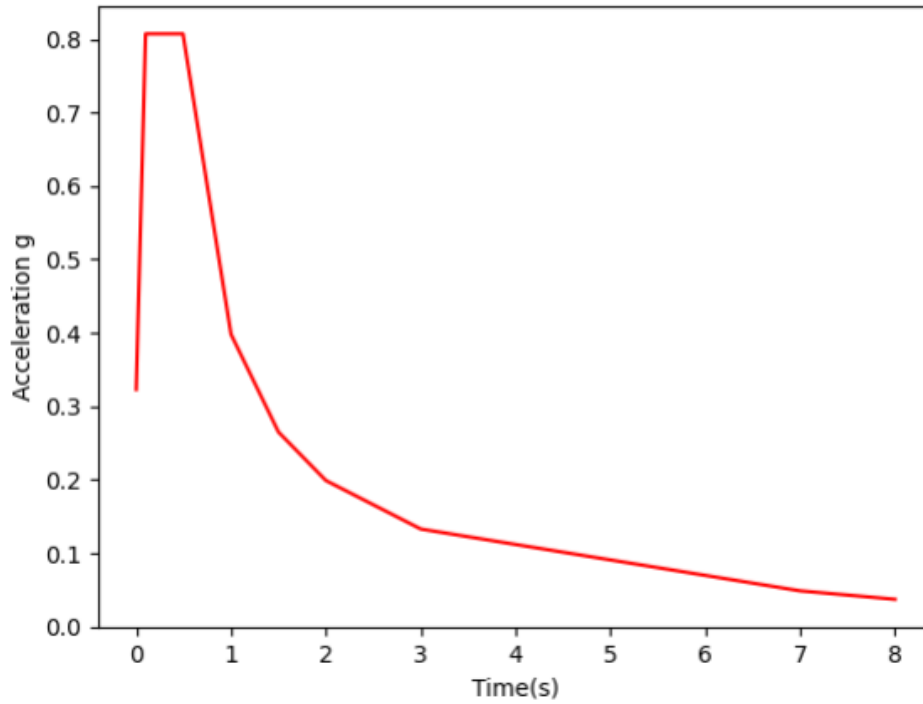
Figure 5.29. Design spectral acceleration of Dead Sea

When comparing the two graphs -depicting the acceleration spectrum for the Dead Sea earthquake and the design acceleration spectrum for the Dead Sea-it becomes evident that the constraints and requirements outlined in JBEC-2018 are sufficient to encompass the values of earthquake acceleration, both those that have occurred and those that may potentially occur. This is visually demonstrated in the accompanying figure.
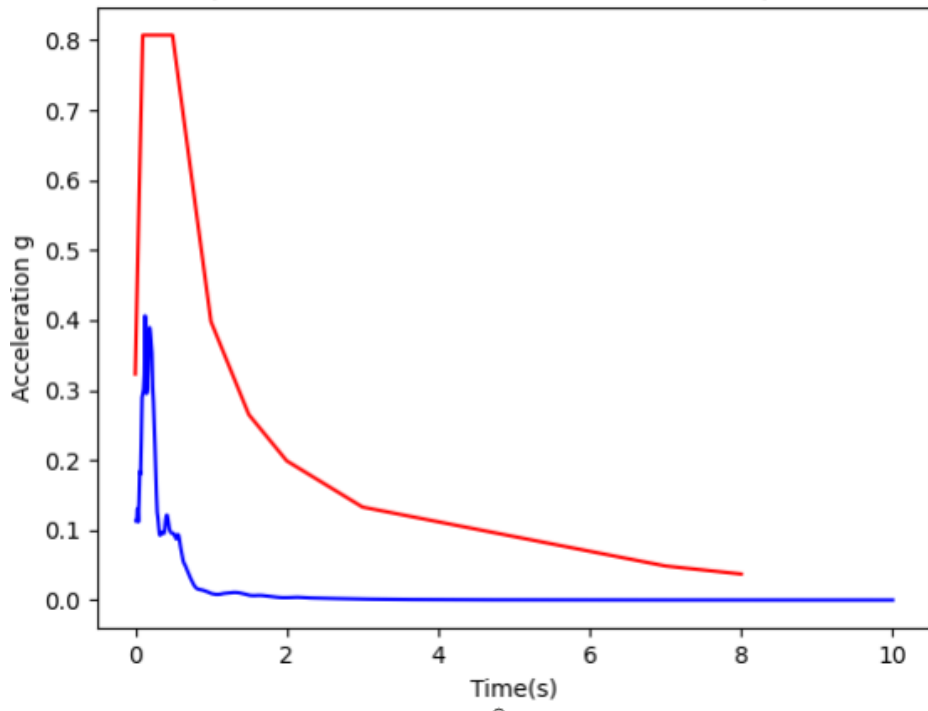
Figure 5.30. Correlation between design spectral acceleration in the Deas Sea area (red color) and the spectral acceleration of the Dead Sea Earthquake (blue color).

CHAPTER 6

6. CONCLUSION AND RECOMMENDATIONS

This study centered on geotechnical earthquake engineering, adhering to the earthquake standards established in Turkey and Jordan. The significance lies in comprehending the seismic impact on soil and assessing resultant damages with implications for human safety. The investigation delved into the regulatory framework's operative in Turkey and Jordan, aiming to discern their commonalities and disparities. The endeavor sought to elucidate the distinctions and parallels, recognizing that both standards necessitate stringent conditions to mitigate potential harm to human life and infrastructure.

Due to the significance of the study, the initial section in chapter one introduces the importance of the geotechnical earthquake engineering field. It emphasizes the study's focus on investigating the geotechnical earthquake engineering standards applied in Turkey and Jordan. The chapter outlines the research problem, poses relevant questions, and discusses the study's objectives and contributions. The primary objectives include comparing and analyzing the geotechnical earthquake engineering standards in Turkey and Jordan, evaluating their effectiveness based on historical earthquake data, and drawing lessons from both regions. The chapter also elucidates the methodology employed in the thesis.

In transitioning to chapter two, clarity and comprehension for researchers are essential. Therefore, providing a concise overview of fundamental concepts in geotechnical earthquake engineering was imperative. This includes discussions on the causes of earthquakes, plate boundaries, faults, seismic waves, and an overview of seismic hazards and soil dynamics. Additionally, the chapter delves into a review of previous research conducted on geotechnical earthquake engineering in Turkey and

Jordan. This review offers insights into seismic events in both countries and explores the relevant standards.

The study identifies one of the most significant factors contributing to earthquakes as quick slips, characterized by abrupt displacements along tectonic faults. This phenomenon leads to a substantial release of accumulated stress and the subsequent release of seismic energy. The fault displacement may result in the burial of one layer under another. The chapter delved into the seismic waves generated during earthquakes and examined their susceptibility to local site conditions and topography. The deformation, such as wave amplification, was explored, emphasizing the notable spatial variability in seismic ground motion and frequency content shifts. This underscores the importance of meticulously considering these factors in the design of constructions.

Moreover, a comparison was drawn among different types of seismic waves. P-waves and S-waves (Body waves) emerged as the fastest, while Rayleigh and Love waves (Surface waves) were slower. It is worth noting that as the speed of the wave increases, the amplitude of the wave decreases.

In examining seismic hazards, it is crucial to emphasize the importance of probabilistic seismic hazard analysis. This analysis considers ground motion intensity and necessitates careful identification of earthquake sources with the potential to generate destructive ground motions. Furthermore, it involves an assessment of potential magnitudes, the distance between the earthquake's epicenter and the affected areas, and various other relevant parameters.

Upon reviewing pertinent studies, it has been established that landslides represent a considerable earthquake hazard, constituting around 27% of all natural hazards in Turkey. This risk is particularly pronounced in Northwestern Anatolia. Additionally, regions in northern Turkey, such as Rize, are vulnerable to landslides, primarily due to the annual occurrence of heavy rainfall. Similarly, areas in Jordan, including Irbid and Jerash, are also prone to landslides. Furthermore, liquefaction was observed in numerous areas subjected to earthquakes in both countries.

In chapter three, the investigation delves deeper into the seismic activities of Turkey and Jordan, conducting a thorough comparison and analysis of the findings. This examination holds significant importance in continually improving seismic standards in both countries. Notably, Turkey exhibits the pivotal North Anatolian Fault System (NAFS) and East Anatolian Fault System (EAFS), crucial in facilitating the

westward motion and interactions of tectonic plates. Conversely, Jordan includes the Dead Sea Transform Fault (DSTF), entangled in the intricate interactions of the Arabian and African Plates, along with the Jordan Rift Valley Fault System. The Anatolian Plate's interactions predominantly influence the fault systems in Turkey, while the Arabian Plate shapes those in Jordan and the rifting processes occurring in the Jordan Rift Valley.

Many investigations into earthquakes in Turkey have highlighted that the buildings that collapsed during seismic events were often old, predating the code updates. Additionally, it was observed that the rules and instructions specified in the code were not consistently applied. The significant earthquake in Kahramanmaraş in 2023 raised concerns, as the maximum acceleration recorded reached a staggering 2.4g, surpassing the design acceleration specified by the code at 1.4g. This underscores the necessity to revisit and reassess this aspect, especially considering lessons learned from earlier earthquakes that led to the improvement of the code in 2018.

The region with active seismicity in Jordan encompasses the Jordan Rift Valley, the Dead Sea area, and the Gulf of Aqaba. However, when comparing the magnitudes of earthquakes in this region with those in Turkey, the magnitudes are generally lower. Furthermore, the buildings that collapsed or sustained significant damage in Jordan were attributed to the low quality of construction and the materials used. This was evident in the Al-Aqaba and Dead Sea earthquakes despite their moderate magnitudes. It should be noted that, at that time, the building codes and regulations had not been updated.

Notable distinctions emerge in comparing the frequency, magnitude, and peak ground acceleration between Turkey and Jordan. Turkey, located in a seismically active region with major fault systems such as the North Anatolian Fault, exhibits a higher frequency of earthquakes. Conversely, Jordan, positioned along the Dead Sea Fault System, has a lower frequency of earthquakes, with significant events like the 1927 Jericho earthquake and the 1995 Gulf of Aqaba earthquake.

Magnitude-wise, Turkey has witnessed some of the world's largest earthquakes, exceeding 7.0 in magnitude and resulting in substantial damage and loss of life. While also experiencing noteworthy earthquakes, Jordan generally has lower-magnitude events, typically below 5. In conclusion, the peak ground acceleration resulting from seismic waves in Jordan is less than in Turkey. Jordan is characterized by fewer earthquakes with significant impact, as indicated in the table.

Table 6.1 Comparison between Turkey and Jordan in earthquake's PGA

Turkey			
Earthquake	Magnitude (Mw)	Buildings Damage	PGA (g)
Kahramanmaraş (2023)	7.8 / 7.5	40000	2.4
Van (October 2011)	7.2	15000	0.17
Edremit (November 2011)	5.7	25	0.09
Kocaeli (August 1999)	7.4	77342	0.4
Düzce (November 1999)	7.2	33000	0.3
Çay-Eber (2002)	6	10000	0.113
Sivrice (2020)	6.8	14747	0.292
Jordan			
Earthquake	Magnitude (Mw)	Buildings Damage	PGA (g)
Gulf of Aqaba (1995)	7.1	Eilat = 57, Cairo = 8, Jordan = 1, all most the building cracks	0.113
Dead Sea (2004)	5.28	Some of the old buildings were damaged	0.157
Jericho (1927)	6.2	Jerusalem = 300, Nablus = 700, Jordan = 500, Ramla & Lod = 100	-

Turkey experiences at least one earthquake annually with a magnitude of 5, making it the third most earthquake-prone country in terms of losses caused by earthquakes and the eighth in terms of the total number of people affected. The highest number of earthquakes was recorded in 2023, exceeding 50,000, including various magnitudes and aftershocks. Conversely, in 2001, the lowest number of earthquakes was observed, totaling 599 (AFAD). In contrast, Jordan encounters an average of 150 earthquakes annually, typically with a magnitude of 2.5. The minimum recorded number of earthquakes in a year is 60 (MEMR). However, it is crucial to emphasize that this does not diminish the importance of reviewing building standards and

earthquake mitigation measures in Jordan, as preparedness and safety remain essential considerations.

In Turkey, several earthquakes have exhibited soil liquefaction, observed in the İzmit Earthquake in 1999, the Kocaeli Earthquake in 1999, and the Van Earthquake in 2011, where liquefaction, particularly in sand boils, and the Sivrice Earthquake 2020 liquefaction-induced sand boils was observed in these earthquake locations.

Amplification and lateral spreading were also noted in the Edremit earthquake of 2011.

In Jordan, Aqaba City, located along the Gulf of Aqaba shore, exhibits susceptibility to liquefaction in some coastal regions. The Dead Sea area in Jordan experiences various soil deformations, including subsidence and landslides. Liquefaction occurs in the region during earthquakes with a magnitude of 6.0 or higher, often accompanied by lateral spreading.

Due to seismic activity, liquefaction is common in both countries, but amplification phenomena are more prevalent in Turkish earthquakes. Turkey has observed boiling sand phenomena more frequently than Jordan. On the other hand, Jordan's earthquakes are characterized by subsidence, lateral spreading (even in non-seismic areas due to water pressure), and occasional tsunamis caused by faults in the nearby sea.

Chapter four delves into Turkey and Jordan's geotechnical earthquake engineering standards. The chapter includes a comprehensive literature review that examines these standards from various perspectives. Notably, the discussion extends to exploring the differences and similarities in the latest versions of these standards. While numerous researchers have extensively covered Turkey's standards, encompassing both general aspects and specific geotechnical earthquake standards, the analysis reveals a notable gap in the literature concerning the review of Jordan's standards, particularly in geotechnical earthquake engineering. This study serves as a pioneering effort, being the first to undertake a comparative analysis between the standards of Turkey and Jordan, with a specific focus on geotechnical earthquake engineering. Consequently, this section contributes significantly to the study's overall goal by addressing and filling the existing gap through meticulous analysis and discussion of the standards.

Through investigations in studies comparing the American standard (ASCE 7-15) with the Turkish Building Earthquake Code of 2018 (TBEC-2018) and that of 2007

(TEC-2007) concerning reinforced concrete buildings, it was observed that the American standard undergoes updates every three to five years, while the Turkish code may see updates every ten to twenty years. The results revealed that ASCE 7-16 allows longer vibration periods with lower spectral acceleration, followed by TBEC-2018 and TEC-2007. There are similarities between ASCE 7-15 and TBEC-2018 regarding soil classification and soil profile requirements. Additionally, TBEC-2018 employs a more refined approach than TEC-2007, considering factors such as site class, design category, occupancy category, building height, and seismic design category. Specific building categories, such as army barracks, schools, and museums, are accorded more significant importance in TBEC-2018 compared to TEC-2007.

The allowable relative displacement between building floors is up to 0.016 mm in TBEC-2018, whereas ASCE 7-16 and TEC-2007 allow up to 0.02 mm, indicating stricter requirements for deformation control during earthquakes.

The TBEC-2018 introduces an updated seismic hazard map, employing a spectral acceleration approach to express hazard levels based on various periods or frequencies of ground motion.

Owing to the significance of soil investigations for construction projects, the Turkish and Jordanian codes necessitate a comprehensive report detailing the soil profile and providing geotechnical design parameters.

The Turkish and Jordanian codes classify soil using shear wave velocity (m/s), average standard penetration resistance (number of blows/m), and soil undrained shear strength. The Turkish code uses symbols (ZA-ZF), while the Jordanian code uses symbols (SA-SF). There are notable differences in the undrained shear strength values for ZC - SC, ZD - SD, and ZE - SE soil classes. For ZC-SC, the Turkish code requires a value greater than 250 kPa, whereas the Jordanian code requires a value greater than 100 kPa. For ZD-SD, the Turkish code requires a value greater than 70 kPa and less than or equal to 250 kPa, while the Jordanian code requires a value greater than 50 kPa and less than or equal to 100 kPa. The Turkish code requires a value of less than 70 kPa for ZE-SE, whereas the Jordanian code requires less than 50 kPa.

Both codes classify soils that require special analysis underclass (ZF-SF), as these soils may be susceptible to failure or collapse under earthquake effects. Such soils include those prone to liquefaction, clay soil, quick clays, and weakly cemented soil. However, there are some differences in the classification criteria between the two codes:

1. In the Jordanian code, for the (SF) class, clay soil with high plasticity must have a depth greater than 7.5 meters and a plasticity index (PI) greater than 75. This implies that the liquid limit (LL) value can be higher than 75% to classify the clay soil as having high plasticity. On the other hand, in the Turkish code, the depth requirement is greater than 8 meters, and the plasticity index (PI) must be greater than 50. This means the Turkish standard classifies the clay soil as having high plasticity when the liquid limit (LL > 50%) indicates that the Turkish standard is more restrictive with clay soil.

2. For soft clay soils with intermediate strength and high depth, the Jordanian code requires the depth to be greater than 36 meters, while the Turkish code requires the depth to be greater than 35 meters. In this case, only the Jordanian code includes a requirement for undrained shear strength ($C_u < 50$ kPa), whereas the Turkish code does not mention it.

The Turkish building code classifies building importance factors into three categories, whereas the Jordanian code utilizes four categories. The categories are seen in the Turkish factor of 3, encompassing both I and II in the Jordanian code. However, a difference arises in structures of moderate importance, with the Turkish code assigning it a factor of 1.2, while the Jordanian code assigns 1.25.

Both standards rely on seismic design criteria based on the forces generated by ground earthquake movements. The requirements consider a design period of 50 years with a 10% probability of exceeding the minimum ground earthquake force, considering a longer earthquake recurrence period of 475 years, with a damping rate of 5% from critical damping.

The study identified variations in the local ground effect coefficients for the short-period region (F_s - F_a) between TBEC-2018 and JBEC-2022. These variations can be attributed to Turkey's seismic and geographical characteristics. TBEC-2018 provides these coefficients for spectral acceleration (S_s) values greater than or equal to 1.50g, while JBEC-2022 specifies values for $S_s > 1.25$g. Both standards exhibit similarities in local ground effect coefficients for the short-period region (F_s and F_a) for certain site types (ZA-SA, ZD-SD). However, differences emerge in coefficients for site types (ZB-SB, ZC-SC, ZE-SE). Notably, for site classification (ZC, SC), TBEC-2018 generally indicates higher values compared to JBEC-2022. Regarding local ground class (ZE-SE), TBEC-2018 tends to have higher values in most cases, except for $S_s \leq 0.25$g, where JBEC-2022 has a higher value.

Primarily, TBEC-2018 emphasizes higher spectral acceleration values, notably evident in the 1.0-second period. TBEC-2018 specifies spectral acceleration values equal to or greater than 0.60g for this period, while JBEC-2022 only provides local ground effect coefficients for 1.0-second spectral acceleration values equal to or greater than 0.50g.

Furthermore, the values of local ground effect coefficients for 1.0-second spectral acceleration coefficients align consistently between the two standards only for site class (ZA-SA), where they maintain a constant value of 0.8 across all spectral acceleration coefficients. However, variations in these values arise for other site classes.

In the comparison of site coefficients for various spectral acceleration coefficients, specifically for local ground effect coefficients at 1.0 second, between TBEC-2018 and JBEC-2022, the following observations emerge:

1. For site class (ZB-SB), JBEC-2022 generally exhibits higher values than TBEC-2018.

2. Values vary in site class (ZC-SC), with some higher in JBEC-2022 and others higher in TBEC-2018.

3. Site class (ZD-SD) generally has higher values in TBEC-2018, except for spectral acceleration values ≤ 0.10g.

4. Site class (ZE-SE) shows higher values in TBEC-2018 for the first two spectral acceleration coefficients, while the value for $S_1 \geq 0.50$g is higher in JBEC-2022.

Regarding defining earthquake design classes, differences were identified between TBEC-2018 and JBEC-2022 in categorizing earthquake design classes based on spectral acceleration coefficients for short periods (SD_S). JBEC-2022 initiates classification from spectral acceleration values less than 0.167g, considering Jordan's exposure to this spectral acceleration. In contrast, TBEC-2018 starts the classification from spectral acceleration values less than 0.33g and continues up to values larger than 0.75g. JBEC-2018, on the other hand, classifies up to 0.5g.

Both codes amplify the building importance factor by multiplying it by (1.5). However, TBEC-2018 stipulates this requirement when the short period's spectral acceleration coefficient (SDs) exceeds 0.65g. In contrast, JBEC-2022 mandates this condition when the spectral acceleration coefficient (SD_S) for a short period exceeds 0.5g, where, according to the seismic conditions in Jordan, this value is relatively high.

As there are some differences between the codes in the part of the structure, they both employ an empirical approach to determine the dominant natural vibration period of a building. In both cases, this is calculated by multiplying an empirical natural vibration period coefficient by the total height of the upper part of the building above the basements [m] raised to a specific power. The key distinction lies in the exponent for the height term: TBEC-2018 fixes it at 3/4, whereas JBEC-2022 determines it based on the empirical natural vibration period coefficient associated with the building type. The empirical natural vibration period coefficient (C_t) also varies between the two codes. For instance, TBEC-2018 is set at 0.08 for steel-framed buildings, while JBEC-2022 uses 0.0724. Similarly, TBEC-2018 sets Ct at 0.07 for other building types, while JBEC-2022 employs 0.0488, highlighting a significant variation.

For deep foundation ties, both codes concur that ties should be designed to withstand tension and compression, not less than 0.10 times the short period spectral acceleration (SD_S) multiplied by the largest sum of dead and live loads on the wedge or column cap.

There are differences in determining the base shear force between the two codes. Both codes use the same equation based on the short period's spectral acceleration, the building's total weight, and the earthquake load reduction coefficient. However, the earthquake load reduction coefficient is treated differently in TBEC-2018 and JBEC-2022. In TBEC-2018, this coefficient is a constant value equal to 4. On the other hand, JBEC-2022 allows for variations, ranging from 1.5 to 8, depending on the type of building. Additionally, JBEC-2022 multiplies the base shear force equation by a factor between 1 and 1.2 for three-story buildings.

The results regarding shallow foundations indicate that both codes agree on the conditions for using shallow foundations. These conditions include when the width of the foundation is greater than the foundation depth, with a general requirement that the foundation depth should be less than 3 meters. Moreover, attention should be paid to groundwater conditions.

TBEC-2018 favors using Hansen's equation to determine the bearing capacity of shallow foundations, while JBEC-2022 prefers Meyerhof's equation. While both equations share similarities, Hansen's equation, an extension of Meyerhof's, requires the determination of additional factors such as foundation soil slope coefficients and foundation base slope coefficients. Hansen's equation is typically applied in more complex cases where these other considerations become significant.

Upon investigation of both codes, the study revealed that TBEC-2018 mandates a more intricate equation for SPT correction. This equation involves corrections for geological stress (depth), rod length, sampler type, drilling drill diameter, and energy ratio. In contrast, JBEC-2022 utilizes a simpler equation, considering only the geological stress (depth) correction coefficient and the field value of the number of blows without correction.

Notable distinctions exist between the two codes. TBEC-2018 emphasizes liquefaction resistance calculation, considering factors like cyclic resistance ratio at earthquake magnitude 7.5 ($CRR_{M7.5}$), design earthquake moment magnitude, short-period design spectral acceleration, and coefficient of stress reduction. In contrast, the Jordanian code (JBEC-2022) primarily focuses on factors such as effective stress, total effective stress, peak horizontal acceleration at the ground surface, and gravitational acceleration. Additionally, it is worth noting that in TBEC-2018, the safety factor against liquefaction must be greater than or equal to 1.10, whereas in JBEC-2022, it must be greater than or equal to 1.0. This variance can be attributed to differences in soil characteristics between Turkey and Jordan. Turkey's soil has lower resistance to liquefaction compared to Jordan's soil. Furthermore, variations in the number and magnitude of earthquakes experienced by each country have also influenced these differing safety factor requirements.

Additionally, regarding the safety factor, a notable difference was observed in the safety factor against overturning retaining walls. TBEC-2018 requires the factor to be greater than 1.3 for incohesive soil, while JBEC-2022 mandates it to be larger than 1.5. Similarly, TBEC-2018 specifies a factor larger than 1.3 for cohesive soil, whereas JBEC-2022 stipulates a requirement of greater than 2.

Both codes are similar in determining the coefficients of active earth pressure (k_a) and passive earth pressure (k_p). However, a notable difference arises in their treatment of dynamic water pressure induced by seismic activity, with the Turkish code providing a more detailed approach to determining dynamic water pressure.

In Chapter Five, the study conducted case studies using the PLAXIS 3D software, employing finite element methods and dynamic analysis. The analysis focused on a circular raft pile foundation designed on sandy soil subjected to a 150 kN/m2 surface load and varying earthquake magnitudes. Two PLAXIS models were created: one for analyzing the Düzce earthquake in Turkey with a moment magnitude of 7.14 and PGA of 0.3g, based on recorded data from stations IRIGM 487 and PEER

RSN (8164). The second model analyzed the Dead Sea earthquake in Jordan with a moment magnitude of 5.28 and PGA of 0.12, based on data from the Ministry of Energy and Mineral Resources of Jordan. Both models shared the same properties, differing only in earthquake magnitude.

In these models, 44 piles with a diameter of 60 cm were distributed within the circular foundation. The study focused on analyzing the deformation of the mesh, foundation, and piles under the combined effects of surface load and earthquake-induced dynamic loads.

By analyzing the results, the study identified a significant difference in the impact of the Düzce earthquake on the mesh compared to the effect of the Dead Sea earthquake. The maximum deformation of the mesh caused by the Düzce earthquake was 35.9 mm, whereas the deformation induced by the Dead Sea earthquake was 11.6 mm. Additionally, the Düzce earthquake substantially affected mesh displacement, resulting in a displacement of 32.5 mm. In comparison, the Dead Sea earthquake caused a displacement of 11.16 mm, indicating a considerable disparity in their influence.

In terms of analyzing the bending moment (M_{11}) due to bending over the horizontal axis of the foundation, the results revealed similarities in the values. Both earthquakes affected element 231 and node 150, resulting in a maximum bending moment of 161.8 kN.m/m. For the Düzce earthquake, the minimum bending moment occurred at element 5 and node 9637, with a value of -93.71 kN.m/m, higher than the minimum value of the Dead Sea earthquake at -93.21 kN.m/m. It's important to note that the sign indicates the direction of the bending moment considerations.

In addition, the results of the analysis of the bending moment over the vertical axis (M_{22}) of the foundation generally show lower values than the bending moment over the horizontal axis of the foundation for both models. The maximum bending moment ($M22$) value for the Düzce earthquake was 142.8 kN.m/m at element 207 and node 140, while the minimum value was -109.7 kN.m/m. These values are slightly higher than the maximum (M_{22}) value of the Dead Sea earthquake, 142.4 kN.m/m, with a minimum value of -109.6 kN.m/m at the same element and node. It is noticeable that the values are very close.

In the analysis of pile deformations, the piles exposed to the Düzce earthquake exhibited significantly higher displacement values, with a maximum displacement of 28.22 mm recorded at element 205 and node 22456. In contrast, the maximum

displacement due to exposure to the Dead Sea earthquake values was much lower, measuring 3.7 mm at element 182 and node 22320.

Moreover, the axial force acting on the piles showed higher values during the Düzce earthquake. The maximum axial force recorded was -920.5 kN.m/m at element 390 and node 22322. Comparatively, for the Dead Sea earthquake values, the maximum axial force at the same element was slightly lower at -918.1 kN.m/m. The values are very close, and the sign indicates compression and tension considerations.

In the analysis of the bending moment around the x-axis of piles (M_2), the results indicate that for the Düzce earthquake, the maximum value recorded was 209.7 kN.m/m at element 463 and node 22786. In comparison, the maximum value due to the Dead Sea earthquake at the same element was 209.3 kN.m/m. A slight difference was observed in the minimum values, where the Düzce values reached -211.6 kN.m/m, while the Dead Sea values were slightly lower at -211.2 kN.m/m. Although the results are close, the Düzce earthquake still exhibited higher values.

In analyzing the bending moment of piles around the third axis (M_3), the results revealed that for the Düzce earthquake, the maximum value occurred at element 270 and node 23255, reaching 160.3 kN.m/m. In contrast, the maximum value for the Dead Sea earthquake was slightly lower at 159.0 kN.m/m. Similarly, for the Düzce earthquake, the minimum recorded value was -177.3 kN.m/m, while for the Dead Sea earthquake, the minimum value was -176.8 kN.m/m. The differences between the maximum and minimum values are relatively small.

The results from both models exhibited close similarities, which can be attributed to various factors. The models shared similar details, including soil and foundation properties, as well as the nature of the structure, with the inclusion of piles that enhance earthquake resistance. Despite differences in earthquake magnitudes and PGAs, the specific ground motions used in the analysis may have similarities. This suggests an indication of the ground motion risk in Jordan. The close results imply that an earthquake with a moment magnitude of 5.28 in Jordan may pose a similar and significant risk as an earthquake with a moment magnitude near 7 in Turkey. This observation aligns with the closeness in requirements between JBEC-2022 and TBEC-2018.

Furthermore, a comprehensive analysis of the design spectral acceleration for both regions was conducted to ascertain the adequacy of the Turkish and Jordanian codes in addressing the earthquakes and ground motions that have occurred or may

occur. This analysis also examined the spectral acceleration resulting from the earthquakes utilized in the models. The process involved gathering various data stipulated by the codes, including determining soil class, short spectral acceleration, and spectral acceleration for a 1.0-second period.

Following this rigorous analysis, the study determined that the Turkish and Jordanian codes incorporate constraints and requirements that render them robust and capable of efficiently managing earthquake-related challenges. This conclusion holds, at least to the extent investigated in this thesis.

For future research, it is recommended to conduct further studies comparing Turkish and Jordanian standards, addressing general aspects, and focusing on geotechnical earthquake engineering. Additionally, exploring the effects of various earthquakes from both Turkey and Jordan on different soil types and applying these findings to the design of various structural elements, including retaining walls and embankments, would be valuable. Multiple studies are suggested for future work, including comparisons between Turkish standards and those used in regions with high earthquake risk, particularly in geotechnical earthquake aspects. Moreover, improving the earthquake database and staying updated on technological advancements is highly recommended, which can assist researchers in conducting more valuable studies.

REFERENCES

Abderahman, N. & Darwish, A. (2001). Geological and geotechnical characteristics of Karameh dam site, north of the Dead Sea, Jordan. *Bull Eng Geol Environ*. (Vol. 60). 291-299.doi: 10.1007/s100640100118.

Abou Karaki, N. Closson, D. & Salameh, E. et al. (2008). Natural, Induced and Environmental Hazards Along the Dead Sea Coast, Jordan. *Hydrogeologie und Umwelt*. (Vol. 14). 1-24.

Ahmad, I. (2023). Key Building Design and Construction Lessons from the 2023 Türkiye–Syria Earthquakes. *School of Architecture and Built Environment*. (Vol. 3, Issue 1). 104-106. doi: 10.3390/architecture3010007.

Akin, M. Ozvan, A. Akin, M. K. and Topal, T. (2013). Evaluation of Liquefaction in Karasu River Floodplain After the October 23, 2011, Van (Turkey) Earthquake. *Natural Hazards.* (Vol. 69). 1551–1575.

Aksoylo, C. Mobark, A. Arslan, M. & Erkan, I. (2020). A Comparative Study on ASCE 7-16, TBEC-2018 and TEC-2007 for Reinforced Concrete Buildings. *Revista de la Construcción.* (Vol. 19, Issue 2). 282-305. doi: 10.7764/RDLC.19.2.282.

Al-Amoush, H. (2016). Landslide Investigation Using Transient Electromagnetic Method (TEM): A Case Study on Al-Ja'ydyya- Salhuob Landslide / Jordan. *Civil and Environmental Research.* (Vol.8, Issue 12). 1-12. doi: 10.7176/CER.

Al-Tarazi, E. (2000). The Major Gulf of the Aqaba Earthquake, 22 November 1995 – Maximum Intensity Distribution. *Natural Hazards*. (Vol. 22). 17–27. doi: 10.1023/A:1008109810031.

Al-Tarazi, E. Sandvol, E. & Gomez, F. (2008). The February 11, 2004 Dead Sea Earthquake ML = 5.2 in Jordan and its Tectonic Implication. *Tectonophysics*. (Vol. 422, Issues 1). 149-158. doi: 10.1016/j.tecto.2006.05.010.

Asimaki, D. & Mohammadi, K. (2018). On the Complexity of Seismic Waves Trapped in Irregular Topographies. *Soil Dynamics and Earthquake Engineering*. (Vol. 114, Issue 29). 424-437.

Atmaca, N. Atmaca, A. and Kilcik, S. (2019). Earthquake Analysis of a School Project with TBDY 2018.*UEMK 2019 Proceedings Book24/25 October 2019 Gaziantep University, Turkey*.

Avni, R. Bowman, D. Shapira, A. & Nur, A. (2002). Erroneous Interpretation of Historical Documents Related to The Epicenter of the 1927 Jericho Earthquake in The Holy Land. *Journal of Seismology*. (Vol. 6). 469–476. doi: 10.1023/A:1021191824396.

Baker, J. (2013). Introduction to Probabilistic Seismic Hazard Analysis. Cambridge University.

Bakir, S. Eser, M. Akkar, Ş. and Iravul, Y. (2011). Shallow Seismic and Geotechnical Site Surveys at the Turkish National Grid for Strong-Motion Seismograph Stations. *Türkiye Earthquake Engineering and Seismology Conference*.

Beklar, T. Demirci, A. Ekinci, Y. and Buyuksarac, A. (2019). Analysis of Local Site Conditions Through Geophysical Parameters at a City Under Earthquake Threat: Çanakkale, NW Turkey. *Journal of Applied Geophysics*. (Vol. 163). 31-39. doi: 10.1016/j.jappgeo.2019.02.009.

Chadha, R. (2023). An Mw 7.8 Earthquake on 6 February 2023 on the East Anatolian Fault, Turkey. *Journal of the Geological Society of India*. (Vol. 99). 449-453. doi: 10.1007/s12594-023-2331-z.

Das, B. (2011). Geotechnical Engineering Handbook. *J. Ross Publishing, Inc*. USA.

Dong, L. & Luo, Q. (2022). Investigations and New Insights on Earthquake Mechanics from Fault Slip Experiments. *Earth-Science Reviews*. (Vol. 228, Issue 104019). doi: 10.1016/j.earscirev.2022.104019.

Duman, T. Çan, T. Emre, Ö. Keçer, M. Doğan, A. Ateş, Ş. and Durmaz, S. (2005). Landslide inventory of northwestern Anatolia, Turkey. *Engineering Geology*. (Vol. 77, Issue 1). 99-114. doi: 10.1016/j.enggeo.2004.08.005.

Elnashai, A. (2000). Analysis of The Damage Potential of The Kocaeli (Turkey) Earthquake of 17 August 1999. *Engineering Structures*. (Vol. 22, Issue 7). 746-754. doi: 10.1016/S0141-0296(99)00104-2.

Elnashai, A. Sarno, L., & Kwon, O. (2015). Fundamentals of Earthquake Engineering from Source to Fragility (2nd Edition). New York: Wiely.

Glass, C. (2013). Dangers from Earthquakes and Faults. *Interpreting Aerial Photographs to Identify Natural Hazards*. 67-95. Doi: 10.1016/C2012-0-06726-9.

Idriss, I. & Boulanger, R. (2008). Soil Liquefaction During Earthquakes. *Earthquake Engineering Research Institute*. United States of America.

Ilki, A. Celep, Z. (2012). Earthquakes, Existing Buildings and Seismic Design Codes in Turkey. *Arabian Journal for Science and Engineering*. (Vol. 37, Issue 2). doi: 10.1007/s13369-012-0183-8.

JBEC. 2022. Jordan Building Earthquake Code. *MEMR. Jordan, 2022*. (in Arabic).

Jimenez, M. Al-Nimry, H. & Khasawneh, A. (2008). Seismic Hazard Assessment for Jordan and Neighboring Areas. *Bollettino di Geofisica Teorica ed Applicata*. (Vol. 49, Issue 1).

Klinger, Y. Avouac, P. Dorbath, L. Abou Karaki, N. & Tisnerat, N. Seismic Behaviour of The Dead Sea Fault Along Araba Valley, Jordan. *Geophysical Journal International.* (Vol. 142, Issue 3).769–782. doi: 10.1046/j.1365-246x.2000.00166.x.

Kramer, S. (1996). Geotechnical Earthquake Engineering. Prentice-Hall International Series in Civil Engineering and Engineering Mechanics.

Mansoor, N. Niemi, T. & Misra, A. (2001). Liquefaction Potential Evaluation Along Active Faults at the Head of the Gulf of Aqaba, Jordan. *International Conferences on Recent Advances in Geotechnical Earthquake Engineering and Soil Dynamics*. (Vol. 26).

Mansoor, N. Niemi, T. & Misra, A. (2004). A GIS-Based Assessment of Liquefaction Potential of The City of Aqaba, Jordan. *Environmental & Engineering Geoscience*. (Vol. 10, Issue 4). 297–320. doi: 10.2113/10.4.297.

Naddaf, M. (2023). Turkey-Syria Earthquake: What Scientists Know. *SafetyLit Journal*, (Vol. 15, Issue 13). doi: 10.1038/d41586-023-00364-y.

Official Website of The Ministry of Energy and Mineral Resources, MEMR, Jordan. (https://www.memr.gov.jo/Default/En).

Official Website of The Ministry of Internal Affairs, Disaster and Emergency Management Presidency (AFAD), Turkey. (https://deprem.afad.gov.tr/).

Ozcep, F. Karabulut, S. Ozel, O. Ozcep, T. Imre, N. and Zarif, H. (2014). Liquefaction-Induced Settlement, Site Effects and Damage in The Vicinity of Yalova City During the 1999 Izmit Earthquake, Turkey. *Journal of Earth System Science*. (Vol. 123). 73–89. doi: 10.1007/s12040-013-0387-7.

Pamuk, A. Kalkan, E. and Ling, H. (2005). Structural and Geotechnical Impacts of Surface Rupture on Highway Structures During Recent Earthquakes in Turkey. *Soil Dynamics and Earthquake Engineering*. (Vol. 25, Issues 8). 581-589. doi: 10.1016/j.soildyn.2004.11.011.

Papazafeiropoulos, G. and Plevris, V. (2023). Kahramanmaraş-Gaziantep, Türkiye Mw 7.8 Earthquake on 6 February 2023: Strong Ground Motion and Building Response Estimations. *Multidisciplinary Digital Publishing Institute, MDPI*. (Vol.13, Issue 5). doi: 10.3390/buildings13051194.

Rafferty, J. (2011). Dynamic Earth Plate Tectonics, Volcanoes, and Earthquakes (1st Edition). *Britannica Educational*. New York.

Rodriguez, C. Bommer, J. & Chandler, R. (1999). Earthquake-Induced Landslides: 1980–1997. *Soil Dynamics and Earthquake Engineering*. (Vol. 18, Issue 5). doi: 10.1016/S0267-7261(99)00012-3.

Sandwell, D. (2001). Exploring the Earth from Mars. *Plate tectonics, Stories of Discovery*. LeGrand, Columbia University.

Sayın, E. Yön, B. Onat, O. et al. (2020). 24 January 2020 Sivrice-Elazığ, Turkey Earthquake: Geotechnical Evaluation and Performance of Structures. *Bull Earthquake Eng*. (Vol. 19). 657–684. doi: 10.1007/s10518-020-01018-4.

Sayın, E. Yön, B. Onat, O. Gör, M. Öncü, M. Tunç, E. Bakır, D. Karaton, M. and Calayır, Y. (2021). 24 January 2020 Sivrice-Elazığ, Turkey Earthquake: Geotechnical Evaluation and Performance of Structures. *Bull Earthquake Eng*. (Vol. 19) 657–684. doi:10.1007/s10518-020-01018-4.

Shearer, P. (2001). Introduction to seismology. *Geophysical Journal International*. Cambridge University. (Vol. 144, Issue 3). doi: 10.1111/j.1751-908X.1994.tb00526.x.

Sluys, L.J. (1992). Wave Propagation, Localization and Dispersion in Softening Solids. dissertation, Delft University of Technology.

Srvulov, M. (2011). Practical Soil Dynamics Case Studies in Earthquake and Geotechnical Engineering. *Springer Dordrecht Heidelberg*. London, New York.

Sucuoglu, H. (2018). New Improvements in the 2018 Turkish Seismic Code. *International Workshop on Advanced Materials and Innovative Systems in Structural Engineering: Seismic Practices*.

Sumer, B. Kaya, A. Hansen, N. (2002). Impact of Liquefaction on Coastal Structures in The 1999 Kocaeli, Turkey Earthquake. *International Offshore and Polar Engineering Conference, Kitakyushu*. Japan.

Tan, O. Tapirdamaz, M. and Yoruk, A. (2008). The Earthquake Catalogues for Turkey. *Turkish Journal of Earth Sciences*. (Vol. 17, Issue 2). 405–418.

Taskin, B. Sezen, A. Tugsal, U. & Erken, A. (2013). The Aftermath of 2011 Van Earthquakes: Evaluation of Strong Motion, Geotechnical and Structural Issues. *Bull Earthquake Eng*. (Vol. 11) 285–312. doi: 10.1007/s10518-012-9356-9.

TBEC. 2018. Türkiye Building Seismic Code. *AFAD, Official Gazetta, 2018*. (in Turkish). Ankara.

Ulusay, R. Aydan, O. Erken, A. Tuncay, E. kumsar, H. and Kaya, Z. (2004). An Overview of Geotechnical Aspects of the Çay-Eber (Turkey) Earthquake. *Engineering Geology*. (Vol. 73, Issues 1). 51-70. doi: 10.1016/j.enggeo.2003.11.005.

Uyeturk, C. Huraj, N. Bayraktarogly, H. and Huseyinpasaogly, M. (2022). Geotechnical Characteristics of Residual Soils in Rainfall-Triggered Landslides in Rize, Turkey. *Engineering Geology*. (Vol. 264, Issue 105318). doi: 10.1016/j.enggeo.2019.105318.

CURRICULUM VITAE